UNIVERSIDADE DE LISBOA
FACULDADE DE CIÊNCIAS

UNIVERSIDAD POLITÉCNICA DE MADRID
ESCUELA TÉCNICA SUPERIOR DE INGENIERÍA Y SISTEMAS DE TELECOMUNICACIÓN
INSTITUTO DE ENERGÍA SOLAR

Large power hybrid PV pumping for irrigation

"Documento Definitivo"

Doutoramento em Sistemas Sustentáveis de Energia
Doutoramento em Ingeniería de Sistemas y Servicios para la Sociedad de la Información

Rita Hogan Teves de Almeida

Tese orientada por:
Luis Narvarte Fernández (IES, UPM)

Miguel Centeno Brito (IDL, FCUL)

Documento especialmente elaborado para a obtenção do grau de doutor

2018

UNIVERSIDADE DE LISBOA
FACULDADE DE CIÊNCIAS

UNIVERSIDAD POLITÉCNICA DE MADRID
ESCUELA TÉCNICA SUPERIOR DE INGENIERÍA Y SISTEMAS DE TELECOMUNICACIÓN
INSTITUTO DE ENERGÍA SOLAR

Large power hybrid PV pumping for irrigation

Doutoramento em Sistemas Sustentáveis de Energia
Doutoramento em Ingeniería de Sistemas y Servicios para la Sociedad de la Información

Rita Hogan Teves de Almeida

Tese orientada por:
Luis Narvarte Fernández (IES, UPM)
Miguel Centeno Brito (IDL, FCUL)

Júri:
Presidente:
- Doutor António P Eduardo Lorenzo Pigueiras, Professor Catedrático, Instituto de Energía Solar – Universidad Politécnica de Madrid (Espanha)

Secretário:
- Doutor Francisco Martinez Moreno, Profesor Ayudante Doctor, ETS de Ingeniería y Sistemas de Telecomunicación – Universidad Politécnica de Madrid (Espanha)

Vogais:
- Doutora Maria Cristina Fedrizzi, Investigadora, Instituto de Energia e Ambiente – Universidade de São Paulo (Brasil)
- Doutor Juan Carlos Canasveras Sanchez, Responsável de I+D, ELAIA (Portugal)
- Doutor Jorge Augusto Mendes de Maia Alves, Professor Associado com Agregação, Laboratório Associado Instituto Dom Luiz, Faculdade de Ciências, Universidade de Lisboa (Portugal)

Documento especialmente elaborado para a obtenção do grau de doutor
Fundação para a Ciência e Tecnologia, PD/BD/105851/2014

2018

To my grandfather Vasco.

ACKNOWLEDGMENTS

The story of this PhD starts well before the writing of this document. In fact, it starts a lot before even thinking about studying PV Irrigation Systems.

It started in 2014, when I applied for the MIT scholarship. At that time, Professor Jorge Maia Alves was very important to me. I want to thank your guidance and support. In fact, I started the PhD because of you and what I miss the most about FCUL is the possibility of talking to you and listening to your wise advices.

In 2015, the PhD got started and a lot of mixed feelings come to my mind. As always, a journey has ups and downs and my PhD journey was not an exception.

I would like to express my gratitude to Miguel Brito for his great support during the first year of my PhD, for the possibility he gave me to come to Spain and for his dangerous adventure trying to get the agreement between both Universities finally signed.

I want to thank to all my open space colleagues in Portugal – Sara, Ivo, Mário, David, Pedro Nunes, Pedro Sousa and Filipe – and the ones who were also in FCUL (although not in the same physical space) – Rodrigo, Filipa, João, José and Nuno. Special thanks to Mário and Ivo: “you were always there when I needed to make the biggest decisions”.

In the summer of 2015 I had the chance to work in an NGO in Cameroon. I wish to thank to the IEEE Smart Village for the opportunity, particularly to Michael Wilson and Martin Niboh. Also, I must thank all the people I met in Cameroon – Ernest, Etienne and Hancheal (the solar team), Roger, David, Kennedy, Rhoda, Carine, Joyce, Hilda, Martin's family and little Ashley. Special thanks to Ernest, Etienne and Hancheal: we passed through a lot of adventurous and experiences together. I feel very proud of Ernest and Etienne for their perseverance and I hope that they continue enjoying the fruits of their labor.

Finally, at the end of 2015/beginning of 2016 the story of PV irrigation systems appeared in my life. Since then, I have two more groups of great people to be thankful – the one at PV Systems Group (IES-UPM) and the MASLOWATEN one.

Let me start by the people at IES. Firstly and foremost, I am very grateful to Luis. I thank you for giving me the opportunity to do my PhD and for sharing your knowledge with me. You gave me not only the possibility to work on MASLOWATEN, but also to be present in all of its stages. You also gave me the opportunity to work on a real project, to work on real

systems, to attend international meetings, to have contact with companies, to present our work worldwide and to grow, both professionally and personally. To summarize, I really want to thank you for your guidance and support. You were always there and I really appreciate that. I also want to thank Eduardo for his useful advices, his great wisdom, his enlightens and his useful help in what concerns the science of writing. I would also like to express my gratitude to Pepe because he shared with me all his knowledge about frequency converters and electronics in general and he taught me the importance of clearly think before starting to do something.

I want to thank my open space colleagues in Spain – Isaac, Celena, Carlos, Luismi, Fran, Imene, Estrella, Remedios, José, Aitor, Rodri, Alberto, José, Gilberto and Roberto. Some of you are no longer with us (here in the workspace) but, somehow, you all positively contribute to my time, work and life in Madrid. I am also thankful to Javier for our discussions and his help with SISIFO. Estrella deserves a special and huge thank because she was there every time I needed, for every reason and always with some word of advice – I think I have gained a Spanish mother.

Thanks to MASLOWATEN I have had the opportunity not only to do this thesis, but also to meet a lot of interesting people. I want to thank all of them for the pleasure and the great opportunity it meant to me to work with all of you. I want to highlight the most involved persons in my thesis. First of all, I really appreciate the support of Miguel Angel, Alberto and Javi (from DOMUS) because they were my first "teachers" outside IES and shared a lot of time and experience. I also want to thank the team at ELAIA, namely Julia, Guilherme, Paula, Juan Carlos, Bennani, Morad and Isham since they were the ones who were actually using the systems and without whose contribution my thesis would not be possible. I am also grateful to David Berengué (from Prógres) and Lauro Antipodi (from Caprari) since they have a lot of knowledge to share and were always available to do it. Finally, I am also thankful to David (from EIC) for his useful help in getting data and information about the world of irrigation.

I also want to express my gratitude to my family and friends. Even if some of my friends are still thinking that doing a PhD is a waste of time, I want to thank Rodrigo, Rui, Filipa, Vera, Diana and Catarina. Furthermore, I want to thank to Joana for her support and enthusiasm every time we met (we should do this more often).

My family was crucial to the success of this work and my life, specially my mother, my sister Maria, my grandpa Vasco and my grandma Teresa. You are, and will always be, an essential

part of my life. You are the ones who were always available for me. I really appreciate your support, your guidance, your friendship, your advices, everything you give to me. I also want to thank my uncles Jorge and Carmo, São, Isaac's parents, my father, my sister Mariana, my grandmother Elisa, my great-aunt Manuela and my godfather as well as his children and grandchildren.

Finally, I am deeply thankful to Isaac: I really appreciate your support both at work and at home; in the good moments and, the most important, in the bad ones. I thank you very much for accompanying me throughout this work and in life, both on a daily basis. You know that the end of this work would not be possible without you and you should also know that I want to be with you forever.

The research presented in this thesis was only possible thanks to the MIT Portugal Program on Sustainable Energy Systems and the Portuguese Science and Technology Foundation (FCT), under the grant PD/BD/105851/2014; as well as the European Union´s Horizon 2020 research and innovation program MArket uptake of an innovative irrigation Solution based on LOW WATer-ENergy consumption (MASLOWATEN), under grant agreement 640771.

Thank you for those who have made this journey unforgettable.

ABSTRACT

The aim of this thesis is to develop technical solutions for the reliable and efficient performance of large-power hybrid photovoltaic (PV) irrigation systems. These solutions have been applied to the design and implementation of two real-scale large-power hybrid PV drip irrigation demonstrators – a 140 kWp hybrid PV-diesel system in Alter do Chão, Portugal, and a 120 kWp hybrid PV-grid system in Tamelalt, Morocco.

Both systems have been working since 2016 and include monitoring systems. In order to do a technical and economic validation of the systems from these monitoring data, it has been necessary to develop new performance indices because, unlike PV grid-connected systems, the operation of this type of systems is affected by factors others than its quality. So, the typical performance ratio (*PR*) has been factorized in 4 distinct indicators: PR_{PV} (which includes the losses strictly related with the PV system), UR_{IP} (which varies with the particular crop and the irrigation period), UR_{PVIS} (which is intrinsic to the PVIS design), and UR_{EF} (which gives an idea of the use of the system, it is influenced by the monthly irrigation scheduling and the availability of water in the source).

The main technical solutions developed include first, an algorithm that allows the elimination of the problems associated with PV-power intermittences caused, for example, by a passing cloud; second, the match between PV production and irrigation needs through the use of a North-South horizontal axis tracker (N-S); and third the integration of the PV system in the pre-existing irrigation network through solutions which maximize the use of PV energy.

This thesis is structured in 2 different parts. The first one presents the results of the technical and economic validation of the demonstrators. In Portugal, the PV share (*PVS*) during the irrigation period is 0.49 (in 2017) and 0.36 (in 2018), and the *PR* is 0.16 (in 2017) and 0.22 (in 2018) extremely influenced by the use of the system (UR_{EF} of 0.29 and 0.44 respectively). In Morocco, in 2017 and 2018, the *PVS* is 0.48 and 0.55, and the *PR* is 0.24 (with a UR_{EF} of 0.32) and 0.29 (UR_{EF} of 0.36) respectively. The economic results show an initial investment cost of 1.2 €/Wp, a payback period of 8.8 years in Portugal and 7 in Morocco and, finally, a Levelized Cost of Energy of 0.13 €/kWh in Portugal and 0.07 €/kWh in Morocco, which leads to savings of 61% and 66% in Portugal and Morocco respectively.

In the second part of the thesis, three other novel contributions for the design of large-power PV irrigation systems are made. The first one is a new type of PV generator structure, the Delta structure, which has the objective to achieve constant in-plane irradiance profiles when

the end-users do not want to install trackers. It is worth noting that the peak power needed in this structure to achieve the same water volume of the N-S tracker is lower than the one needed with the typical static structure oriented to the Equator.

The second study evaluates the losses in a PV irrigation system depending on the number of PV modules in series of a PV generator. It is possible to conclude that these losses are irrelevant in most situations, casting doubts about the complex designs that are being offered by the market to avoid them. In places with very high mean temperatures, in a stand-alone PV system, these losses can be eliminated with the increase in the number of PV modules in series. On the other hand, in a hybrid PV-grid system it is impossible to eliminate the losses, but they can be minimized.

Finally, a new pump selection method for PV irrigation systems working at a variable frequency is proposed. A simulation exercise carried out for three different places in the Mediterranean zone shows that the water volume pumped by a PV irrigation system with a pump selected with this new method is 7.3 to 20.5% higher than the one pumped with the pump selected with the traditional method.

KEYWORDS: PV systems; hybrid PV systems; PV irrigation systems; water pumping; performance indices

RESUMEN

El principal objetivo de esta tesis es el desarrollo de soluciones técnicas para el funcionamiento fiable y eficiente de sistemas híbridos de riego fotovoltaico (FV) de alta potencia. Estas soluciones técnicas se han aplicado al diseño e instalación de dos demostradores de riego FV por goteo a escala real – uno de 140 kWp híbrido FV-diésel en Alter do Chão, Portugal, y otro de 120 kWp híbrido FV-red en Tamelalt, Marruecos.

Los dos sistemas están en pleno funcionamiento desde el 2016 y ambos cuentan con sistemas de monitorización. Para validar técnica y económicamente ambos demostradores a partir de estos datos de monitorización, ha sido necesario desarrollar nuevos índices de calidad de su operación ya que, a diferencia de los sistemas FV de conexión a red, el funcionamiento de este tipo de sistemas se ven afectados por factores ajenos a su calidad. Así, el tradicional *performance ratio* (*PR*) ha sido factorizado en 4 indicadores distintos: PR_{PV} (que incluye las pérdidas relacionadas con el sistema FV), UR_{IP} (que varía con el cultivo y su periodo de riego), UR_{PVIS} (que depende del diseño del sistema de riego FV), y UR_{EF} (que cuantifica la utilización real del sistema por el usuario).

Las principales soluciones técnicas desarrolladas incluyen, primero, un algoritmo que permite eliminar los problemas asociados a la intermitencia de la potencia FV causada, por ejemplo, al efecto del paso de nubes; segundo, el ajuste entre la producción FV y la demanda de agua a través de la utilización de seguidores de eje norte-sur horizontal (N-S); y, tercero, la integración de los sistemas FV en los sistemas de riego que ya existían en las fincas mediante configuraciones de diseño que permiten maximizar el aprovechamiento de la energía solar.

La tesis se estructura en 2 partes. En la primera se presentan los resultados de la evaluación técnica y económica de los dos demostradores. El de Portugal muestra penetraciones FV durante el periodo de riego de 0.49 (en 2017) y 0.36 (en 2018), y *PR* de 0.16 (en 2017) y 0.22 (en 2018) fuertemente influenciados por la utilización del usuario (UR_{EF} de 0.29 y 0.44 respectivamente). En el caso de Marruecos la penetración FV, en 2017 y 2018, es de 0.48 y 0.55, y el *PR* de 0.24 y 0.29 (UR_{EF} de 0.32 y 0.36), respectivamente. A nivel económico, la inversión inicial en ambos sistemas es 1.2 €/Wp, el período de retorno de la inversión es 8.8 años en Portugal y 7 en Marruecos y, finalmente, el *Levelized Cost of Energy* es 0.13 €/kWh en Portugal y 0.07 €/kWh en Marruecos, llevando a ahorros del 61% y 66% en Portugal y Marruecos, respectivamente.

En la segunda parte de la tesis, se realizan otras tres contribuciones novedosas para el diseño de sistemas de riego FV de alta potencia. La primera es un nuevo tipo de estructura, llamada Delta, que tiene por objetivo conseguir un perfil constante de irradiancia con una estructura estática para los casos en que los usuarios no deseen instalar seguidores solares. Es interesante subrayar que la potencia pico necesaria en esta estructura para llegar al mismo volumen de agua del sistema con seguidor N-S es más pequeña que la necesaria con la típica estructura estática orientada al ecuador.

El segundo estudio evalúa las pérdidas en un sistema de riego FV dependiendo del número de módulos en serie del generador FV. Se puede concluir que en la mayor parte de los casos, estas pérdidas no son significativas por lo que carecen de sentido los complejos diseños que está ofreciendo el mercado para evitar estas pérdidas. En localizaciones con muy altas temperaturas medias, en un sistema aislado estas pérdidas disminuyen con el aumento del número de módulos en serie, mientras que en un sistema híbrido con la red eléctrica estas pérdidas son inevitables independientemente del número de paneles, aunque se pueden minimizar.

Finalmente, se propone un nuevo método de selección de bombas para sistemas de riego FV a frecuencia variable. Un ejercicio de simulación hecho para 3 lugares distintos de la cuenca mediterránea demuestra que el volumen de agua bombeada por un sistema de riego FV con una bomba seleccionada por este nuevo método tiene incrementos entre el 7.3 y el 20.5% cuando se compara con una bomba seleccionada con el método tradicional.

PALABRAS CLAVE: sistemas FV; sistemas híbridos FV; sistemas de riego FV; bombeo de agua; índices de funcionamiento

RESUMO

O principal objetivo de esta tese é o desenvolvimento de soluções técnicas para o funcionamento fiável e eficiente de sistemas híbridos de rega fotovoltaica (PV) de alta potência. Estas soluções técnicas foram aplicadas ao desenho e instalação de dois demonstradores híbridos PV para irrigação gota-a-gota em dois olivais reais da empresa ELAIA – um sistema híbrido PV-diesel de 140 kWp em Alter do Chão, Portugal; e um sistema híbrido PV-rede de 120 kWp em Tamelalt, Marrocos.

Os dois demonstradores estão em pleno funcionamento desde 2016 e ambos contam com sistemas de monitorização. Para validar técnica e economicamente os dois demonstradores a partir dos dados de monitorização foi necessário desenvolver novos índices de desempenho uma vez que, ao contrário do que ocorre em sistemas PV de ligação à rede, o funcionamento de sistemas de rega PV é influenciado por fatores externos à qualidade da sua instalação. Assim, o tradicional *performance ratio* (*PR*) foi fatorizado em 4 indicadores: PR_{PV}, UR_{IP}, UR_{PVIS}, UR_{EF}. O primeiro, PR_{PV}, contabiliza as perdas estritamente relacionadas com o sistema fotovoltaico (e pode ser comparado ao *PR* de um sistema de ligação à rede). O UR_{IP} depende do cultivo e indica as perdas associadas ao período de rega. O UR_{PVIS} está relacionado com o desenho do sistema de irrigação PV (sendo influenciado, por exemplo, pelo tipo de irrigação, pela relação entre a potência consumida e a instalada e pela estrutura do gerador PV). O quarto e último indicador, UR_{EF}, indica a utilização real do sistema (relacionando a irradiância utilizada com a útil num sistema de rega PV).

As principais soluções técnicas desenvolvidas incluem o desenvolvimento de um algoritmo para eliminar os problemas associados à intermitência da potência PV causados, por exemplo, por uma passagem de nuvens (este algoritmo foi patenteado); o ajuste entre a produção PV e as necessidades de rega foi solucionado através da utilização de seguidores de eixo Norte-Sul horizontal (N-S); e, finalmente, o sistema PV foi perfeitamente integrado no sistema de rega pré-existente nas herdades mediante configurações de desenho que permitem maximizar o aproveitamento da energia solar PV.

Esta tese está estruturada em duas partes. Na primeira são apresentados os dois demonstradores em estudo. Para cada um deles é feita uma análise dos sistemas pré-existente e atual. De seguida, simulações para dois cenários (um otimista e um pessimista) foram desenvolvidas para estimar o desempenho dos novos sistemas híbridos. Finalmente, os dados

de monitorização permitiram fazer uma análise detalhada do desempenho real dos sistemas durante as campanhas de rega de 2017 e 2018.

No caso de estudo em Portugal, em 2017, a penetração PV foi 0.49, e o *PR* durante o período de rega foi 0.16 (extremamente influenciado por um UR_{EF} de 0.29). Estes valores são consequência da baixa utilização do sistema devido à sequia verificada ao longo do ano. De facto, o sistema funcionou apenas 94 dias e maioritariamente durante a noite. Em 2018, o desempenho no mês de agosto é particularmente interessante. O sistema funcionou, em média, 16 horas por dia (quase 7h30 apenas com PV), a penetração PV foi de 0.53 e o *PR* de 0.56. Neste caso, o UR_{EF} é 0.99, o PR_{PV} 0.83 e o UR_{PVIS} 0.68. Nos restantes meses do ano um problema com o sistema de fertirrigação obrigou a uma elevada utilização do gerador diesel. Ainda assim, durante o período de rega, a penetração PV é 0.36 e o *PR* 0.22. Neste último caso, os valores de PR_{PV} e UR_{PVIS} são semelhantes aos do mês de agosto (0.80 e 0.60 respetivamente), sendo a principal diferença o UR_{EF} que baixa de 0.99 a 0.44. No caso de Marrocos, a penetração PV é 0.48 em 2017 e 0.55 em 2018 e o *PR* é 0.24 e 0.29 respetivamente. Este *PR* é influenciado, maioritariamente, pelos valores de UR_{EF} (0.32 em 2017 e 0.36 em 2018).

A nível económico, o investimento inicial é de 1.2 €/Wp nos dois sistemas, o tempo de retorno do investimento é 8.8 anos em Portugal e 7 em Marrocos e, finalmente, o *Levelized Cost of Energy* é 0.13 €/kWh no caso de Portugal e 0.07 €/kWh no caso de Marrocos, o que significa poupanças de 61% e 66% em Portugal e Marrocos, respetivamente.

Adicionalmente, outros três estudos sobre sistemas de rega PV de alta potência são apresentados: um novo tipo de estrutura estática chamada Delta, as perdas de energia associadas ao número de módulos em série neste tipo de sistemas, e finalmente um novo método de seleção de bombas para sistemas de irrigação PV de alta potência.

Relativamente à estrutura Delta, o principal objetivo era obter um perfil constante de irradiância sem utilizar seguidores solares. Verificou-se que esta opção (que consiste em instalar metade da potência pico do gerador PV orientada a Este e a outra metade a Oeste com uma inclinação de 60º) é bastante interessante em sistemas de irrigação PV. A potência pico necessária neste caso é inferior à necessária com a típica estrutura estática orientada ao Equador. Se o objetivo é alcançar a mesma quantidade de água da estrutura com seguidor N-S nos meses de rega, então a potência pico necessária na estrutura Delta é 1.75 vezes a

necessária no caso deste seguidor. Além disso, um índice para estudar quão constante é o perfil foi utilizado e os resultados mostram que durante o período de rega alcança-se 0.99.

Relativamente ao estudo da influência do número de módulos em série, as perdas de energia PV foram calculadas para um sistema PV autónomo que bombeia de um poço a um depósito e para um sistema híbrido PV-rede a pressão e caudal de água constantes. Estas duas configurações foram analisadas em dois locais com temperaturas ambiente médias distintas (Villena, Espanha e Marraquexe, Marrocos) e para valores de tensão impostos pela bomba ou pela rede elétrica distintos. De seguida, realizaram-se duas extrapolações dos resultados obtidos. A primeira estabelece-se para permitir a seleção do número de módulos PV em série dependendo da média anual da temperatura máxima e a segunda dependendo da tensão da rede à qual o sistema vai ser ligado. Pode-se concluir que, na maioria dos casos, estas perdas não são significativas e, nesse seguimento, não têm sentido as soluções complexas que o mercado está a oferecer para eliminar estas perdas. Em locais com temperaturas médias muito altas, no caso dos sistemas isolados, as perdas diminuem (e podem ser eliminadas) com o aumento do número de módulos em série no gerador PV. Por outro lado, no caso dos sistemas híbridos PV-rede estas perdas podem ser minimizadas, mas são inevitáveis independentemente do número de módulos em série.

No que diz respeito ao método de seleção de bombas, um novo método é proposto uma vez que o tradicional seleciona a bomba com base na máxima eficiência no ponto de trabalho (a 50 ou 60 Hz). Ora, num sistema PV, a bomba pode funcionar a frequências e pontos de trabalho distintos e por isso o método de seleção deve ser adaptado a essas características. Este novo método foi desenvolvido e o procedimento foi implementado no SISIFO (uma ferramenta de simulação de sistemas PV desenvolvida no Instituto de Energia Solar da Universidade Politécnica de Madrid). Posteriormente, foi feita uma comparação entre o desempenho de uma bomba selecionada com o método tradicional e outra com o novo método. Esta comparação foi realizada em três locais distintos da área mediterrânea: Madrid, Marraquexe e Nice. Os resultados demonstram que o volume de água bombeada ao largo de um ano aumenta entre 7.3 e 20.5%, enquanto a eficiência da bomba aumenta entre 4.3 e 5.3% quando se compara a bomba selecionada com o novo método com a bomba selecionada com o método tradicional.

PALAVRAS-CHAVE: sistemas PV; sistemas híbridos PV; sistemas de rega PV; bombagem de água; índices de desempenho

CONTENTS

ACKNOWLEDGMENTS ..... **III**

ABSTRACT ..... **XI**

RESUMEN ..... **XIII**

RESUMO ..... **XV**

LIST OF FIGURES ..... **XXI**

LIST OF TABLES ..... **XXV**

NOMENCLATURE ..... **XXVII**

1. INTRODUCTION **1**

1.1 Brief summary of the historical milestones in photovoltaic pumping 6

1.1.1 PV water pumping systems for irrigation *10*

1.2 Limitations of PV irrigation technology in the current state of the art and the MASLOWATEN project 13

1.3 The need of hybrid systems 16

1.4 Objectives and main contributions of this thesis 17

FIRST PART: DESIGN, IMPLEMENTATION AND PERFORMANCE ANALYSIS OF HYBRID PV IRRIGATION SYSTEMS **21**

2. A 140 KWP HYBRID PV-DIESEL IRRIGATION SYSTEM IN PORTUGAL **23**

2.1 Introduction 23

2.2 The Alter do Chão irrigation system 24

2.2.1 The pre-existing only-diesel system *24*

2.2.2 The hybrid PV-diesel system *26*

2.2.3 The PV generator *29*

2.2.4 Performance scenarios *30*

2.3 Performance indices for hybrid PV systems 32

2.3.1 Performance indices for the two scenarios *35*

2.4 In-the-field performance 37

2.4.1 Commissioning of the system *37*

2.4.2 Real performance in 2017 ..... *37*

2.4.3 Real performance in 2018 ..... *38*

2.5 Economic analysis 39

2.5.1 Net Present Value, Internal Rate of Return and Payback Period *40*

2.5.2 Levelized Cost of Energy *40*

2.5.3 Results *42*

3. A 120 KWP HYBRID PV-GRID IRRIGATION SYSTEM IN MOROCCO **45**

3.1 Introduction 45

3.2 The Tamelalt irrigation system 45

3.2.1 The pre-existing only-grid system *45*

3.2.2 The hybrid PV-grid system *47*

3.2.3 The PV generator *49*

3.2.4 Performance scenarios *49*

3.3 Performance indices 51

3.3.1 Performance indices for the two scenarios *52*

3.4 In-the-field performance 53

3.4.1 Commissioning of the system *53*
3.4.2 Real performance in 2017 ..... *54*
3.4.3 Real performance in 2018 ..... *55*
3.5 Economic analysis 56

SECOND PART: CONTRIBUTIONS TO THE DESIGN OF PV IRRIGATION SYSTEMS 59

4. PV ARRAYS WITH DELTA STRUCTURES FOR CONSTANT IRRADIANCE DAILY PROFILES 61

4.1 Introduction 61
4.2 The Delta structure 62
4.2.1 Irradiance profiles *64*
4.2.2 Ground Cover Ratio *66*
4.2.3 Electrical losses *67*
4.3 Comparative performance analysis 70

5. ON THE NUMBER OF PV MODULES IN SERIES FOR LARGE-POWER IRRIGATION SYSTEMS 77

5.1 Introduction 77
5.2 Limitation of the number of PV modules in series and impact in the PV irrigation system performance 78
5.3 Energy losses versus number of PV modules in series 80
5.3.1 Methodology *80*
5.3.2 Losses for the stand-alone PV irrigation system to a water pool *84*
5.3.3 Losses for the hybrid PV-grid irrigation system at constant power *85*
5.4 Discussion of the results 86
5.4.1 Stand-alone PV irrigation system to a water pool *86*
5.4.2 Hybrid PV-grid irrigation system at constant power *87*
5.4.3 Summary and generalization of results *89*
5.5 Design of solutions to avoid energy losses 93

6. A NEW PUMP SELECTION METHOD FOR LARGE-POWER PV IRRIGATION SYSTEMS AT A VARIABLE FREQUENCY 95

6.1 Introduction 95
6.2 The traditional pump selection method 96
6.3 The new selection method for PV irrigation systems at a variable frequency 101
6.4 Pump selection method and PV irrigation system performance 106
6.5 Implementation in SISIFO 109

7. CONCLUSIONS AND FUTURE RESEARCH LINES 111

7.1 Conclusions 111
7.2 Future research lines 115

8. PUBLICATIONS 117

8.1 International peer reviewed journals 117
8.2 Conference proceedings 118
8.3 Patents 119
8.4 Other publications during the doctorate not related to the thesis 119

9. REFERENCES 121

LIST OF FIGURES

Figure 1 – Percentage of the irrigated areas regarding the utilized agricultural area (UAA) [%] in 2013 [14]. 3

Figure 2 – Percentage of energy used in agriculture and forestry in the World, Europe, southern Europe and southern European countries in 2011 (it includes, but it is not limited to, the energy needed to irrigate) [18]. 4

Figure 3 – PV pumping system for irrigation in Capim Grosso, Brasil [42]..... 9

Figure 4 – Engineer conducting performance evaluation after 8 years of operation in Chihuahua, Mexico [43]... 9

Figure 5 – Components of a PV irrigation system: PV generator, frequency converter, motor-pump and water tank. 11

Figure 6 – Solar water pump in India (photograph from Raghav Agarwal, [58]). 12

Figure 7 – PV irrigation system in Tizi, Morocco [30]. 12

Figure 8 – (a) Pre-existing irrigation system configuration: The electric power at the output of the diesel generator, P_{AC}, is controlled in order to keep the hydraulic pressure constant at the input of the irrigation network, p_1. Black and blue lines represent electricity and water ways respectively. (b) Cycling evolution of AC power (P_{AC}) and pressure (p_1 and p_2) due to water filtering and filter cleaning periods. 25

Figure 9 – Hours per day of a) Irrigation scheduling, b) Daytime. 26

Figure 10 – Hybrid PV irrigation system configuration. A PV generator, a new motor-pump, and two FCs have been added to the pre-existing configuration of Figure 1. The new components are marked in orange, while the previous ones are in green. 27

Figure 11 – Available PV power thresholds with hysteresis for the different operating modes – "Only PV", Hybrid and "Only Diesel". 28

Figure 12 – (a) Aerial view of the hybrid PV-diesel drip irrigation system. (b) Detail of the three motor-pumps and the water filter bench. The additional third pump is easily identifiable. 29

Figure 13 – Incident irradiance profile on the tracker during the autumn equinox and the summer solstice. 30

Figure 14 – Energy flows involved in a hybrid PV irrigation system. 33

Figure 15 – Graphical representation of the different irradiations considered: (a) $\int \boldsymbol{G_{IP}}$ is the irradiation during the irrigation period, (b) $\int \boldsymbol{G_{useful}}$ is the useful irradiation during the IP determined by the design of the PV irrigation system; and (c) $\int \boldsymbol{G_{used}}$ is the irradiation used effectively by the system. 34

Figure 16 – The pre-existing irrigation system. 46

Figure 17 – Hours per day of a) Irrigation scheduling, b) Daytime. 46

Figure 18 – Hybrid PV-grid system configuration. If ones compare this configuration with the one presented in Figure 16, the PV generator and the PLC were added, as well as the frequency converters (which replace the soft-starters). 48

Figure 19 – Different components of the system: (a) PV generator. (b) Frequency converters and PLC boxes. (c) Motor-pumps. 49

Figure 20 – Graphical representation of the different irradiations considered: (a) $\int \boldsymbol{G_{IP}}$ is the irradiation during the irrigation period, (b) $\int \boldsymbol{G_{useful}}$ is the useful irradiation during the IP determined by the design of the PV irrigation system; and (c) $\int \boldsymbol{G_{used}}$ is the irradiation used effectively by the system. 51

Figure 21 – The Delta structure, $\Delta S(\beta)$: The PV array is distributed in two halves. One half is oriented to the West while the other half is oriented to the East. For presentation clarity, the latter is not pointed out in the figure. 63

Figure 22 – The in-plane global irradiance over a ΔS(60) measured on a clear day close to the Summer Solstice (23rd June 2017) at IES-UPM. In-plane global irradiance in the East- and West-oriented halves of the ΔS(60) are presented in blue and green respectively. The average value is in red. It is seen that constancy is almost achieved during the middle 8 hours of the day. Variations near 8 h and 20 h are due to shadows from surrounding objects..... 63

Figure 23 – The in-plane global irradiance evolution during the Spring Equinox (green), the Summer Solstice (red), and the Winter Solstice (blue) days at Figueirinha, Silves, Portugal. The highest constancy index is obtained during the Summer Solstice (0.974), followed by the Spring Equinox (0.971), the lowest value being obtained during Winter Solstice (0.839)..... 65

Figure 24 – The constancy index and yearly irradiation for different angles of inclination (from 0 to 90^0) for the ΔS(β). As expected, the maximum constancy index is obtained for an inclination of 60^0 (0.948). The green point represents the yearly irradiation for S(25)..... 66

Figure 25 – Spacing between adjacent rows in ΔS(β) (a), S(β) (b), and 1xh (c)..... 66

Figure 26 – The evolution of yearly energy yield in Figueirinha for the three structures considered..... 67

Figure 27 – DC power with 1 and 2 MPPTs, as well as electrical mismatching losses over a typical day of June. The monthly mean of electrical mismatching losses is 2%..... 69

Figure 28 – Electrical mismatching losses over a typical year. The yearly mean value is 2.4%. 69

Figure 29 – System (blue solid line) and pump curves (orange solid line represents 50 Hz and the points marked with circles have been obtained from manufacturer information, the remaining dashed lines corresponds to frequencies different from 50 Hz)..... 71

Figure 30 – The yearly AC energy produced by a PVGCS with ΔS(60) and S(25) normalized by the AC energy produced by a 40 kWp 1xh (E_{AC}/E_{AC1xh}) as a function of its PV peak power normalized by the 40 kWp peak power of 1xh (P^*/P^*_{1xh}). The two points with E_{AC}/E_{AC1xh} =1 represent the required oversizing of ΔS(60) and S(25) PV peak power to equal the performance of the 40 kWp 1xh. 72

Figure 31 – Water volume pumped by a PVIS with ΔS(60) and S(25) normalized by the water volume pumped by a 40 kWp 1xh (Water volume/Water volume$_{1xh}$) as a function of its PV peak power normalized by the 40 kWp peak power of 1xh (P^*/P^*_{1xh}). The continuous lines represent yearly values and dashed lines show the water volume pumped during the irrigation period. The points with *Water volume*/*Water volume*$_{1xh}$ =1 represent the required oversizing of ΔS(60) and S(25) PV peak power to equal the performance of the 40 kWp 1xh. 72

Figure 32 – AC power of PVGCS (a) and water flow of PVIS (b) for a characteristic day of June for the three structures in the study..... 74

Figure 33 – P-V curve of the stand-alone PV irrigation system to a water pool. The PV energy losses are calculated integrating along the whole irrigation period the difference of the maximum power that could be generated by the system and the power that is really producing due to the limitation of $V_{DC_{BUS\_PUMP}}$..... 82

Figure 34 – P-V curve of the hybrid PV-grid system. The PV energy losses are calculated integrating the difference of $P_{p=cte}$ and the PV power corresponding to $V_{DC_{BUS\_GRID}}$: (a) $P_{MPP} \geq P_{p=cte}$; (b) $P_{MPP} < P_{p=cte}$..... 83

Figure 35 – Frequency of occurrences of hourly V_{oc}>800 V in the N-S structure. 85

Figure 36 – PV energy losses: (a) Losses when $P_{MPP} > P_{p=cte}$ occur if the PV generator voltage for $P_{p=cte}$, $V_{DC_{PV\_p=cte}}$, is less than $V_{DC_{BUS\_GRID}}$, and they can be eliminated increasing the number of PV modules in series; (b) Losses when $P_{MPP} < P_{p=cte}$ depend on the difference between $V_{DC_{BUS\_GRID}}$ and $V_{DC_{PV\_p=cte}}$ and can be reduced but also increased when varying the number of PV modules in series..... 88

Figure 37 – Evolution of the losses along the year for the case of $V_{DC_{BUS\_GRID}} = \mathbf{587}$ V for a hybrid PVIS at constant pressure in Marrakech and depending on the number of PV modules. 89

Figure 38 – Losses depending on the temperature of the location for a stand-alone PVIS to a water pool. The abscissa axis is expressed in terms of a temperature offset regarding the yearly mean maximum temperature in Villena. 90

Figure 39 – Losses depending on $V_{DC_{BUS\_PUMP}}$ for a stand-alone PVIS to a water pool. 91

Figure 40 – Losses in a hybrid PV-grid irrigation system at constant power depending on the temperature. The abscissa axis is expressed in terms of a temperature offset regarding the yearly mean maximum temperature in Villena. 92

Figure 41 – Losses for a hybrid PV-grid irrigation system at constant power in Villena depending on $V_{DC_{BUS\_GRID}}$. 92

Figure 42 – Proposal of design to avoid overvoltages at the FC input when it is necessary to use 21 PV modules in series. 93

Figure 43 – PV pumping system from a well to a water tank. The figure illustrates the static head (H_{st}), the drawdown and the head of the water tank, (H_{pool}). The total manometric head is the addition of H_{st}, drawdown, H_{pool} plus the friction losses. 97

Figure 44 – System curve, *H-Q* pump curve and characteristic points to select a pump. 98

Figure 45 – Three possible pumps for a certain duty point. Pump A has its BEP too far to the left in respect to the duty point; Pump C has its BEP too far to the right in respect to the duty point. Pump B has the BEP close to the duty point and the pump would be the selected according to the traditional pump selection method. 99

Figure 46 – Preferred operating region to bring about the lowest energy and maintenance cost and to reduce the risk of system problems since hydraulic excitation forces and cavitation risk attain a minimum close to the BEP [137]. 99

Figure 47 – List of the suitable pumps offered by PumpTutorNG tool for the duty point *H*= 288 m and *Q*= 227 m^3/h. 100

Figure 48 – *H-Q* curves of the pumps offered by PumpTutorNG tool for the duty point *H*= 288 m and *Q*= 227 m^3/h. 100

Figure 49 – Pumps with the highest slope. The E10S55/15A+MAC12340C-8V (a) and E12S50/11A+MAC12340C-8V (b) models show the ratio between the lowest and the highest head of 2.3 and 2.0 respectively. 102

Figure 50 – Detail of the *H-Q*, power-*Q* and efficiency-*Q* of both pumps. In both cases, the duty point is in the right-hand third of the *H-Q* curve. 103

Figure 51 – Determination of the lowest operating frequency for the E10S55/15A+MAC12340C-8V pump (a) and the E12S50/11A+MAC12340C-8V pump (b). The values are 38 Hz and 39 Hz respectively. 104

Figure 52 – H-Q, power-Q and efficiency-Q curves at the frequencies used to calculate EFF_{IRR} for the E10S55/15A+MAC12340C-8V pump (a) and the E12S50/11A+MAC12340C-8V pump (b). Only the efficiency values for 50Hz are shown but the procedure is similar for the rest of the frequencies. 105

Figure 53 – Monthly yield with both the proposed pump and the traditional one. 107

Figure 54 – Comparison of the *H-Q* curves of several possible pumps for a certain duty point as shown by SISIFO – curves at 50 Hz are shown in (a), while the ones at start frequency are in (b). The system curve is also included. 110

Figure 55 – Comparison of the volume of water pumped by four possible pumps during (a) the twelve months of a year and (b) during the pumping hours of the characteristic day of July. 110

LIST OF TABLES

Table 1 – ON(1)/OFF(0) status of the different operating modes. 28

Table 2 – PV energy and volume of water pumped (from PV and from diesel) in the Optimistic and Pessimist scenarios. Daily working hours are also given for “Only PV” and “Hybrid” modes with the threshold of 95 kW to transit between these two modes. 31

Table 3 – Parameters of the simulation. 32

Table 4 – Simulated performance indices for the Optimistic and Pessimist scenarios (NA means not applicable). 36

Table 5 – Expected and actual STC power of the PV generator and FCs and motor-pumps efficiencies. 37

Table 6 – Real operational data in 2017. 38

Table 7 – Real performance indices in 2017. 38

Table 8 – Real operational data in 2018. 39

Table 9 – Real performance indices in 2018 (NA means not applicable). 39

Table 10 – Economic data for the Alter do Chão PV-diesel drip irrigation system. 43

Table 11 – Economic results of the Alter do Chão PV-diesel drip irrigation system. 43

Table 12 – PV energy, volume of water pumped (from PV and from grid) and daily working hours in the Pessimist and Optimistic scenarios. 50

Table 13 – Parameters of the simulation. 50

Table 14 – Simulated performance indices for the Optimistic and Pessimist scenarios. 52

Table 15 – Expected and actual STC power of the PV generator and FCs and motor-pumps efficiencies. 53

Table 16 – Real operational data in 2017. 54

Table 17 – Real performance indices from August to November 2017. 54

Table 18 – Real operational data in 2018. 55

Table 19 – Real performance indices from a period of 2018. 55

Table 20 – Economic data for the Tamelalt PV-grid drip irrigation system. 56

Table 21 – Economic results of the Tamelalt PV-grid drip irrigation system. 56

Table 22 – Constancy index values, for three representative days and for three different PV array structures. 65

Table 23 – The separation between structures (L) and 1/GCR for the three structures in the study. 67

Table 24 – Characteristics of the PV irrigation system. 70

Table 25 – AC energy for a PVGCS and water volume for a PVIS for a 40 kWp 1xh. NA means not applicable. 71

Table 26 – PV generator size needed to guarantee the same yearly AC energy (for a PVGCS) or water volume (for a PVIS) than a 40 kWp 1xh 73

Table 27 – Yearly mean of the constancy index (k_C) applied to AC power of a PVGCS and to water flow for PVIS for the three structures in the study. 75

Table 28 – The required values of $V_{DC_{BUS\_PUMP}}$ depending on $V_{AC_{PUMP}}$. 79

Table 29 – $V_{DC_{BUS\_GRID}}$ values corresponding to different $V_{AC_{GRID}}$. 80

Table 30 – PV generator size, frequency converter and pumping characteristics of the stand-alone and hybrid PVIS. 81

Table 31 – Maximum and minimum monthly mean ambient temperatures (T_{Mm}, T_{mm}) in Villena and Marrakech. 81

Table 32 – PV energy losses of the stand-alone PV irrigation system in Villena (Vi) and Marrakech (Ma) for 20 to 22 PV modules in series and for the three values of $V_{DC_{BUS\_PUMP}}$ 84

Table 33 – PV energy losses of the hybrid PV-grid irrigation system at constant power in Villena (Vi) and Marrakech (Ma) for 20 to 22 PV modules in series and for the two values of $V_{DC_{BUS\_GRID}}$ 85

Table 34 – PV energy losses of the hybrid PV-grid irrigation system at constant power in Marrakech (Ma) for 20 to 22 PV modules in series. 88

Table 35 – Optimum number of PV modules in series to reduce the losses at the FC input for the stand-alone PV irrigation system to a water pool. 89

Table 36 – Optimum number of PV modules in series to reduce the losses at the FC input for the hybrid PV-grid irrigation at constant power. 90

Table 37 – Values of the pump efficiency at the four frequencies used to calculate EFF_{IRR}. 106

Table 38 – PV generator size, inverter and pumping characteristics. 107

Table 39 – Performance and annual efficiency of both pumps, that selected with the new method proposed here and that selected with the traditional method. 107

Table 40 – Performance comparison of the pumps selected with the new (Pump A: E10S55/15A+MAC12340C-8V) and the traditional method (Pump B: E12S55/9B+MAC12340C-8V) in the characteristic days of the months of May, June and July. 108

Table 41 – Increase in the pumped water and efficiency obtained with the pump selected with the new method proposed here for to other locations: Marrakech and Nice. 109

NOMENCLATURE

Parameter	Description	Unit
B	In-plane direct irradiance	W/m^2
β	Inclination angle	º
β_c	Coefficient of variation in the voltage with the temperature of the solar cell	V/ºC
$CAPEX$	Capital Expenditures	€
CEC_n	Annual price of the diesel/grid electricity	€
CF	Cash Flow	€
$CF_{PV,n}$	Cash Flow of the PV for year n	€
CR	Capital Repayment	€
DI	Debt Interest	%
E_{AC}	AC energy	kWh
E_{AC1xh}	AC energy of 1xh	kWh
E_d	Diesel energy	kWh
EFF_{IRR}	Irrigation efficiency	p.u.
E_g	Energy supplied by the grid	kWh
E_d^H	Energy supplied by the diesel generator in “Hybrid” mode	kWh
E_{Hyd}	Hydraulic energy	kWh
E_d^O	Energy supplied by the diesel generator in “Only Diesel” mode	kWh
E_{PV}	PV energy	kWh
$\eta_{DC/AC}$	Efficiency of the FC	p.u.
η_{Hyd}	Hydraulic efficiency	p.u.
η_{int1}	Efficiency at intermediate motor-pump frequency	p.u.
η_{int2}	Efficiency at intermediate motor-pump frequency	p.u.
η_{max}	Efficiency at maximum motor-pump frequency	p.u.
η_{min}	Efficiency at minimum motor-pump frequency	p.u.
η_P	Ratio real power versus nominal power of the PV generator	p.u.
η_T	Thermal efficiency of the PV generator	p.u.
F_{ML}	Electrical mismatching losses	%
G	In-plane global irradiance	W/m^2
G*	Irradiance at Standard Test Conditions	W/m^2

γ	Power temperature coefficient of the PV modules	W/ºC
GCR	Ground Cover Ratio	p.u.
$G_{dm(0)}$	Monthly mean daily horizontal irradiation	Wh/m^2
G_{IP}	Irradiance during the IP	W/m^2
G_{md}	In-plane irradiance at midday	W/m^2
G_{used}	Irradiance effectively used by the system	W/m^2
G_{useful}	Available useful irradiance during the IP	W/m^2
h	Inflation rate	%
H	Pumping head	m
HDR	Hybrid diesel ratio	p.u.
H_{dyn}	Dynamic level of the water in the well	m
$H_{friction}$	Friction losses	m
HMT	Total Manometric Head	m
H_{pool}	Height of the water pool	m
IIC	Initial Investment Cost	€
IRR	Internal Rate of Return	%
I_{SC}	Short-circuit current	A
K_0	No-load parameter (Schmid model)	p.u.
K_1	Linear losses parameter (Schmid model)	p.u.
K_2	Joule losses parameter (Schmid model)	p.u.
k_c	Constancy index	p.u.
K_p	Proportional gain	p.u.
l	Loan maturity	%
LCOE	Levelized Cost of Energy	€/kWh
$LCOE_{CS}$	Levelized Cost of Energy of the current system	€/kWh
$LCOE_{PS}$	Levelized Cost of Energy of the previous system	€/kWh
$LCOE_{PV}$	Levelized Cost of Energy of PV	€/kWh
L_{EW}	Separation between rows of the PV generator in East-West direction	p.u.
L_{NS}	Separation between rows of the PV generator in North-South direction	p.u.
μ	Mean value	p.u.
NPV	Net Present Value	€

N_s	Number of PV modules in series	p.u.
σ	Standard deviation value	p.u.
$OPEX$	Operating expense	€
$OPEX_0$	Operating expense at year 0	€
P^*	Nominal power of the PV generator	kW
P^*_{1xh}	Peak power of 1xh	kW
p_1	Water pressure at the water outlet to the plants	m
p_2	Water pressure at the output of the pumps	m
P_{AC}	AC power	kW
PB	Payback period	year
P_{Δ}	Power of the Delta structure	kW
P_{MPP}^{Δ}	Maximum power of Delta with one MPPT	kW
P_E	Power of the East side of the Delta structure	kW
P_i	Power of the i side of the Delta structure (where i can be East or West)	kW
P_i^*	Peak power of the i side of the Delta structure (where i can be East or West)	kW
$P_{p=const}$	Constant PV power	kW
PE_n	Energy consumed by the diesel generator or the grid	kWh
PR	Performance Ratio	p.u.
PR_{PV}	PR considering only losses strictly associated with the PV system itself	p.u.
PVE_n	Energy that after the installation of the PV system is not consumed by the diesel generator	kWh
PVS	PV share	p.u.
PVS^H	PV share characteristic solely to the “Hybrid” mode	p.u.
P_W	Power of the West side of the Delta structure	kW
Q	Water flow	m^3/h
r	Real interest rate	%
s	Additional spread	%
S_n	Annual savings	€
T_C	Cell temperature	ºC
T_C^*	Cell temperature at Standard Test Conditions	ºC

T_{d}	Derivative time	s
T_{i}	Integral time	s
T_{Mm}	Maximum monthly mean ambient temperatures	ºC
T_{mm}	Minimum monthly mean ambient temperatures	ºC
UR_{EF}	Ratio of the irradiation required to keep P_{AC} stable during the irrigation scheduling to the same irradiation during the IP	p.u.
UR_{IP}	Ratio of the total irradiation throughout the irrigation period to the total annual irradiation	p.u.
UR_{PVIS}	Ratio of the irradiation strictly required to keep P_{AC} equal to the stable AC power requirement to the total irradiation throughout the IP	p.u.
V_{AC}	AC voltage	V
$V_{\mathrm{AC_{PUMP}}}$	AC voltage of the grid	V
$V_{\mathrm{AC_{PUMP}}}$	output AC voltage of the pump	V
$V_{\mathrm{DC_{BUS\_GRID}}}$	DC bus voltage established by the grid	V
$V_{\mathrm{DC_{BUS\_PUMP}}}$	DC bus voltage imposed by the pump	V
$V_{\mathrm{m}}^{\mathrm{diesel}}$	Water volume pumped by diesel	m^3
V_{MPP}	Maximum Power Point Voltage	V
V_{MPP}^{Δ}	Maximum power point voltage of the whole Delta structure	V
V_{MPP}^{i}	Maximum power point voltage of each side of the Delta structure (where i can be East or West)	V
V_{m}^{PV}	Water volume pumped by PV	m^3
V_{OC}	Open-circuit voltage	V
$V_{\mathrm{p=const}}$	Voltage at constant PV power	V
V_{t}	Thermal voltage of a PV module	V
$Water\ volume_{\mathrm{1xh}}$	Water volume of 1xh	m^3
WT_{day}	Daily working time	h

Abbreviations

AC	Alternate Current
DC	Direct Current
1xh	Single North-South horizontal axis tracker

BEP	Best Efficient Point
ΔS(60)	Delta structure
FAO	Food and Agriculture Organization (of the United Nations)
FC	Frequency Converter
FENACORE	Spanish Federation of Irrigation Communities
FENAREG	Portuguese Federation of Irrigation Associations
GTZ	German Cooperation Agency
IES-UPM	Solar Energy Institute, Universidad Politécnica de Madrid
IP	Irrigation Period
Ma	Marrakech
MASLOWATEN	MArket uptake of an innovative irrigation Solution based on LOW WATer-ENergy consumption
MP	Motor-pump
MPP	Maximum Power Point
MPPT	Maximum Power Point Tracking
PAEGC	Powering Agriculture: An Energy Grand Challenge for Development
PID	Porportional, Integral, Differential
PRODEEM	Program for Energy Development of States and Municipalities
PRS	Solar Regional Program
PV	Photovoltaics
PVGCS	PV Grid-Connected System
PVGIS	Photovoltaic Geographical Information System
PVIS	PV irrigation system
S(25)	Static structure oriented to the South and tilted 25º
STC	Standard Test Conditions
UAA	Utilized Agricultural Area
Vi	Villena

CHAPTER 1

INTRODUCTION

Photovoltaic (PV) electricity prices have declined below 0.1 €/kWh [1], which means that PV is currently able to compete with almost any other energy sources and in almost all scenarios. Therefore, the general problem of the PV engineering can be understood as the problem of adapting the particular characteristics of PV to a specific application.

This is well solved for two particular situations: grid-connected PV systems with low levels of PV penetration (that is currently the majority of the PV market, with 385.7 GW of installed capacity until 2017 [2]) – which has led, namely, to the inclusion of protections and support in the regulations of active and reactive power – and stand-alone PV systems – which include a battery to cover the deficits of radiation.

Currently, PV systems are also becoming more attractive to the market of large-power irrigation systems since energy is a key input for irrigation services.

According to the Food and Agriculture Organization of the United Nations (FAO) the food needed in 2050 to feed the rising world population will be 60% higher than the one in 2015 [3]. This increase in food production will only be possible with an increase of the irrigated land.

Worldwide, irrigation needs vary with water availability, climate, topography and geology. The structure of irrigation is also affected by regional activities, infrastructures and social customs [4]. In 2007, according to Schoengold & Zilberman in [5], irrigation systems represented 20% of agricultural land worldwide, 40% of the world food by volume and more than 50% of the value of agricultural production.

Water is a critical asset for the competitiveness of the agricultural sector – 1 ha of irrigated land produces 5 to 6 times more than 1 ha of dry land [6], [7]. [8]. Accordingly, agriculture is a high water consuming sector [9] – currently, agriculture consumes around 70% of the freshwater demand in the world; in 2012, it accounted for around 33% of total water use in Europe, reaching up to 80% in a significant part of southern Europe [10]; in 2000 it was responsible for around 30% of total water use in Europe (in the southern countries this value was over 60% and in the northern ones it varied from almost zero to over 30% [11]).

Southern European countries rely heavily upon irrigation for their crop production [10] and therefore water becomes a limiting factor. In fact, the irregularity and unpredictability of rain forces irrigation [6] and it is also a way to mitigate the adverse effects of climate change [6]. Moreover, agriculture employed a high percentage of the economically active population [6] (e.g., in 2010, 9.8 % in Spain [12], 13.5% in Portugal [13]). On the other hand, in more humid and low-temperature areas, irrigation is a way both to increase and stabilize the farmer incomes (irrigation reduces the risks in case of low rainfall or droughts) [10].

The distribution of irrigated land in Europe, in 2013, can be seen in Figure 1 [14]. As expected, the highest share of irrigated land is located in southern Europe. The national values of the irrigated area as a percentage of the utilized agricultural area (UAA) in these countries was 34.4% in Greece, 33.6% in Malta, 24.3% in Italy, 22.6% in Cyprus, 13.5% in Portugal and 13.4% in Spain. Even so, Spain had, in absolute terms, the largest area of irrigated land in Europe, with 2.9 million ha. The mean value across the 28 countries of the European Union was 6.2% [15].

For instance, in Spain, in 2010, the UAA represented 47% of the country area (23.7 million ha) and the average size of farms was 24 ha. Even so, 50% of the farms had less than 5 ha (occupied less than 5% of the national UAA) and 5% of the farms had 100 ha or more (represented 55% of the UAA and accounted for 63% of the total standard output, which is the average monetary value of the agricultural output at farm-gate price, in €/ha). Nevertheless, it is interesting to note that there was a tendency towards the increase of large farms. The irrigable area was 15% of the UAA and the average water consumption was 5470 m^3/ha [12]. Currently, the irrigated land in Spain occupies 22% of the UAA, which means 3.7 million ha [16]. According to Abadía cited in [17], the average contracted power in Spain is 2 kW/ha. This means that a farm of 100 ha or more needs 200 kW or more.

In Portugal, also in 2010, the UAA represented 40% of the country area. A tendency towards the disappearance of small farms in favor of the bigger ones also occurred in this country. Nevertheless, the average size of the farms was 12 ha, with 50% of the farms with less than 2 ha and only 2% with 50 ha or more. These last ones occupied 58% of the national UAA and represented 23.7% of the total standard output of the country. The irrigable area was 14% of the UAA [13].

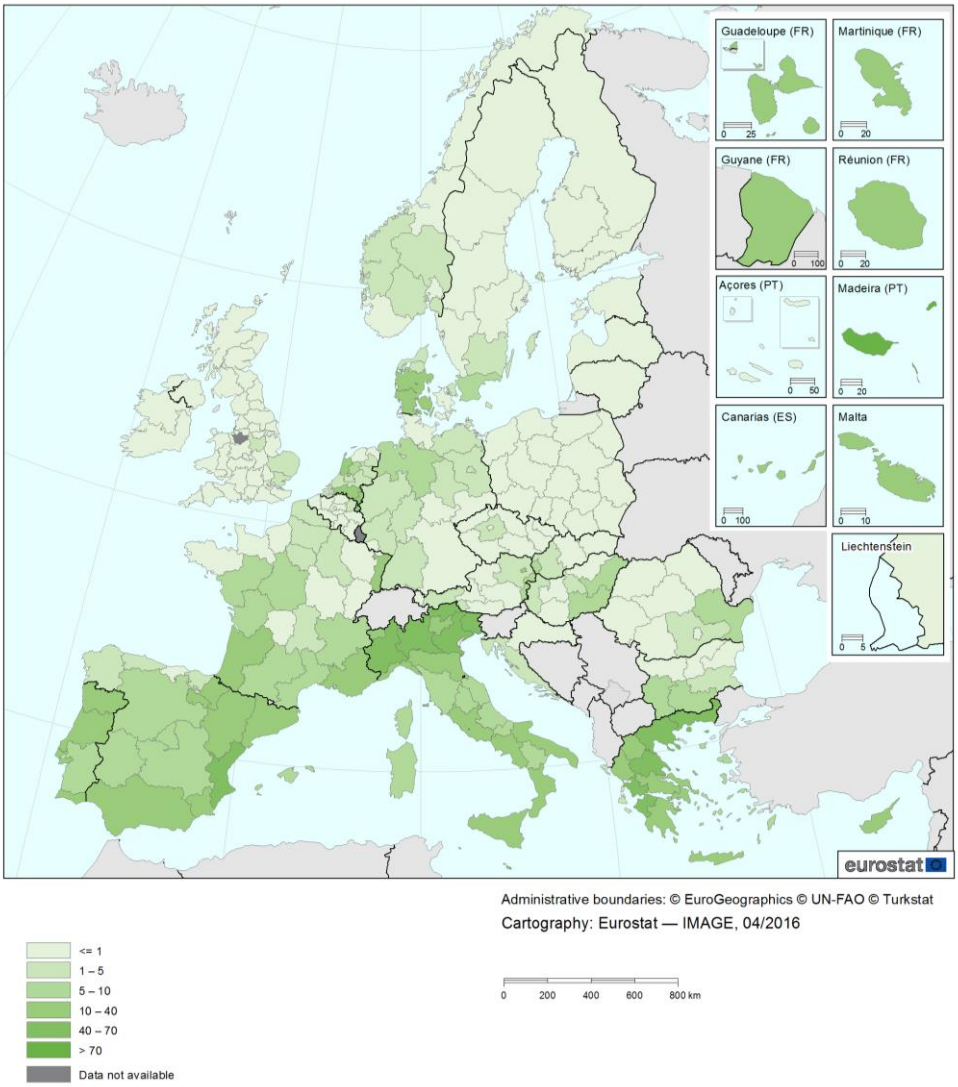

Figure 1 – Percentage of the irrigated areas regarding the utilized agricultural area (UAA) [%] in 2013 [14].

Traditionally, most of the irrigation in Europe has consisted of open-channel gravity-based system that consumes a huge amount of water and almost zero energy [11]. More efficient irrigation systems are being implemented within Europe through the change from this kind of systems to pressurized networks (in which water consumption is reduced at the price of increasing energy use) [9], [6], [7], [10]. Spain is the best representative example of this modernization. According to FENACORE (the Spanish Federation of Irrigation Communities), from 2000 to 2016 the share of gravity-based systems decreased from 59% to 27%, while the share of drip systems increased from 17% to 49% [18].

It can be concluded that this modernization has not only increased the water efficiency and productivity but has also improved the operation and maintenance of the irrigation systems and enhanced the working conditions of the farmers [7]. Even so, it also increased both the investment and energy demand [7]. It follows that higher energy costs are currently observed

in the farms. Hence, farmers are looking for solutions to reduce these costs and ensure the profitability of their farms [9].

The share of energy used in the World, Europe, southern Europe and southern European countries in agriculture and forestry in 2011 is revealed in Figure 2 (data obtained from FAO [19]). As expected, the highest share is verified in the southern Europe region, 2.60%.

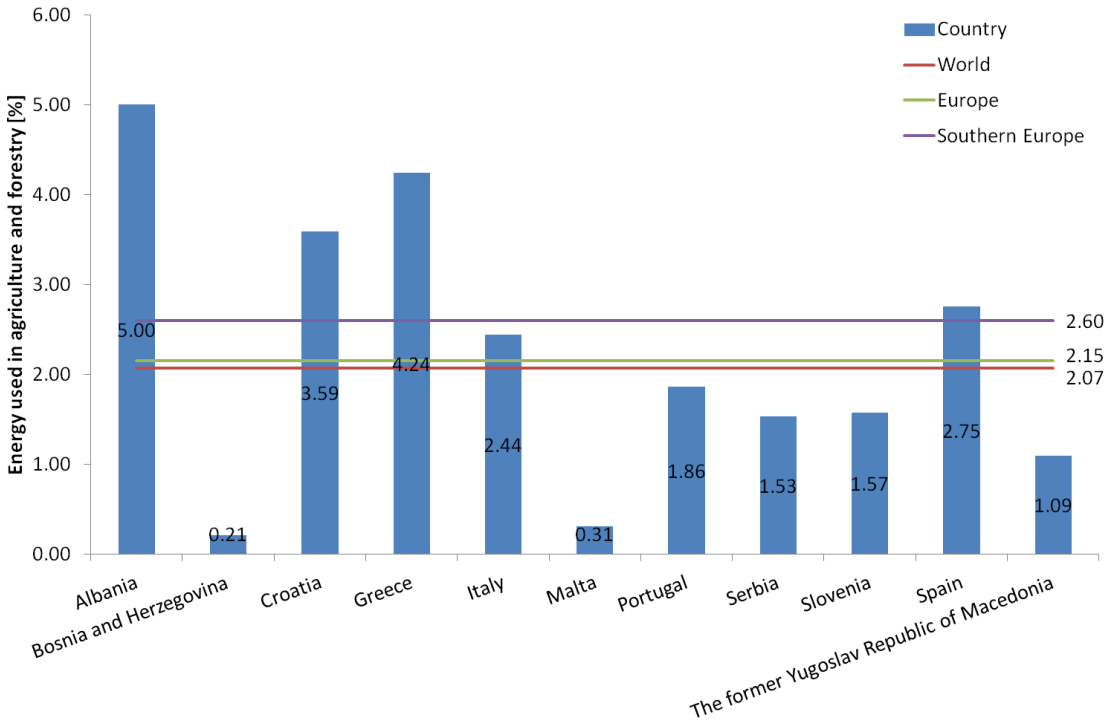

Figure 2 – Percentage of the energy used in agriculture and forestry in the World, Europe, southern Europe and southern European countries in 2011 (it includes, but it is not limited to, the energy needed to irrigate) [19].

If ones focus again in the case of Spain, in 2011, 2.75% of the national energy was used in agriculture and forestry (see Figure 2). Later, in 2016, 2.5% of the total electricity consumption was in the category "agriculture, livestock, forestry, hunting and fisheries" [20]. It is important to mention that these previous values included, but are not limited to, irrigation. Currently, and according to estimations done by FENACORE, irrigation accounts for 2.1-2.2% of the national electricity consumption.

Still, in Spain, the energy consumption to irrigate increased 1800% from 1950 to 2010, while the water used decreased by 21% [21]. According to the Spanish National Institute of Statistics cited in [7], the energy consumed for irrigation has increased 70% from 1996 to 2011 (2136 GWh in 1996 to 3647 GWh in 2011). In Portugal, the energy consumption to irrigate increased 665% from 1960 to 2014 (from 200 kWh/ha to 1534 kWh/ha respectively) [6].

Moreover, the increase in energy prices is also negatively affecting the feasibility of agriculture in southern Europe [22], [23]. In Spain, the price of energy for irrigation has risen due to the liberalization of the electricity market in 2003 and the elimination of special irrigation rates in 2008 [9]. According to FENACORE, the price of electricity for the Irrigator Communities increased 1250% from 2008 to 2013 [24]. Similarly, in Portugal, the electricity market was also liberalized, the seasonal electricity contracts were eliminated in 1983 and a 40% discount and a program called "Green Electricity" ended in 2005 [25]. From 1999 to 2014, the energy part of the electricity bill increased by 25% [25].

In Spain, the average price of the power term alone increased by 288% from 2008 to 2014 [9]. In Portugal, from 1999 to 2014, the electricity tariffs just for using the system increased 773% [25]. Currently, the high tariffs of the fixed terms of the electricity bill (which need to be paid for the 12 months of the year even if the system is used only during 6) represent 20 to 30% of the electricity bill in Portugal [6]. The seasonal profile of irrigation is reflected in electricity consumption. For instance, in Portugal, a study performed by FENAREG (the Portuguese Federation of Irrigation Associations), in partnership with IMValores sv and Green Egg, found that 90% of the annual electricity consumption in irrigation is between April and September (with July and August being responsible for 61%) [6].

Following the tendency towards the increase of large farms, large powers are currently needed. Furthermore, given the modernization of agriculture in southern Europe, greater energy consumption and hence higher energy costs are becoming a critical matter in this region. Accordingly, productive agriculture needs to decrease its costs in order to guarantee the sustainability of the sector and to allow competitiveness.

As pointed out in [8], research and development projects are needed to promote the use of stand-alone PV systems for irrigation both for communities of irrigators and private farms. According to FENAREG, the current biggest challenge in the agricultural sector is to reduce the energy bill associated with water pumping [26]. Three solutions are proposed by FENAREG: the return to seasonal contracted power tariffs, the real liberalization of the electricity market, and a national program to implement renewable energy systems [27]. In what concerns this last recommendation, FENAREG appealed to the Portuguese Government, in May 2018, to create specific support to the installation of PV systems in the public irrigation sector (for example, through the Common Agricultural Policy or the PDR2020) [26]. FENAREG considers that PV can contribute to the reduction of the irrigation costs [26].

In this framework, the end-users (farmers, agro-industries and irrigator communities) are seeking for alternatives to their conventional energy sources (national grid and diesel generators [28]) that satisfy their needs of large power at reasonable costs. According to [5] there is the need to develop technologies to decrease the cost of groundwater abstractions in order to face the effects of rising energy prices. Moreover, in [7], authors said that it is necessary to analyze the application of wind and PV for medium and large size farms since renewable energy systems, mainly solar, are only used in small farms with small water requirements (not exceeding 10 kW).

Furthermore, it can be pointed out that in 2014 electric irrigation pumps consumed around 62 TWh worldwide [29], with the southern Europe representing almost 40% of this consumption [30], which means a potential market of 16 GWp of PV irrigation systems in this region [31].

Likewise, the north of Africa is also a very interesting market. For instance, in Morocco, in 2011, irrigated land represented 5% of the UAA [32] and, in 2009, 15% of the energy consumed in the country was devoted to agriculture and forestry [19]. According to the Ministry of Energy, Mines, Water and Environment, cited in [31], the annual electric consumption in this region is estimated to yield 2500 GWh, which leads to a potential market of PV irrigation system of 1.5 GWp.

Large-power PV irrigation systems are thus becoming more attractive to overcome the problem of increasing energy consumption and electricity costs. Hence, this thesis intends to adapt the characteristics of large-power PV generators to the need for irrigation of modernized agriculture.

1.1 Brief summary of the historical milestones in photovoltaic pumping

The history of PV water pumping systems begins in 1973, when Dominique Campana attended UNESCO's solar summit in Paris [33]. After this, she thought about using PV to pump water. So, in the mid-1970s she coordinated the installation of the first PV water pumping system. This system was installed in Corsica, France, and included a Guinard DC pump fed by Philips PV modules [33], [34].

Father Bernard Vespieren was one of the first visitors of this system. At that time, he had a Non-Governmental Organization in Mali, called “Mali Aqua Viva”, which, among other things, supported the installation of hand pumps for drinking water. Excited with the good

performance of the solar pump in Corsica [31], he introduced the first PV pump in Africa in 1977 [34].

After these first experiences, many other PV pumping programs were developed. In 1978, Newkirk, according to [35], did a bibliography of the published material on PV water pumping systems. He found 7 publications about systems in the Soviet Union, 2 in France, 1 in Germany and 3 in the USA. The ones outside the USA had peak powers ranging from 300 Wp to 1 kWp. Regarding the ones in the USA, detailed information was only available for a 25 kWp system feeding a 7.5 kW pump for 12 hours a day in the months of July and August. It was installed in the summer of 1977 in Nebraska, sponsored by the United States Department of Energy.

Between 1979 and 1981, the United Nations Development Program, with the support of the World Bank and the Intermediate Technology Development Group, implemented a pilot project to test and evaluate PV pumping systems with powers ranging from 100 to 300 Wp used in small-scale irrigation systems in Mali, Philippines and Sudan [36]. A great potential was found but none of the products were approved to large-scale deployment. An improvement in the reliability and a cost reduction (the PV modules price was about 16 USD/Wp in 1978 [37]) were recommended as a result of the project [38]. Between 1977 and 1990 around 200 systems were installed in Mali, with a total installed power of 220 kWp [34], [38].

Following the experience in Mali, the countries of the Permanent Interstate Committee for Drought Control in Sahel (Burkina Faso, Cape Verde, Chad, Gambia, Guinea-Bissau, Mauritania, Nigeria, and Senegal), in cooperation with the European Commission, launched the Solar Regional Program (PRS) in the early 1990s [39]. The main objective of this project was to improve the water access to the population (both in quantity and quality), as well as improving their economic conditions through the irrigation of vegetables and fruit trees [38], [39]. This project allowed the installation of 1040 systems, with a total PV power of 1.3 MWp [38], [39].

This program was the first one in the PV pumping field which included technical specifications and quality control procedures [38]. For this reason, these systems presented lower failures rates but these procedures only went from the borehole to the entry of the water pool. Some problems occurred in the distribution networks and the main lesson learned was that every component of the whole system should be carefully tested [38].

Also in the early 1990s, from 1990 to 1994, the German Cooperation Agency (GTZ), in partnership with the local governments, developed the "PVP Program" with the objective of demonstrating the maturity of the technology and its real costs. The program installed 90 PV pumping systems, with a total power of 180 kWp, in Argentina, Brazil, Indonesia, Jordan, Philippines, Tunisia and Zimbabwe (according to Anhalt, cited in [38]).

During the 1990s some other national projects arose. As an example, in 1993, India had the largest number of solar pumps in the world, with more than 1000 systems for village water supplies [34]. In Morocco, more than 100 PV pumps had been installed by the Ministry of the Interior, while it was estimated that around 100 more had been installed privately [34]. Moreover, in Brazil, the Program for Energy Development of States and Municipalities (PRODEEM), established by the Brazilian Federal Government in December 1994 to install mainly PV systems, carried out 6 International Biddings since May 1996. Along the six phases, almost 2500 PV water pumping systems were installed, with a total power of 1.4 MWp (Figure 3 shows one of these systems). The main objective of this project was to supply water mainly for human consumption but also for animals and small-scale irrigation [40]. A couple of studies identified some drawbacks of this program such as the delay in the implementation of the systems, the poor technical assistance and the lack of participation of the end-users [41]. In addition, according to [41], an analysis in the Northeast region showed that from the 801 installed systems, 18% presented problems in the controllers/inverters and 25% in the helical pumps. Still in the Northeast region, in Petrolina, the city hall evaluated 30 PV pumping systems of this project [42]. This evaluation was done in 2002-2003 and, according to Petrolina (2002) cited in [39], only 65.6% of the systems were still working, 20.7% were broken or were not in use and the remaining 13.7% had been stolen. In January 2005, a new inspection was done and, according to Borges Neto (2005) cited in [39], only 4 of the initial 30 systems were still in operation.

Figure 3 – PV pumping system for irrigation in Capim Grosso, Brazil [43].

Finally, in Mexico, between 1994 and 2000, 206 PV water pumping pilot systems (with a total power of 101 kW and benefiting around 10000 people) were installed in the framework of the Mexican Renewable Energy Program [44]. From July 2003 to March 2004 a survey was carried out in 46 of these systems. Results demonstrated that 26 systems had presented failures in some of the components, from which 8 had been replaced and the systems continue to work. Accordingly, 18 systems were not working. As in the PRODEEM, most failures occurred in the pumps. According to [44], 54% of the problems were related to the pumps, 21% to the controllers/inverters, 17% to borehole-related issues and 8% of the systems were dismantled.

Figure 4 – Engineer conducting performance evaluation after 8 years of operation in Chihuahua, Mexico [44].

The project "Implementation of a PV water pumping program in the Mediterranean countries", developed under the MEDA program (a cooperation program supported by the European Union) in the beginning of the 2000s, also deserves attention. Fifty-two PV water pumping systems were installed: 10 in Algeria, 29 in Morocco and 13 in Tunisia (with a total power of 59, 138.7 and 58.3 kWp respectively) [45]. In this project, four standardized services were proposed in order to allow a higher quality control procedure: 850, 1750, 2600 and 5500 m^4/day [46]. Before the beginning of this project, a few other systems had been

installed in Morocco [47]. It is remarkable that the development of a professionalized structure allowed its maintenance along 12 years [47]. Once more, the majority of the failures was not related to the PV components but with the lack of water in the boreholes.

The technological evolution in these programs went from dedicated inverters and centrifugal pumps specifically dedicated to PV applications to both standard frequency converters and AC centrifugal pumps [48]. This contributed to an increase in the reliability and efficiency of the systems due to the use of well-proven components. Since this equipment was extensively used in industrial applications, a decrease in price was also verified and the availability of spare parts and the access to maintenance tasks significantly improved.

The year 2009 can be seen as a turning point for PV irrigation because the PV modules cost decreased dramatically [1] and, as a consequence, PV systems become affordable for the agriculture sector in general [49] and for PV irrigation systems in particular [50], [51], [52], [53]. Although technical problems associated with the greater power required for agricultural irrigation limited their introduction into the market, this market becomes extremely interesting.

1.1.1 PV water pumping systems for irrigation

Although the first projects of PV water pumping systems were mainly devoted to drinkable water to the populations, there were some cases of systems applied to irrigation worldwide [36], [38]. According to [34], the predominance of drinkable water supply was due not only to the smaller water quantities needed in drinking water but also due to the high social value of domestic water when compared to the one for irrigation.

A PV water pumping system for irrigation is commonly made up of a PV generator, a frequency converter (FC), a standard centrifugal pump and a water tank and/ or an irrigation network (Figure 5) [48] and usually requires more power than a PV pumping system for drinkable water. A PID (Proportional, Integral, Differential) algorithm for motor control (implemented in the FC) automatically adjusts the output voltage and frequency to the PV DC power available [54], [55]. A maximum power point tracking algorithm is usually included in order to maximize the PV energy production [49], [56], [57].

These systems can be classified into two types: pumping to a water pool (at a variable pressure and water flow) from where irrigation is done by gravity and direct pumping (with constant pressure and water flow for each irrigation sector usually through drippers).

Regarding their energy source, they can be stand-alone or hybrid depending, among others, on the number of irrigation hours per day.

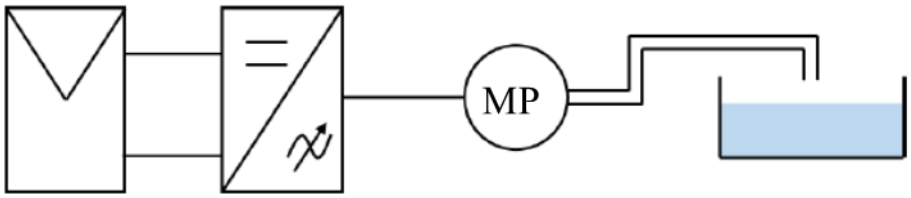

Figure 5 – Components of a PV irrigation system: PV generator, frequency converter, motor-pump and water tank.

From 1980 to 2000, most of the publications were focused on the economic feasibility of PV water pumping systems for irrigation, forgetting the technical barriers to satisfy the needs of professional farmers. One of the reasons for this economic concern was the almost constant need for drinkable water throughout the year, which does not happen with the water for irrigation. In this last case, a large variation from month to month is usually observed (and may be null in some periods) [34], [36]. The main consequence of this is that the system will be oversized in some months of the year, endangering its economic feasibility.

In 1993, according to [34], and considering economic factors, the use of water for irrigation was only possible if the water was at very low heads or if it was surface water. Accordingly, the maximum area possible to irrigate with PV was less than about 1 ha. Later, in 2000, Campen was still recording that the use of PV in irrigation systems was limited to low-power systems [39]. In 2006, Odeh made a study on the economic viability of PV water pumping systems and found out that systems up to 11 kWp were becoming feasible and could be a profitable investment [58].

In the last few years, a huge amount of national and international programs were launched to promote PV water pumping systems for irrigation. For example, 2016 IRENA report on Solar Pumping for Irrigation [59] mentions three of them: India pretends to install 100000 PV pumps by 2020 (an Indian system can be seen in Figure 6), Morocco 100000 by 2022, and Bangladesh 50000 by 2025. For instance, in India, the fuel prices have increased by more than 250% since 2000, which leads the Government of India to support and promote solar pumping systems [60]. Even so, according to [60], the most available commercial pumps underperform in the field (due to poor design, low efficient and mismatch of components).

Figure 6 – Solar water pump in India (photograph from Raghav Agarwal, [59]**).**

Finally, an international big project also deserves attention: Powering Agriculture: An Energy Grand Challenge for Development (PAEGC). It was launched in 2012 by the United States Agency for International Development, the Swedish International Development Cooperation Agency, the German Federal Ministry for Economic Cooperation and Development, the Duke Energy, and the Overseas Private Investment Corporation, to provide technical support, business acceleration, financing support and policy support to farmers in low-income countries [61]. It is a project devoted to all kind of support in what concerns the energy-water-food nexus in these countries. Accordingly, it includes, but it is not limited to, low-power PV water pumping systems for irrigation.

Lastly, it is important to underline that the last reviews published about PV water pumping systems (including PV water pumping systems for irrigation) are still reporting only small-power systems [57], [62], [63], [64]. For example, the largest system presented in the review of Wazed has 11 kWp [63], while the largest one in the Sontake review has 15 kWp [64]. In [31], a 20 kWp system in Tizi (Morocco) is described (see Figure 7). Therefore, it can be said that the experience in PV water pumping systems for irrigation is limited to low-power [31].

Figure 7 – PV irrigation system in Tizi, Morocco [31].

1.2 Limitations of PV irrigation technology in the current state of the art and the MASLOWATEN project

The current state of the art of PV water pumping systems for irrigation is limited to 20 kWp due to technical, economic and social aspects that hamper extent to greater powers. Hereinafter, we will adopt the nomenclature "PV pumping systems for irrigation" for the low-power systems and "PV irrigation systems" for the larger-power ones (PVIS).

In what concerns the technical limitations, the most relevant issues are:

- Problems associated with PV-power intermittences.

  The frequency converters adjust both the output voltage and the frequency to the PV-power available which, in turn, depends on the in-plane incident irradiance. Two types of PV-power variations affect the system performance: the variation throughout the day that can be calculated mathematically and the variation due to passing clouds that occurs in a random way [31], [65], [66], [22].

  This latter variation is essential to the reliability of large-power PVIS [67]. In fact, the quick intermittence of PV power due to the passing of clouds (up to 80% of PV-power variation in one minute [68]) can translate into control instabilities leading to a sudden motor shutdown encompassing water hammer and AC overvoltage that seriously threaten the integrity of both the hydraulic and electric components [31], [69]. Particularly, the deep boreholes and large water flows lead to strong water hammers which can damage or decrease the lifetime of the hydraulic components of the system [31]. On the other hand, the electric components can be damaged due to the overvoltage caused both by the abrupt stop of the FC and the long length of the wires between the FC and the motor-pump.

- The need to match PV production and irrigation needs of the farmer.

  The PV energy, the availability of water in the source and the water needs of each particular crop change throughout the year [34], [36]. As pointed out in [70], when designing a PV irrigation system, both solar energy and water resources should be taken into account. In the same way, the yearly production of the PV generator should be as similar as possible to the yearly profile of water demand. Since the water pumped should be adapted to the needs of the crop, which is normally high in summer

months and null in winter months, it is good news that the water requirement is higher when more solar energy is available [36], [71], [72].

In what concerns the intra-daily variations, this match of PV production and irrigation needs is also crucial. A constant profile of water flow is required (which means that a constant profile of PV power should be achieved) both in pumping to a water pool and direct pumping systems. In the first case, the borehole should not be stressed out with peaks of water flow. In direct pumping, that requires constant pressure and water flow and, therefore, constant power, this constancy is even more important. It is easy to understand that the typical static structure oriented to the Equator does not fulfill this requirement.

- The difficulty in the integration of the PV system in the pre-existing irrigation systems that are very diverse.

  A significant part of the potential PV irrigation market will be the retrofitting of already existing irrigation systems fed by the national grid or diesel generators [73]. This suggests that the characteristics of the pre-existing irrigation system need to be studied in detail to adapt the PV system to it. It seems easy but it is not since it requires a deep knowledge of the previously installed irrigation system, namely its irrigation network, motor-pumps, power source, irrigation automatism (if any), irrigation scheduling, and type of irrigation: to a water pool or direct pumping (through drippers, sprinklers or pivots). Moreover, it is also critical to know possible restrictions and irrigation scheduling. There are some irrigation networks that force irrigation during the night since the needed number of irrigation hours is higher than the number of sun hours.

  Furthermore, an irrigation controller that executes the irrigation programs according to the irrigator operator desire is usually presented in the pre-existing irrigation system. However, when integrating the PVIS, if the irrigator operator wants to irrigate, the system will only work if there is enough PV-power available to run the pump. Accordingly, it is easy to understand that it is necessary that the PV controller sends this information to the irrigation controller. This integration would be also very useful to the irrigator operator since he would be able to continue with his habits of just programming the irrigation controller.

- The tuning of the frequency converter.

  The plug and play PV pumping systems available for low-power needs do not work for large-power PVIS. This happens because the PID controller of the frequency converter is affected by the characteristics of the hydraulic system and cannot be tuned in the factory but on-site. Therefore, in large-power PVIS it is necessary to tune the PID controller once the PVIS has been installed.

In addition to the technical issues, some economic and social aspects also appear:

- The high initial investment cost (which means that if there is not an appropriate financing mechanism available it is hard to install the system).
- The low confidence of the end-user on the reliability of a new technology such as PVIS.
- The pre-conceived idea of the end-users that PV only works for low-power applications and that the land surface needed to install the PV generator is too much.

MASLOWATEN, a H2020 European Project for the market uptake of large-power PVIS that lasted from September 2015 to August 2018 [74] faced these limitations. The project included the design, installation and operation of 5 real-scale large-power demonstrators with powers from 40 to 360 kWp working in real facilities of farmers, cooperatives, agro-industries and irrigator communities to show their reliability and economic feasibility. The final goal was to introduce them to the market. The demonstrators cover the different possible configurations of the irrigation systems: water pumping to a pool at a variable water flow and direct pumping to the irrigation network through sprinklers, pivots or drip systems at a constant pressure and water flow; powered by stand-alone PV systems or hybrid systems combining PV with the grid or with diesel generators. The project considered also the development of the needed tools for the bankability and market uptake of PVIS: technical specifications [50] and quality control procedures, a simulation tool [75] and business plans. MASLOWATEN also transferred the technology to 27 European small and medium enterprises, typically, installers that are close to the farmers.

This thesis has been developed in the framework of MASLOWATEN project and, specifically, in the aspects related to large-power hybrid PVIS.

1.3 The need for hybrid systems

The hybrid solutions are imperative in a variety of situations. First, if the irrigation network requires more irrigation hours than those available with PV (usually due to the diameter of the pre-existing tubes), a hybrid system is indispensable because otherwise, the system will not be able to deliver the water needed by the crop. So, in this case, the main purpose of the hybrid system is to cover the night demand.

Second, when there are peaks of irrigation in some periods, one possibility is to oversize the PV generator [76], although this may not be the most economical solution and a hybrid system should be considered [49]. It must be pointed out that a diesel generator can be rented for only one month (instead of doing it along the whole irrigation period). In this case, the main purpose of the hybrid system is a response to the peak consumption.

Third, a hybrid system can be installed only to get the irrigator operator confidence in the PV system. In this case, the hybrid was not strictly needed in terms of energy consumption but can act as a backup system. An important aspect that should be considered in these situations is the possible rebound effect in water consumption. Since electricity during the day tends to be free, the irrigator operator can think about using the amount of money saved to increase their irrigation hours and start irrigating during night-time, which will lead to a rise in both energy and water consumption. The control of the water consumption by water authorities would avoid this problem but it is surprising that the use of water meters to account the volume of water used is not usual [77], [78].

Finally, since PV power is variable in time [22], [65], [66], the use of hybrid systems can also be a possible strategy to solve the problems associated to the PV-power intermittences.

The use of hybrid PV systems has the advantage of improving the reliability of the system [66], [76], increase the efficiency in power use, decrease energy costs and emissions [66]. Furthermore, in [73], it is mentioned that a hybrid system may be a cost-effective solution for large-power PVIS, particularly if diesel generator or grid electricity are already being used.

1.4 Objectives and main contributions of this thesis

The objective of this thesis is the **development of technical solutions** for the reliable and efficient performance of **large-power hybrid PV irrigation systems**.

These technical solutions have been applied in the design and implementation of two real-scale large-power PVIS:

- A 140 kWp hybrid PV-diesel drip irrigation system in Portugal in a super-intensive olive plantation of 195 ha;
- A 120 kWp hybrid PV-grid drip irrigation system in Morocco in an intensive olive trees farm of 233 ha.

Both systems differentiate in the type of hybridization – while in Portugal the hybridization is carried out in the hydraulic part of the system, in Morocco the PV and the grid are electrically hybridized.

The technical solutions provided by this thesis tackle the aforementioned limitations and are the following:

- The problems associated with PV-power intermittences.

  Instabilities have been addressed by specific FC control algorithms. These procedures, applied to the large-power hybrid PVIS of Portugal, take advantage of the possibility of power regeneration of the centrifugal pumps and have been patented [79]. This way, instead of a sudden stop of the motor-pump, its frequency is reduced but the motor-pump does not stop. It is easy to understand that this procedure does not eliminate the PV-power variability, but it removes the problems associated with it [31]. Furthermore, it is important to mention that the use of batteries was not considered as an option to solve this problem because of reliability and economic feasibility reasons.

  In the case of the hybrid PVIS of Morocco, this limitation is directly solved due to the electric hybridization of the system.

- The match between PV production and irrigation needs.

  The use of a North-South horizontal axis tracker was the solution adopted in both systems. This is very interesting both for pumping to a water pool or direct pumping. It presents four main advantages: it maximizes the water pumped during the irrigation period (the match between the yearly water demand of the crops and the yearly profile of irradiance is very good, much better than with the typical static structure facing the Equator [80]); the daily profile of irradiance is almost flat in this type of tracker during the irrigation months [80], [81]; it allows the enlargement of the irrigation hours per day when compared to the typical static structure facing the Equator (the system will start pumping earlier in the morning and will keep working until later in the afternoon, [31], [49], [80]); and it requires less nominal power to pump the same water volume than PV static structures [31], [80]. Apart from technical considerations, an economic analysis with current prices shows that the installed tracker prices are below 0.2 €/Wp [82], while PV module prices are around 0.4 €/Wp [83], [84] which means that the selection of the tracker should be made if one considers the total costs of the system [31].

- The integration of the PV system in the pre-existing irrigation system.

  One of the PVIS was integrated into a pre-existing only-diesel system in Portugal, while the other was integrated into a pre-existing only-grid system (the one in Morocco). In both cases, the already existing irrigation infrastructure and the irrigation scheduling were kept.

  In the case of Portugal, the hybrid system was needed in order to fulfill the irrigation needs of the farm. The daily irrigation hours during the summer months are as high as 17 hours, more than the sun hours. Moreover, the introduction of the PV generator in the irrigation system might also lead to the possibility of reducing the number of months of renting the diesel generator, which will obviously translate into additional financial benefits.

  Conversely, the system of Morocco is a hybrid one due to the end-user desire – this occurs since this system belongs to a big agro-industry that wants to guarantee that the pumps will run whenever they want. If the use of the PV system is maximized by the end-user, the grid will only work as a back-up.

- The tuning of the FCs.

  Specific tuning procedures have been developed to adapt the PID control of the FC to the characteristics of the pre-existing irrigation system. These procedures consisted in three main steps: preliminary configuration, the definition of the proportional gain (K_p), and the integral time (T_i). The derivative time (T_d) is usually unfeasible (and not used) due the high electrical noise presented in this type of systems.

  These procedures have been applied to the tuning of the FCs of the two demonstrators and their correct performance has been checked in commissioning tests and through the monitoring data during two years of operation.

Both systems have been working since 2016 and two years of monitoring data have been analyzed in this thesis. To appropriately evaluate the performance of the systems new performance indices have been proposed and, based on them, the technical and economic evaluation is presented.

This analysis is included in the first part of this document. Chapter 2 presents the design, implementation and evaluation of the hybrid PV-diesel drip irrigation system in Portugal, while chapter 3 presents the results of the hybrid PV-grid drip irrigation system in Morocco.

Furthermore, the second part of this document deals with other contributions to the design of large-power PVIS:

- a new type of PV generator structure – the Delta structure – that provides constant PV profiles but with static structures (chapter 4);
- an evaluation of the PV energy losses due to the limitation of the number of PV modules in series in PVIS (chapter 5);
- a new pump selection method for PV irrigation applications, which considers that these systems work at a variable frequency (chapter 6).

Finally, conclusions and future research lines are presented in chapter 7, and the publications elaborated in the framework of this thesis in chapter 8.

FIRST PART: DESIGN, IMPLEMENTATION AND PERFORMANCE ANALYSIS OF HYBRID PV IRRIGATION SYSTEMS

The first part of this thesis describes the design, implementation and performance analysis of two real-scale large-power drip irrigation systems:

1) A 140 kWp hybrid PV-diesel system in Portugal (with hybridization in the hydraulic part);
2) A 120 kWp hybrid PV-grid system in Morocco (with hybridization in the electric part).

Both systems were designed to maximize the use of PV energy and the two hybridizations were patented [85], [86].

CHAPTER 2

A 140 KWP HYBRID PV-DIESEL IRRIGATION SYSTEM IN PORTUGAL

2.1 Introduction

Diesel generation typically supplies electricity at about 3.5 kWh per liter, which represents a fuel consumption cost of around 0.3 €/kWh. Meanwhile, PV electricity prices have declined below 0.1 €/kWh [1]. Thus, PV hybridization with pre-existing diesel based irrigation systems is becoming increasingly attractive, as pointed out by several authors [28], [59], [87], [88].

This chapter describes the design, implementation and operational performance of a 140 kWp hybrid PV-diesel installed in Alter do Chão (Portugal) for the drip irrigation of 195 ha of super-intensive olive trees. This system belongs to ELAIA, which is part of Sovena Group, one of the biggest producers of olive oil in the world.

The design has paid attention to the problem of integrating the novelty of PV into the existing diesel system. Furthermore, an important consideration is that, apart from the technical quality of the components, the performance of the PV system is not only affected by intrinsic-to-design characteristics (for example, pumping at a given head requires the irradiance to be higher than a certain threshold, which implies corresponding irradiation losses) but also by circumstances external to the system. In fact, the PV system only works when water is both available at the source and required by the plants. The corresponding useful period (and, again, corresponding irradiation losses) substantially varies from case to case and from year to year. This chapter also proposes new performance indices for distinguishing between PV system quality and PV system use.

This chapter is structured as follows: section 2.2 includes a description of the Alter do Chão irrigation system, both the pre-existing only-diesel system and the current hybrid PV-diesel system. Section 2.3 is dedicated to the presentation of performance indices for hybrid PV systems. Section 2.4 is about the in-the-field performance of the system, during the irrigation campaigns of 2017 and 2018. The economical validation is detailed in section 2.5.

2.2 The Alter do Chão irrigation system

2.2.1 The pre-existing only-diesel system

The yearly and daily evolution of the electric power requirements of the irrigation system need to be deeply understood to afford the PV system design. The pre-existing system, Figure 8 (a), was made up of two centrifugal pumps (Caprari MEC-MRS 100-2D 45 kW) fueled by a 250 kVA diesel generator through a soft-starter and a 55 kW FC. The first pump is always kept at nominal frequency (50 Hz) while the second one is controlled by the FC in such a way that the water pressure at the water outlet to the plants, p_1, is kept constant at 5.7 bar. Since the water filter at the input of the irrigation network is progressively becoming clogged with water impurities, the pressure at the output of the pumps, p_2, and, in turn, the AC power demand, P_{AC}, increases over time. There is also a filter cleaning device (fcd) that automatically reverses the water flow (from the output to the input of the filter) when the differential pressure at the filter, p_2-p_1, reaches 1 bar until the filter becomes clean. That typically happens once an hour and takes 5 minutes. During such short cleaning periods, the p_1 suddenly decreases (because water is used for cleaning and not to irrigate the plants) and, consequently P_{AC} increases up to a certain limit imposed by the FC. Figure 8 (b) shows this cycling evolution of p_1, p_2 and P_{AC}. In addition, the system also includes a fertirrigation device which is not included in Figure 8(a).

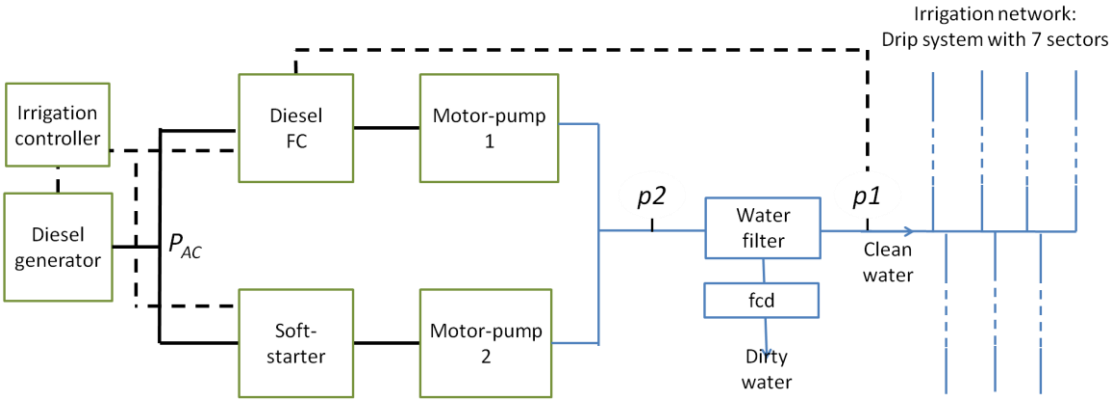

(a)

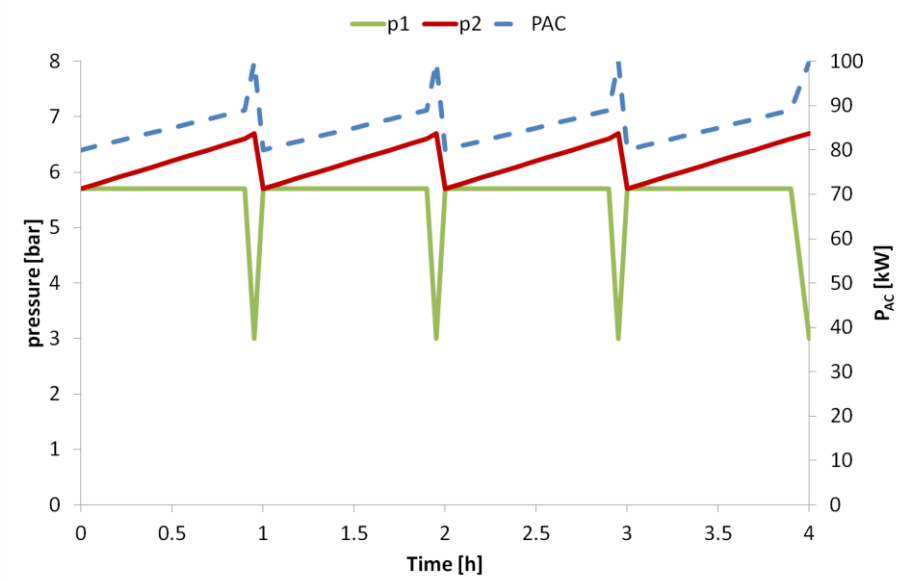

(b)

Figure 8 – (a) Pre-existing irrigation system configuration: The electric power at the output of the diesel generator, P_{AC}, is controlled in order to keep the hydraulic pressure constant at the input of the irrigation network, p_1. Black and blue lines represent electricity and waterways respectively. (b) Cycling evolution of AC power (P_{AC}) and pressure (p_1 and p_2) due to water filtering and filter cleaning periods.

On the other hand, the pipe network is divided into 7 different irrigation sectors covering areas corresponding from 27 to 30 ha and requiring water flows from 217 to 244 m^3/h. The irrigation period (IP) is typically from May to October. Each day, every sector is activated sequentially and consequently, the water flow varies from 217 to 244 m^3/h following a timetable which is drawn up weekly by the operator responsible for the irrigation in accordance with the water needs of the olive trees (related to the difference between the evapotranspiration and the rain). It must be understood that, for a given volume of water, the irrigation time is a consequence of the section of the pipe network. This is implemented practically by means of an irrigation controller (Agronic 4000, from Progrés) which automatically commands the shifts of the irrigation sectors and the diesel generator. This way, the daily irrigation time varies from week to week and the P_{AC} required varies throughout the day in accordance with the different water requirements of the activated sector (this variation is in addition to the cycling behaviour due to the filter cleaning system). The key information to bear in mind is that, apart from the power peaks associated to the filter cleaning requirements, P_{AC} varies from 70 to 80 kW of stable power due to the different power demands of the sectors. The intensive cultivation of olive trees usually has its maximum water demand in July (around 500m^3/Ha) that obliges the irrigation operator to schedule approximately 2.5 h of irrigation per shift, per day. The irrigation lasts 17 h/day during this month, longer than the daily sun hours. Figure 9 shows an example of the weekly irrigation scheduling for a typical year. The figure also shows the sunlight hours, which is sometimes

shorter than the irrigation schedule. This is the main reason for using a hybrid, i.e. not only PV, irrigation system.

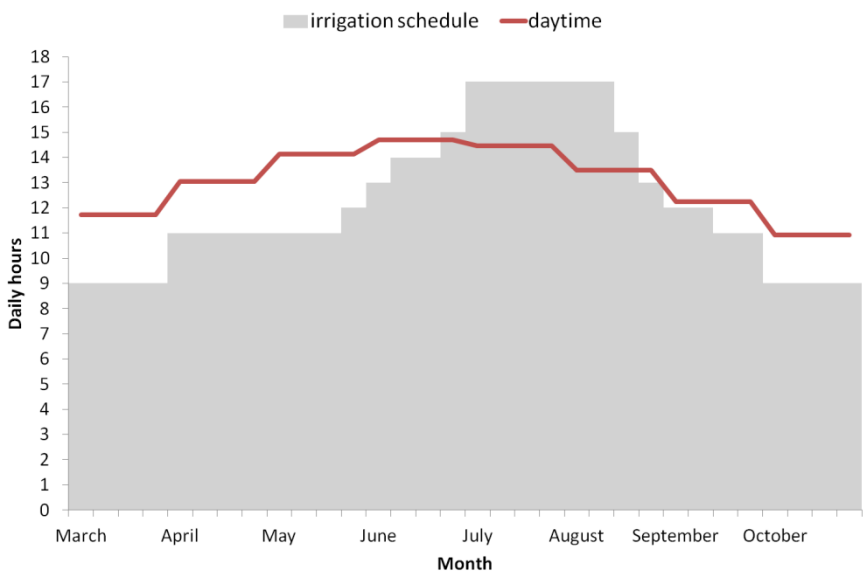

Figure 9 – Hours per day of a) Irrigation scheduling, b) Daytime.

The water inlet to the pumps is made up of a 300 m^3 regulation tank (about one and a half hours of consumption) which, in turn, receives water from an external dam. In years with severe droughts, water is often restricted. These restrictions can affect both the daily volume and availability throughout the day. Sometimes water is not only scarce but mainly available at night.

It is worth commenting that this pre-existing irrigation system is a representative case of the complexity of the irrigation infrastructures of modern agro-industries constituting the potential market for large-power PVIS.

2.2.2 The hybrid PV-diesel system

Inspired by concepts of the Diffusion of Innovations theory [89], we tried to minimise the technical risk perceived by the irrigation operator. The PV system design adheres to three main considerations. First, the pipe network and the irrigation scheduling are fully preserved. As a consequence, and according to Figure 9, stand-alone PV is not enough and the hybridization with the pre-existing diesel system is required (possible changes in the pipe network to reduce the irrigation hours per day are not economically feasible).

Second, PV hybridization has been implemented, as Figure 10 shows, by means of a 140 kWp PV generator, a new pump identical to the pre-existing ones (motor-pump 3) and two

additional 55 kW FCs (two Omron 3G3RX-A4550 acting as PV master FC and PV slave FC). A contactor was added to enable the change of energy source of the motor-pump 2 that can now be fed by the PV or diesel generators. Strictly speaking, this third pump could be avoided but it is the price to be paid for obtaining the confidence of the irrigator operator. Even though, this additional pump barely affects the economic feasibility of the new system. For the same reason, we have also implemented an emergency button to allow the quick disconnection of all this new equipment, thus restoring the original "Only Diesel" configuration.

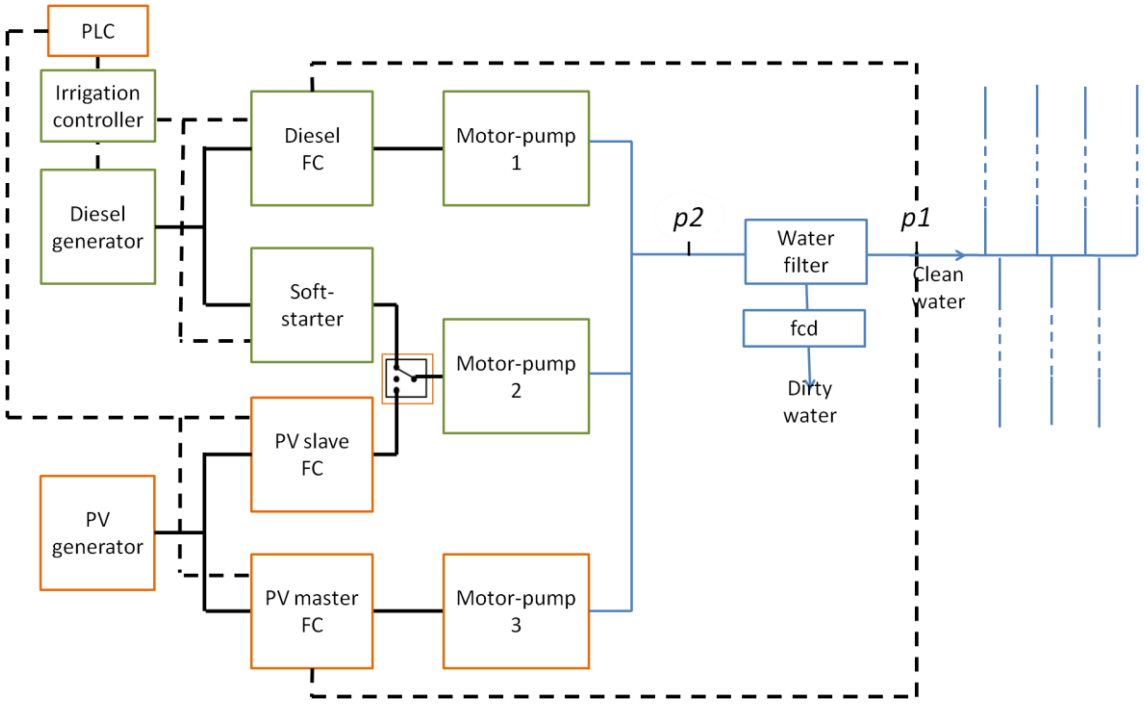

Figure 10 – Hybrid PV irrigation system configuration. A PV generator, a new motor-pump, and two FCs have been added to the pre-existing configuration of Figure 1. The new components are marked in orange, while the previous ones are in green.

Third, to maximize the use of PV energy and therefore to minimize the diesel consumption, three operating modes are available: "Only PV", "Hybrid" and "Only Diesel". Table 1 includes the ON/OFF status of the main components of the system in each case. The rotation between these modes follows the dynamics of the PV power available in accordance with the threshold values established in Figure 11. In practice, the I_{SC} and V_{OC} of a reference module are used for measuring the PV operation conditions: in-plane irradiance, G, and cell temperature, T_C. Then, the available PV power at the output of the FC, P_{AC}, is calculated by a dedicated PLC as:

$$P_{AC} = P^* \frac{G}{G^*} \times \eta_P \times \eta_T \times \eta_{DC/AC} \qquad \text{(Eq. 1)}$$

where P* is the nominal power of the PV generator, η_P is the ratio real power versus nominal power of the PV generator which includes the losses due to mismatching, dirtiness and ageing of the PV generator, $\eta_T=1+\gamma(T_C-T_C^*)$ is the thermal efficiency of the PV generator (γ is the power temperature coefficient of the PV modules) and $\eta_{DC/AC}$ is the efficiency of the FC.

It must be noted that the threshold for changing from the "Only PV" to "Hybrid" modes is somewhat higher than the required stable P_{AC} (80 kW). This is necessary to assure the stable behavior of the system. As revealed during the initial tests, below this value the surge in power demand due to the cleaning of the filters often translates into control instabilities.

Table 1 – ON(1)/OFF(0) status of the different operating modes.

	Diesel		PV	
Mode	**Soft-starter**	**FC**	**Master FC**	**Slave FC**
"Only PV"	0	0	1	1
"Hybrid"	0	1	1	0
"Only Diesel"	1	1	0	0

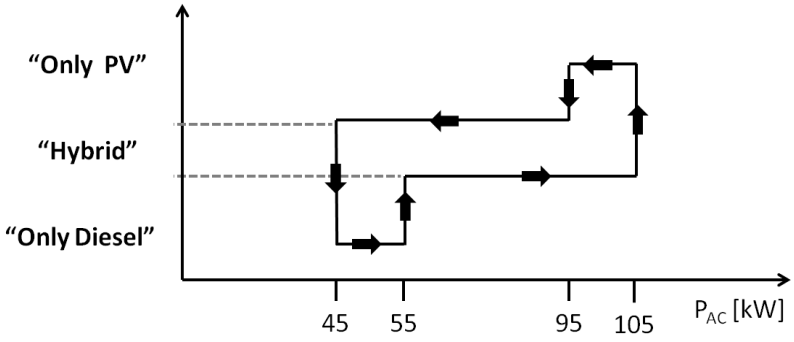

Figure 11 – Available PV power thresholds with hysteresis for the different operating modes – "Only PV", Hybrid and "Only Diesel".

Figure 12 shows (a) an aerial view of the hybrid PV-diesel system, and (b) the three motor-pumps and the water filter bench.

(a)

(b)

Figure 12 – (a) Aerial view of the hybrid PV-diesel drip irrigation system. (b) Detail of the three motor-pumps and the water filter bench. The additional third pump is easily identifiable.

In line with the pioneering nature of the MASLOWATEN project, the system is carefully monitored by means of one-minute records of: G, T_c, P_{DC}, $p1$, water flow, AC frequency, voltage and current of each FC.

2.2.3 The PV generator

The PV generator design obeys two key ideas. First, a North-South horizontal axis tracker has been selected because it provides a good adaptation between solar radiation availability and water needs. This is for two different reasons. On the one hand, the daily profiles of G are reasonably constant during the IP, which obviously matches well with the constant power requirement of drip irrigation. An in-depth look at the constancy of irradiance profiles has been published previously [80]. On the other hand, the yearly evolution of daily irradiation is better adapted to the water required by the plants than static or two-axis PV arrays [50].

Second, the PV power of the PV generator has been selected so that on clear days, the PV generator suffices for powering all the irrigation system at midday on the equinox days, which use to be the limits of the irrigation period. Figure 13 shows the daily profile of G, for the equinox and for the summer solstice. Note that most time G remains equal to or larger than the midday value, G_{md}. Then, assuming the irradiance on a surface perpendicular to the Sun is $G^* = 1000$ W/m^2 and ignoring the diffuse component, the G_{md} on these days is given by:

$$G_{\mathrm{md}} = G^* \cdot \cos(\emptyset) \qquad \text{(Eq. 2)}$$

where φ is the latitude of Alter do Chão. Now, introducing (2) into (1) and making reasonable assumptions for η_P=0.96, η_T =0.9 and $\eta_{DC/AC}$=0.95, assuring $P_{AC} \geq 80$ kW leads to $P^* \geq 125$ kW. For reasons of modularity (PV modules of 250 W, strings of 20 modules and trackers

with 7 rows) the final P* was established as 140 kW. It is worth nothing that this PV generator occupies 3000 m^2, which represents 0.15% of the total farm area.

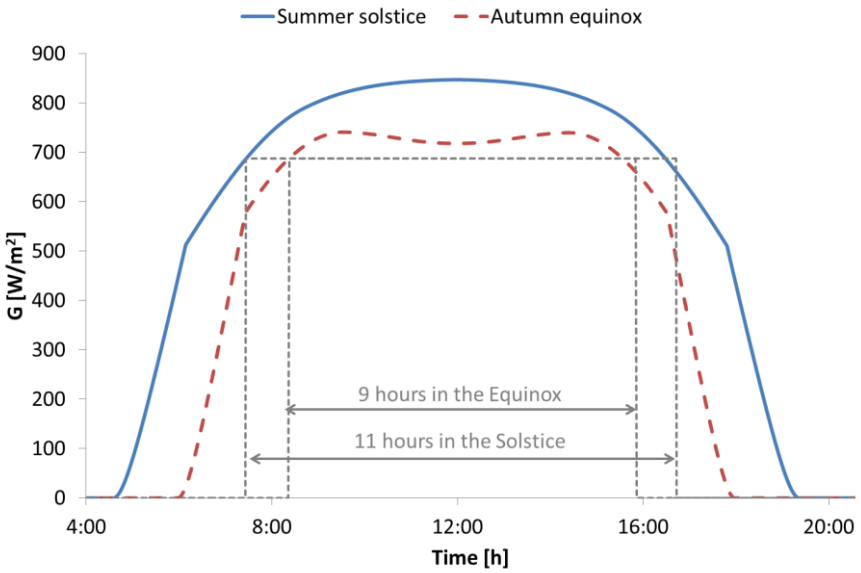

Figure 13 – Incident irradiance profile on the tracker during the autumn equinox and the summer solstice.

It should be noted that this rule (PV power at midday on the equinox is equal to the stable power required for pumping) is just a rough guesswork. At first glance, it might appear that this rule is equivalent to assuring that the irrigation system is fully powered by PV most of the time. However, this is not completely true. As mentioned before, avoiding instabilities during filter cleaning periods changes the operation to hybrid modes even at times when the available PV power is larger than that suggested by this rule. For this reason, the option for large PV peak power, even at the price of reducing the *PR* value would also be a possible option and, finally, this is the reason at the root of establishing 95 kW for the transition between the "Only PV" and the "Hybrid" modes.

2.2.4 Performance scenarios

The annual performance of the hybrid PV system is very dependent on the corresponding water availability circumstances, which typically vary between two extremes.

On the one hand, an Optimistic Scenario defined by the absence of water restrictions. Then, the water needs of the plants are fully covered and water is available throughout the day. That means the irrigation system gets the maximum use of the PV potential during the irrigation period, working in either "Only PV" or "Hybrid" modes. On the other hand, a Pessimistic Scenario defined by severe water restrictions. Then water provision to the plants is restricted to assure survival and minimum production. Table 2 shows the result of combining water

availability and PV potential for these two scenarios. The details of the water restrictions in these scenarios have been suggested by the previous experience of the irrigator operator. PV energy, E_{PV}, water volume pumped by PV and by diesel, V_m^{PV} and V_m^{diesel} , respectively; and daily working time, WT_{day}, in "Only PV" or "Hybrid" modes are given for each month and for the full irrigation period. It is worth noting that the figures for these scenarios are restricted to the irrigation period and daytime. Additional water can be pumped by diesel during the night, but this has been disregarded here because it is not related to PV hybridization. PV simulations have been carried out with SISIFO, a freely-available software tool specifically developed within the MASLOWATEN framework [75]. Solar climate data are as given by PVGIS [90] and Table 3 includes some of the parameters of the simulation. Note that water restrictions in the Pessimistic Scenario mean that only 39% of the PV potential is finally used.

Table 2 – PV energy and volume of water pumped (from PV and from diesel) in the Optimistic and Pessimist scenarios. Daily working hours are also given for "Only PV" and "Hybrid" modes with the threshold of 95 kW to transit between these two modes.

Optimistic Scenario					
Month	E_{PV} **[kWh]**	V_m^{PV} **[m^3]**	V_m^{diesel} **[m^3]**	WT_{day}	
				"Only PV"	**"Hybrid"**
March	9235	33480	33480	0.0	9.0
April	10956	39720	39480	0.0	11.0
May	18735	67920	19200	6.5	5.2
June	19860	72000	21600	7.0	6.0
July	22574	81840	14880	9.0	4.0
August	19165	69480	12360	7.7	3.3
September	10758	39000	38520	0.1	10.7
October	9235	33480	33480	0.0	9.0
Total	**120517**	**436920**	**213000**		
Pessimistic Scenario					
May	13339	48360	3720	6.0	1.0
June	17874	64800	14400	7.0	4.0
July	11122	40320	0	5.4	0.0
August	3244	11760	0	1.6	0.0
September	1622	5880	5880	0.0	1.6
Total	**47201**	**171120**	**24000**		

Table 3 – Parameters of the simulation.

Parameter		Value/ option
Solar climate data		PVGIS
Real power vs nominal power [%]		96
DC/AC conversion [%]		95
Hydraulic part	**Motor-pump [%]**	69
	Filter [%]	80
	Cleaning and other [%]	90

2.3 Performance indices for hybrid PV systems

This section proposes a set of indices for qualifying the design and operation of a general hybrid PV system. First, the energy balance is described in Figure 14 and quantified by means of three ratios defining the PV share (*PVS*), the PV performance (*PR*), and the hydraulic efficiency (η_{Hyd}). The following equations apply:

$$PVS = \frac{E_{\mathrm{PV}}}{E_{\mathrm{PV}} + E_{\mathrm{d}}} \quad \text{(Eq. 3)}$$

$$PR = \frac{E_{\mathrm{PV}}}{P^*/G^*} x \frac{1}{\int G dt} \quad \text{(Eq. 4)}$$

$$\eta_{Hyd} = \frac{E_{\mathrm{Hyd}}}{E_{\mathrm{PV}} + E_{\mathrm{d}}} \quad \text{(Eq. 5)}$$

where E_{PV} and E_{d} are the energy supplied by the PV generator and the diesel generator respectively, E_{Hyd} is the hydraulic energy and η_{Hyd} is the efficiency of the hydraulic system. The following comments apply.

On the one hand, from the PV engineering point of view, the two operational modes involving diesel are different. In the case of systems designed for being powered mainly by PV during the daytime, the "Only Diesel" mode becomes relevant mainly at night-time and is somewhat out of PV concerns. On the other hand, the "Hybrid" mode only occurs during daytime and is directly related to the design of the PV system. Therefore, it is interesting to distinguish between a *PVS* characteristic of the overall operation, which is of interest to the user, and a PVS^{H} characteristic solely to the "Hybrid" mode. That can be easily done by defining a hybrid diesel ratio, *HDR*, as:

$$HDR = \frac{E_d^H}{E_d^H + E_d^O} \quad \text{(Eq. 6)}$$

where E_d^H and E_d^O are the energy supplied by the diesel generator in "Hybrid" and "Only Diesel" operation modes respectively. Then, Eq. 3 can be rewritten as:

$$PVS = \frac{E_{PV}}{E_{PV} + E_d^H/HDR} \quad \text{(Eq. 7)}$$

and

$$PVS^H = PVS(HDR = 1) \quad \text{(Eq. 8)}$$

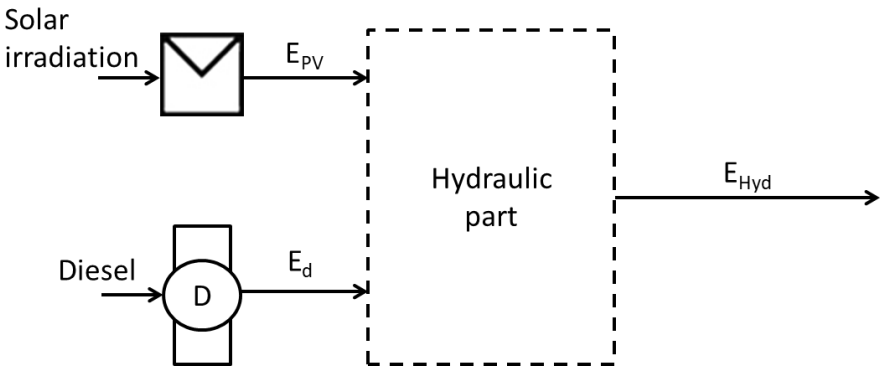

Figure 14 – Energy flows involved in a hybrid PV irrigation system.

Furthermore, the *PR* is widely used in general PV environments and provides an indication of both the technical quality of the PV system's equipment and the efficient use of the available irradiation. It is interesting to distinguish between irradiation losses for three essentially different reasons: the non-irrigation period, the intrinsic characteristics of the PV system design and the external circumstances. For that, the *PR* is factorized as follows:

$$PR = \frac{E_{\mathrm{PV}}}{\mathrm{P}^*/\mathrm{G}^*} \mathrm{x} \frac{1}{\int G\mathrm{dt}} \mathrm{x} \frac{\int_{\mathrm{IP}} G\mathrm{dt}}{\int_{\mathrm{IP}} G\mathrm{dt}} \mathrm{x} \frac{\int G_{\mathrm{useful}}\mathrm{dt}}{\int G_{\mathrm{useful}}\mathrm{dt}} \mathrm{x} \frac{\int G_{\mathrm{used}}\mathrm{dt}}{\int G_{\mathrm{used}}\mathrm{dt}} \quad \text{(Eq. 9)}$$

where IP is the irrigation period determined by the crop and its water needs; G_{useful} is the available useful irradiance during the IP determined by the relationship between the P*, the PV generator structure and the type of irrigation system - water pool or constant pressure; and G_{used} is the irradiance effectively used by the system. To clarify these concepts, G during IP, G_{IP}, G_{useful}, and G_{used} are shown in Figure 15 for a constant pressure system like that analyzed in this chapter. It can be shown that G_{IP} is the total irradiance during the irrigation period determined by the water needs of the olive trees (Figure 15-a). G_{useful} is the irradiance required to deliver the 80 kW needed to pump at a constant pressure of 5.7 bar (Figure 15-b). It is worth noting that with irradiances below G_{useful} it will not be able to pump because the

required pressure would not be reached and irradiances higher than G_{useful} will be partially wasted because the system works at constant pressure. Finally, G_{used} is the part of G_{useful} that has been used effectively due to the availability of water and the irrigation scheduling (Figure 15-c). In this last figure, the irradiance from 7 am to 2 pm was wasted due to the irrigation scheduling or the lack of water during this day and not because of technical problems in the PV system or the needs of the crop.

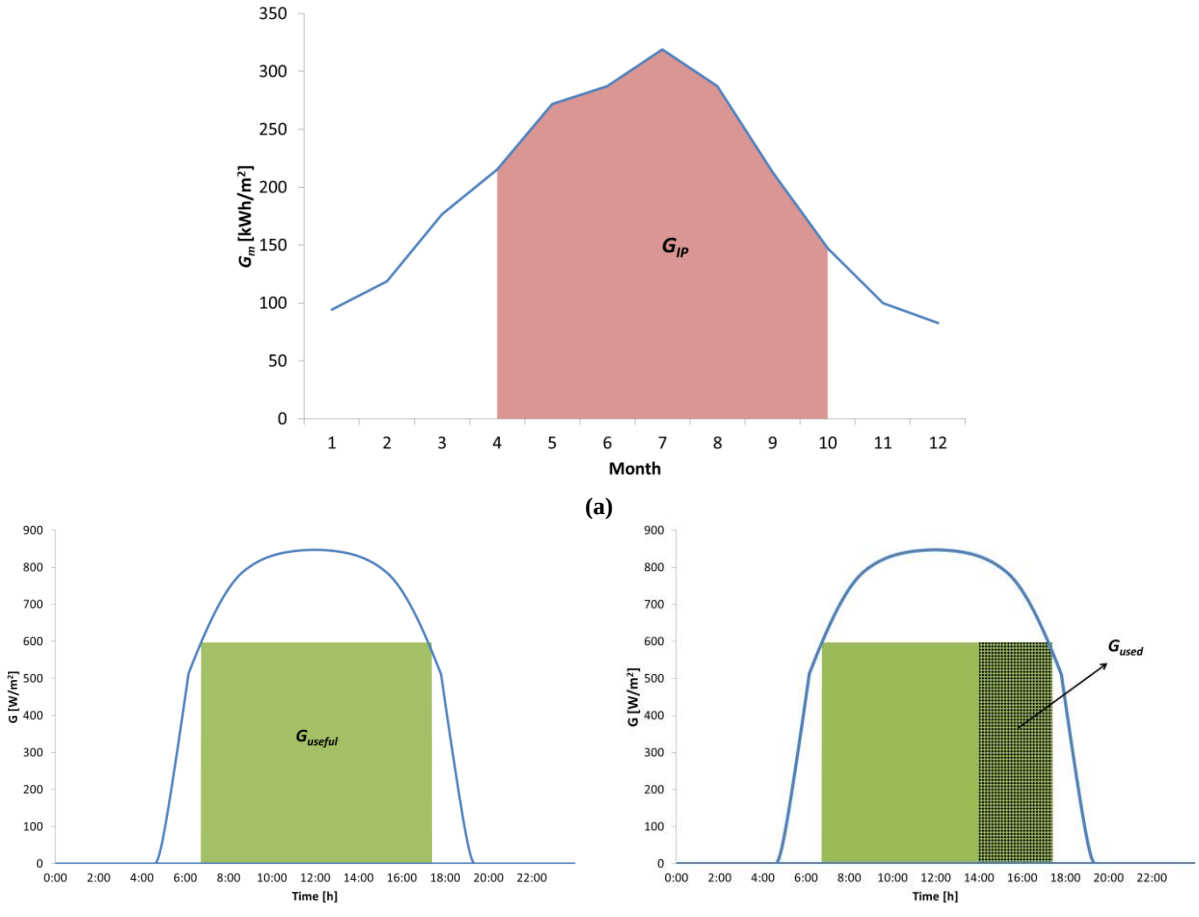

Figure 15 – Graphical representation of the different irradiations considered: (a) $\int G_{IP}$ is the irradiation during the irrigation period, (b) $\int G_{useful}$ is the useful irradiation during the IP determined by the design of the PV irrigation system; and (c) $\int G_{used}$ is the irradiation used effectively by the system.

Now, it is possible to rewrite Eq. 9 as:

$$PR = PR_{PV} \times UR_{\mathrm{IP}} \times UR_{\mathrm{PVIS}} \times UR_{\mathrm{EF}} \qquad \text{(Eq. 10)}$$

where:

$PR_{\mathrm{PV}} = \frac{E_{\mathrm{PV}}}{P^*/G^*} x \frac{1}{\int G_{\mathrm{used}} \mathrm{dt}}$	This is the PR considering only losses strictly associated with the PV system itself, i.e., actual versus nominal peak power, dirtiness, thermal and DC/AC conversion losses. It is intrinsic

	to the technical quality of the PV component and its maintenance.
$UR_{\mathrm{IP}} = \frac{\int_{\mathrm{IP}} G\mathrm{dt}}{\int G\mathrm{dt}}$	This is the ratio of the total irradiation throughout the irrigation period to the total annual irradiation (Figure 15-a). It is intrinsic to a given crop. Note that it is one if the analysis is done on a month inside the irrigation period.
$UR_{\mathrm{PVIS}} = \frac{\int G_{\mathrm{useful}}\,\mathrm{dt}}{\int_{\mathrm{IP}} G\mathrm{dt}}$	This is the ratio of the irradiation strictly required to keep P_{AC} equal to the stable AC power requirement (80 kW, see section 2.2.1) to the total irradiation throughout the IP (Figure 15-b). It is intrinsic to the PVIS design; specifically it depends on the type of irrigation system (direct pumping or pumping to a water pool), the ratio between the PV peak power and the stable PV power required for irrigation, and on the tracking geometry.
$UR_{\mathrm{EF}} = \frac{\int G_{\mathrm{used}}\,\mathrm{dt}}{\int G_{\mathrm{useful}}\,\mathrm{dt}}$	This is the ratio of the irradiation required to keep P_{AC} stable during the irrigation scheduling to the same irradiation during the IP.

Finally, when the PV system is hybridized with already existing diesel facilities as in the Alter do Chão case, the diesel-efficiency, which is usually expressed in terms of the specific fuel consumption (liters per kWh) is really not a matter for the PV engineer and can be disregarded.

It might be thought that using as much as 9 indices for describing the performance of a PV system is just too complex. However, we think this is in coherence with the intrinsic complexity of large modern irrigation and not particularly cumbersome to implement within the automatic control frame characteristic of this type of irrigation. Moreover, it must be understood that the set of these 9 indices constitute a general evaluation frame that becomes reduced for simpler irrigation. For example, for stand-alone PV systems pumping to a water pool throughout the year, which is likely the most commonly imagined PV irrigation system, E_{d} = 0; *PVS* = 1; UR_{IP} = 1 and UR_{EF}= 1. Hence, the relevant indices are just the *PR* and UR_{PVIS}.

2.3.1 Performance indices for the two scenarios

Table 4 shows the values of the performance indices for the two scenarios. At first glance, one can expect a higher PVS^{H} in the Optimistic Scenario, although this does not happen because

the lower the number of irrigation hours, the higher the PVS^{H} (if the irrigation is centered at midday).

The annual *PR* for the Optimistic Scenario is 0.37, while that for the Pessimistic Scenario is 0.15. These values might be surprising when considering that typical values in grid connection, which is currently the most extended PV application, range from 0.75 to 0.90 [91], [92], [93]. However, it must be understood that the economic framework of grid and diesel electricity generation differs considerably. The typical cost of diesel electricity is about 0.3 €/kWh. Thus, assuming that the PV electricity cost for being competitive in grid connection is about 0.05 €/kWh, it is easy to deduce that PV can compete with diesel electricity for $PR > 0.8/(0.3/0.05) = 0.13$. A detailed analysis shows that the PR_{PV} is similar in both cases; the UR_{IP} is lower in the Pessimistic Scenario due to the low use of the system both on a monthly and daily basis; the monthly UR_{PVIS} is the same in both cases since this index is only related to the design of the PVIS. Finally, the UR_{EF} is 1 in the Optimistic Scenario since the system is maximizing the use of PV, which does not happen in the Pessimist Scenario. The η_{Hyd} remains unchanged.

Table 4 – Simulated performance indices for the Optimistic and Pessimist scenarios.

Optimistic Scenario							
Month	PVS^{H}	***PR***	PR_{PV}	UR_{IP}	UR_{PVIS}	UR_{EF}	η_{Hyd}
March	0.50	0.37	0.90	1.00	0.41	1.00	0.50
April	0.50	0.36	0.89	1.00	0.41	1.00	0.50
May	0.78	0.49	0.87	1.00	0.57	1.00	0.50
June	0.77	0.49	0.85	1.00	0.58	1.00	0.50
July	0.85	0.51	0.83	1.00	0.61	1.00	0.50
August	0.85	0.48	0.84	1.00	0.57	1.00	0.50
September	0.50	0.36	0.86	1.00	0.42	1.00	0.50
October	0.50	0.45	0.89	1.00	0.50	1.00	0.50
IP	**0.67**	**0.45**	**0.86**	**1.00**	**0.67**	**1.00**	**0.50**
Annual	**0.67**	**0.37**	**0.86**	**0.83**	**0.67**	**1.00**	**0.50**
Pessimistic Scenario							
May	0.93	0.35	0.87	1.00	0.57	0.71	0.50
June	0.82	0.45	0.85	1.00	0.58	0.90	0.50
July	1.00	0.25	0.84	1.00	0.61	0.49	0.50
August	1.00	0.08	0.84	1.00	0.57	0.17	0.50
September	0.50	0.05	0.86	1.00	0.42	0.15	0.50
IP	**0.88**	**0.25**	**0.85**	**1.00**	**0.56**	**0.52**	**0.50**
Annual	**0.88**	**0.15**	**0.85**	**0.60**	**0.56**	**0.52**	**0.50**

2.4 In-the-field performance

2.4.1 Commissioning of the system

Commissioning tests have been carried out after the PV system was set up in 2016. In accordance with MASLOWATEN technical specifications [16], a visual and infrared inspection of the PV arrays and characterization of the energy behavior of the main system components (STC power of the PV generator, and FCs and motor-pumps efficiencies) were carried out. Table 5 summarizes the key results in comparison with the expectations established at the design phase. The hydraulic efficiency is 5% lower than expected (45% versus 50%). Possible reasons are related to the filter cleaning dynamics and with a slightly improper position of the pumps due to some space restrictions. We are investigating this point further.

Table 5 – Expected and actual STC power of the PV generator and FCs and motor-pumps efficiencies.

	STC power [kW]	Efficiency	
		FCs (electric)	Motor-pumps and filter (hydraulic)
Expected	134.7 (-3.8% of nominal)	0.95	0.50
Actual	136.9 (-2.2% of nominal)	0.93	0.45

Despite the system being in routine and proper operation since 2016, monitoring data are only available from 2017.

2.4.2 Real performance in 2017

A brief analysis of the 2017 irrigation campaign is presented. It was critically influenced by a very dry year and, therefore, the months of April and May suffered a moderate drought and those from June to September a severe drought [94]. Due to this lack of water, the system only worked for 94 days totaling 943 hours (from the end of April to the end of September), which represents 66% less than what it could work according to its potential. Note that in the months of August and September the system only pumped for 85 hours (37 h in August and 48 h in September, 89% less than the Optimistic Scenario).

Table 6 and Table 7 show the results in a similar way to Table 2 and Table 4 respectively, in this case for the real data measured on the farm. The volume of pumped water is 68% less than the Optimistic Scenario and very similar to that of the Pessimistic one. The main difference between the Pessimistic Scenario and the real data is that in the latter, the “Only

Diesel" mode is included due to water restrictions during the sunlight hours, which obliges the user to irrigate during the night.

Table 6 – Real operational data in 2017.

Month	E_{PV} [kWh]	V_m^{PV} [m^3]	V_m^{diesel} [m^3]		WT_{day} [hours]		
			"Hybrid"	"Only Diesel"	"Only PV"	"Hybrid"	"Only Diesel"
April	1960	5880	2346	414	0.5	0.6	0.1
May	12480	37440	13105	14015	3.9	2.3	2.5
June	11701	32618	6714	42902	4.3	1.1	7.2
July	6293	17559	3620	14804	2.3	0.6	2.6
August	1872	5001	689	1849	0.7	0.1	0.4
September	1525	3958	3065	3049	0.3	0.6	0.6
Total	**35832**	**102457**	**29540**	**77034**			

In this case, real data on the irradiance and cell temperature are considered and for this reason, the UR_{PVIS} is different from that obtained in the scenarios. The *PR* is lower due to the use of the system during the night and the η_{Hyd} is lower for the reasons explained in section 2.4.1. For example, in the month of June, the PVS^H is equal to that of the Pessimistic Scenario (with a *PVS* of 0.39). The *PR* is lower than before mainly because the UR_{EF} decreases from 0.90 to 0.51.

Table 7 – Real performance indices in 2017.

Month	*PVS*	*HDR*	PVS^H	*PR*	PR_{PV}	UR_{IP}	UR_{PVIS}	UR_{EF}	η_{Hyd}
April	0.68	0.85	0.71	0.07	0.83	1.00	0.62	0.13	0.45
May	0.58	0.48	0.74	0.33	0.81	1.00	0.65	0.63	0.45
June	0.39	0.14	0.83	0.28	0.78	1.00	0.69	0.51	0.47
July	0.47	0.20	0.83	0.14	0.78	1.00	0.70	0.26	0.46
August	0.66	0.27	0.88	0.05	0.81	1.00	0.69	0.08	0.46
September	0.40	0.50	0.56	0.04	0.81	1.00	0.75	0.07	0.45
IP	**0.49**	**0.28**	**0.78**	**0.16**	**0.79**	**1.00**	**0.69**	**0.29**	**0.46**
Annual	**0.49**	**0.28**	**0.78**	**0.11**	**0.79**	**0.68**	**0.69**	**0.29**	**0.46**

2.4.3 Real performance in 2018

The system is also being monitored throughout the current irrigation campaign (2018). In this case, water restrictions are not affecting the campaign (the daily mean working time was between 9 and 16 hours) but a problem in the fertirrigation system until the end of July negatively affects the performance of the system, since there was the need to use the diesel system until this time. The real operational data and the performance indices are presented in Table 8 and Table 9 respectively.

The month of August deserves attention. It is the only month in which the system was working without external influences. In this month the system worked, on average, 16 hours per day. This implies that the "Only Diesel" mode is needed since the system needs to run also during the night. Even so, the number of working hours in "Only PV" mode is similar to the one of the Optimistic Scenario (which supposes 11 hours of irrigation per day, 7.7 hours only with PV. Furthermore, it is interesting to verify that the obtained indices are very close to the ones of the Optimistic Scenario. For example, the PVS^{H} is 0.82 (versus 0.85 in the Optimistic Scenario) and the *PR* is 0.56 (0.08 higher than in the Optimistic Scenario due to the higher UR_{PVIS}, which is equal to 0.68 in 2018 and to 0.57 in the Scenario).

Finally, the hydraulic efficiency should be discussed. The obtained value (0.55) is greater than expected (0.50) and higher than the one measured during the characterization of the system (0.45) and during 2017 (0.46). A possible explanation to this can be related with the water source – in 2018 more water is available and it is cleaner than before (which decreases the losses represented in Table 5 due to both "cleaning and other" and "filter").

Table 8 – Real operational data in 2018.

Month	E_{PV} **[kWh]**	V_m^{PV} **[m³]**	V_m^{diesel} **[m³]**		WT_{day} **[hours]**		
			"Hybrid"	**"Only Diesel"**	**"Only PV"**	**"Hybrid"**	**"Only Diesel"**
May	3478	10652	2271	56213	1.2	0.3	7.7
June	5040	15936	4497	40842	2.5	0.9	8.0
July	11425	36021	6290	59158	2.5	0.9	8.6
August	20948	55547	14322	41226	7.4	2.2	6.5
Total	**40891**	**127500**	**27379**	**197439**			

Table 9 – Real performance indices in 2018.

Month	***PVS***	***HDR***	PVS^{H}	***PR***	PR_{PV}	UR_{IP}	UR_{PVIS}	UR_{EF}	η_{Hyd}
May	0.15	0.04	0.82	0.12	0.87	1.00	0.59	0.22	0.54
June	0.26	0.10	0.78	0.19	0.83	1.00	0.63	0.37	0.56
July	0.35	0.10	0.85	0.30	0.85	1.00	0.64	0.56	0.56
August	0.53	0.26	0.82	0.56	0.83	1.00	0.68	0.99	0.55
IP	**0.36**	**0.12**	**0.82**	**0.22**	**0.80**	**1.00**	**0.60**	**0.44**	**0.55**

2.5 Economic analysis

Experimental data of diesel consumption and water use are available for the irrigation campaigns of 2016 and 2017 (this data is measured by ELAIA operators and, consequently, were not dependent on the monitoring system installed with the PV part of the system).

Irrigation in both years was very different due to the previously mentioned lack of water in 2017. On the other hand, 2016 was a standard year from the point of view of irrigation since it was possible to give to the plants all the water they need.

Accordingly, two different situations are studied along 25 years (the period of warranty of the PV modules, normally used for PV investments): case study A considers that all the 25 years are equal to 2016, while case study B is a combination of 2016 and 2017 data and considers that each 5 years there is a year like 2017 and the remaining ones are like 2016. As pointed out in [95], in one out of ten years, in semi-arid areas, there is a drought event caused by seasonal rainfall below minimum seasonal plant water requirement. This means that case study A can be seen as an optimistic solution and case study B as a pessimist one.

The economic feasibility study is carried out based on four different indicators: the Net Present Value (*NPV*), the Internal Rate of Return (*IRR*), the Payback Period (*PBP*) and the Levelized Cost of Energy (*LCOE*).

2.5.1 Net Present Value, Internal Rate of Return and Payback Period

In order to estimate the *NPV*, the *IRR* and the *PBP* for an investment, the annual Cash Flows (*CF*) need to be calculated for the whole lifetime of the system. In this study profit is the economic savings derived from reducing diesel consumption due to the use of the PV system. In other words, the viability of the PV system is evaluated in terms of the variation in the *CF* before and after the installation of the PV generator. *CF* for the year n, is given by:

$$CF_{\mathrm{PV,n}} = \begin{cases} -IIC, & \mathrm{n} = 0 \\ S_{\mathrm{n}} - OPEX - DI, & \mathrm{n} \neq 0 \end{cases} \quad \text{(Eq. 11)}$$

where *IIC* is the Initial Investment Cost also known as *CAPEX* – Capital Expenditures, S_{n} is the annual savings by not using the diesel generator, *OPEX* (Operating Expense) is the annual operational expense and *DI* is the debt interests. In more detail, the S_{n} is given by:

$$S_{\mathrm{n}} = PVE_{\mathrm{n}} \times CEC_{\mathrm{n}} \quad \text{(Eq. 12)}$$

where PVE_{n} is the energy that, after the installation of the PV system, is not consumed by the diesel generator, and CEC_{n} is the annual price of the diesel. CEC_{n} is calculated by the following equation:

$$CEC_{\mathrm{n}} = CEC_{\mathrm{n-1}} \times (1 + h + s) \quad \text{(Eq. 13)}$$

where *h* is the inflation rate and *s* is an additional spread. This spread is applicable over the diesel price in order to reflect the most exact price evolution of this commodity throughout the 25 years.

Regarding the *OPEX*, costs related to the maintenance, insurance and security costs associated only to the PV system were considered. Finally, in order to calculate the *DI*, the following equation is used [96]:

$$DI_{\mathrm{n}} = IIC \times D - CR \quad \text{(Eq. 14)}$$

where *CR* is the Capital Repayment and it is associated with the loan maturity (*l*) that in this case was considered as 6 years. *D* is the debt ratio that was considered 70% and the *CR* is given by the following equation [96]:

$$CR = \frac{IIC \times D}{l} \quad \text{(Eq. 15)}$$

The variation in *CF* for the year n when substituting the diesel energy (ΔCF_{n}) is given by the following [96]:

$$\Delta CF_{\mathrm{n}} = \frac{CF_{\mathrm{PV,n}}}{(1+r)^{\mathrm{n}}} \quad \text{(Eq. 16)}$$

where *r* (the real interest rate) can be calculated by the following equation [96]:

$$r = \frac{(i-h)}{(1+h)} \quad \text{(Eq. 17)}$$

where *i* is the interest rate.

With the ΔCF_{n}, it is possible to calculate the *NPV* (Eq. 18) [96]. The *NPV* is the sum of all the cash flows discounted to the present using the time value of money [96]. If the *NPV* is greater than zero, it is expected that value will be created for the investor. If it is less than zero, it is expected that value will be destroyed for the investor.

$$NPV = \sum_{\mathrm{n}=0}^{N} \Delta CF_{\mathrm{n}} \quad \text{(Eq. 18)}$$

Finally, it is possible to calculate the *IRR* as well as the *PBP*. The first one is defined as the real interest rate that would make the *NPV* equals to zero after the 25 years of lifetime of the project (i.e. the real interest rate at which the initial investment is returned at the end of the lifetime of the project). The *PBP* is defined as the number of years (n) for which *NPV* is equal

to zero (i.e. the period required for the initial investment to be returned with the present value of cash flows, disregarding the real interest rate).

2.5.2 Levelized Cost of Energy

The levelized cost of energy (*LCOE*) is the most common indicator used by entities in order to compare different energy technologies. According to [97], the sum of the annual values of the *LCOE* ($LCOE_n$) multiplied by the energy generated annually (E_n) should be equal to the sum of the values of the costs of the project (see Eq. 19).

$$\sum_{n=0}^{N} \frac{LCOE_n \times E_n}{(1+r)^n} = \sum_{n=0}^{N} \frac{Costs_n}{(1+r)^n} \quad \text{(Eq. 19)}$$

If we do the same rearrange done in [97] and [98], assuming a constant value per year, the *LCOE* is given by the following equation:

$$LCOE = \frac{\sum_{n=0}^{N} \frac{Costs_n}{(1+r)^n}}{\sum_{n=0}^{N} \frac{E_n}{(1+r)^n}} \quad \text{(Eq. 20)}$$

where the numerator of Eq. 20 is the total lifecycle cost of the system and the denominator, the lifetime energy production. Based on this equation we are able to calculate different *LCOE*s for each energy source. For a PV application ($LCOE_{PV}$) we consider the costs as the following:

$$LCOE_{PV} = \frac{IIC + \sum_{n=1}^{N} \frac{OPEX_n}{(1+r)^n}}{\sum_{n=0}^{N} \frac{PVE_n}{(1+r)^n}} \quad \text{(Eq. 21)}$$

On the other hand, the *LCOE* of the previous system ($LCOE_{PS}$), in this case, the only-diesel system, is calculated as:

$$LCOE_{PS} = \frac{\sum_{n=0}^{N} \frac{CEC_n \times (PVE_n + PE_n) + OPEX_n}{(1+r)^n}}{\sum_{n=0}^{N} \frac{(PVE_n + PE_n)}{(1+r)^n}} \quad \text{(Eq. 22)}$$

where PE_n is the energy consumed by the diesel generator.

In the case of a hybrid system, the *LCOE* of the system ($LCOE_{CS}$) is given by:

$$LCOE_{\mathrm{CS}} = \frac{IIC + \sum_{\mathrm{n}=0}^{N} \frac{CEC_{\mathrm{n}} \times PE_{\mathrm{n}} + OPEX_{\mathrm{n}}}{(1+r)^{\mathrm{n}}}}{\sum_{\mathrm{n}=0}^{N} \frac{(PVE_{\mathrm{n}} + PE_{\mathrm{n}})}{(1+r)^{\mathrm{n}}}} \quad \text{(Eq. 23)}$$

2.5.3 Results

Table 10 includes the main economic data used in both study cases. The *IIC* of the system is 170277.03 € (1.22 €/Wp), while the *OPEX* at year zero ($OPEX_0$) is 3064.8 €. The values for *h* [99] and *i* [100] are the average value along the last 10 years, *r* is calculated based on these two values and *s* is an estimated value based on information obtained from the different end-users.

Table 10 – Economic data for the Alter do Chão PV-diesel drip irrigation system.

	Values
***IIC* [€]**	170277.03
***IIC* per Wp [€/Wp]**	1.22
***OPEX*$_0$ [€]**	3064.8
***h* [%]**	1.19
***i* [%]**	0.82
***r* [%]**	-0.37
***s* [%]**	3

It can be seen in Table 11 that the economic results are very interesting: an *IRR* of 15% and 13%, a *PBP* of 8.8 and 10.1 years (less than half of the lifetime of the system), and an $LCOE_{cs}$ of 0.12 and 0.15 €/kWh in case studies A and B respectively. The *LCOE* of the only-diesel system, $LCOE_{PS}$, is 0.32 €/kWh, which means that savings are 61% in case study A and 53% in case study B.

Table 11 – Economic results of the Alter do Chão PV-diesel drip irrigation system.

Case study	**A**	**B**
***NPV* [€]**	634767	549184
***IRR* [%]**	15	13
***PBP* [years]**	8.8	10.1
***LCOE*$_{CS}$ [€/kWh]**	0.13	0.15
Savings [%]	61	53

CHAPTER 3

A 120 KWP HYBRID PV-GRID IRRIGATION SYSTEM IN MOROCCO

3.1 Introduction

This chapter describes the design, implementation and operational performance of a 120 kWp hybrid PV-grid system installed in Tamelalt (Morocco) for the drip irrigation of 233 ha of intensive olive trees. This system also belongs to ELAIA.

The design of this system also considers the problem of integrating the novelty of the PV system, in this case, in a pre-existing only-grid system.

This chapter is structured in the same way as the previous one: section 3.2 includes a description of the Tamelalt irrigation system, both the pre-existing only-grid system and the current hybrid PV-grid system. Section 3.3 is devoted to the presentation of performance indices for two different scenarios. Section 3.4 is about the in-the-field performance of the system and section 3.5 about the economic feasibility.

3.2 The Tamelalt irrigation system

3.2.1 The pre-existing only-grid system

The pre-existing irrigation system (Figure 16) was composed by drip emitter devices and two centrifugal surface pumps of 45 kW fed from the national electric grid. Each pump works through a soft-starter at a constant frequency of 50 Hz. Accordingly, and to guarantee constant pressure along the farm, pressure regulating valves are installed. The system also includes a water filter and an fcd, which work as in the case of Alter do Chão.

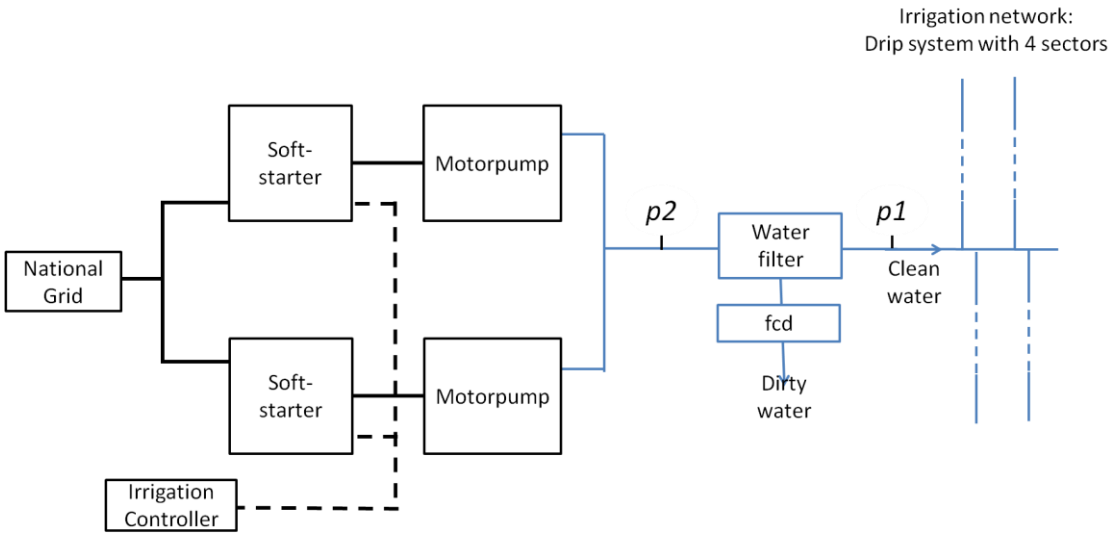

Figure 16 – The pre-existing irrigation system.

The IP is typically all year round. The pumps work with a pressure setpoint of 4 bar after the bank of filters, giving each one a flow between 180 and 200 m^3/h according to the irrigation sector. The farm is divided into 4 sectors with areas ranging from 56 to 60 Ha. Daily, each sector is activated sequentially (through the irrigation controller, an Agronic 4000, from Progrés) in accordance with a weekly irrigation schedule done by the operator responsible for the irrigation. An example of this weekly irrigation schedule for a typical year is shown in Figure 17.

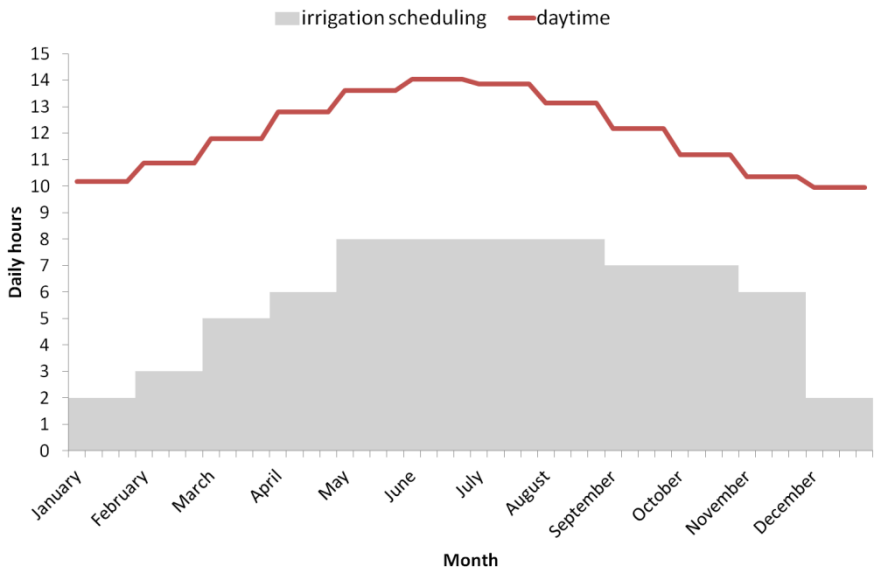

Figure 17 – Hours per day of a) Irrigation scheduling, b) Daytime.

The water to the irrigation pumps comes from a 25000 m^3 reservoir. Four submersible pumps (two of 30 kW and two of 37 kW), also fed from the grid, extract water from four different wells to this reservoir.

This only-grid drip irrigation system is representative of the great number of systems present in the current market.

3.2.2 The hybrid PV-grid system

As in the case of Portugal, the design of the PV system was done taking into account the characteristics of the irrigation system already installed in the field and the end-user desire in order to reduce the degree of novelty. So, first of all, the pipe network and the irrigation schedule are preserved.

Second, this system is also a hybrid one. In this case, the hybridization is done because the end-user wants to keep the connection to the previous energy source to guarantee that they will be able to irrigate whenever they need. Therefore, hybridization could be seen as the price to pay to have the confidence of the user. It should be mention that this system cannot inject energy into the grid. The reason is twofold. First, the injection of PV electricity to the grid is nationally regulated, which means that different countries have different laws. Furthermore, even within the same country, this regulation can change within time and this will lead to uncertainties in the investment. Second, if we are able to prove the technical and economic feasibility of the system without sales to the grid, we are guaranteeing that in the worst-case scenario the system will be profitable.

The new and current system (Figure 18) includes a PV generator of 120 kWp, electrically divided into two equals fields of 60 kWp, each one feeding one frequency converter of 55 kW (Omron 3G3RX-A4550) – which replaces the previous soft starters – and two 45 kW pumps (Caprari – MEC-AS4/125C+ FELM 45KW 4P). This system has the hybridization in the electric part, which means that each FC receives electricity from both the national grid and the PV generator.

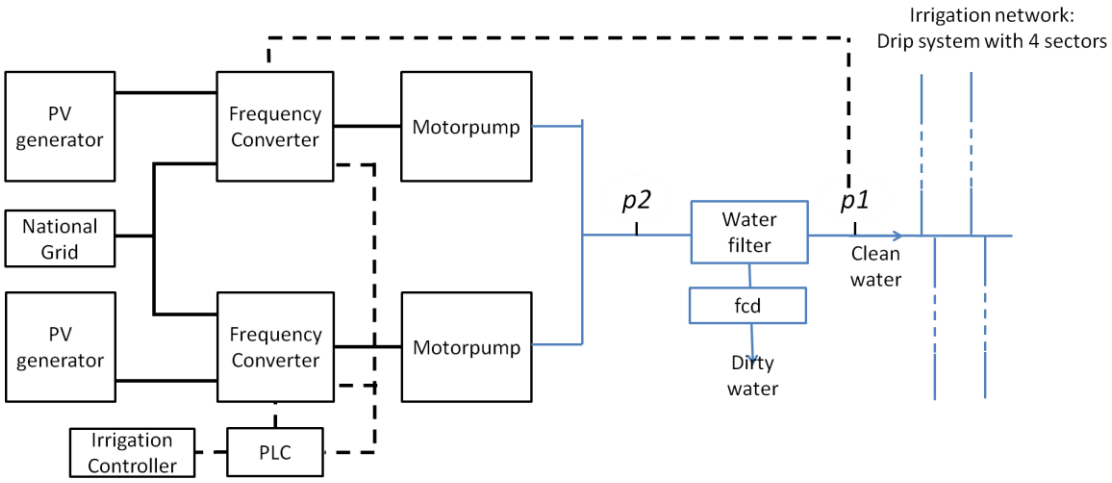

Figure 18 – Hybrid PV-grid system configuration. If ones compare this configuration with the one presented in Figure 16, the PV generator and the PLC were added, as well as the frequency converters (which replace the soft-starters).

Finally, three operating modes are available: "Only PV", "Hybrid" and "Only Grid". The configuration adopted in this system allows the maximization of the use of the PV production if the voltage at the maximum power point of the PV generator is higher than the DC voltage imposed by the grid in the DC bus of the frequency converter. This was done for the first time in this site and a patent was already accepted [86]. The two frequency converters work in a master-slave mode, i.e., one of the frequency converters (the master) controls the pressure in the irrigation system and sends an analog signal (representing the frequency) to the other frequency converter (the slave).

Figure 19 shows the main components currently used in the system.

(a)

(b)

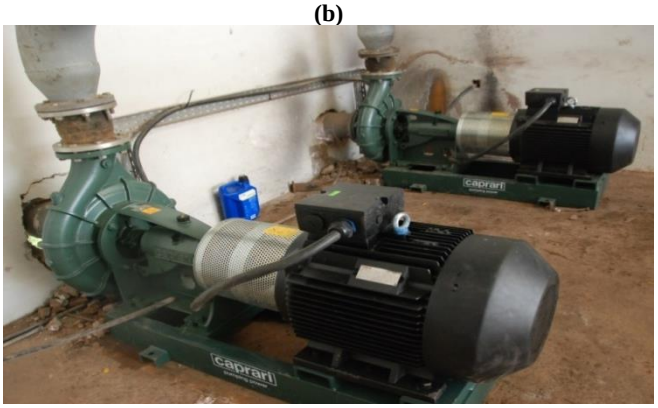

(c)

Figure 19 – Different components of the system: (a) PV generator. (b) Frequency converters and PLC boxes. (c) Motor-pumps.

As in the case of Alter do Chão, this system is also being monitored but an additional variable is measured: the current absorbed from the national grid.

3.2.3 The PV generator

This PV generator is also installed in a North-South horizontal axis tracker and its peak power is the power needed at midday on the equinox days to run both pumps. So, with Eq. 1 and 2 and making the same assumptions as in the case of Alter do Chão (η_P=0.96, η_T =0.9 and $\eta_{DC/AC}$=0.95), guaranteeing $P_{AC} \geq$ 80 kW implies that $P^* \geq$ 114 kW, which leads to P^* equal to 120 kW.

3.2.4 Performance scenarios

Two scenarios are also presented here (an Optimistic and a Pessimistic one) based on the number of irrigation hours suggested by the irrigator operator and indicated in Table 11. It can be seen that the maximum number of irrigation hours per day is 8 h, which means that if the end-user irrigates during daytime the system will always have energy coming from the PV generator. Table 11 also includes the PV energy and the water volume pumped with PV and grid, V_m^{PV} and V_m^{grid}, respectively. The PV simulations were also done with SISIFO and using PVGIS database, and Table 13 includes the main parameters of the simulation. A general

overview of Table 11 shows that in the Optimistic Scenario the irrigation period is the whole year, while in the Pessimistic one the IP goes from March to November. The number of irrigation hours along the year for the Optimistic Scenario is 2134 h, while in the Pessimist Scenario they are 53.4% lower.

Table 12 – PV energy, volume of water pumped (from PV and from the grid) and daily working hours in the Pessimist and Optimistic scenarios.

Optimistic Scenario				
Month	E_{PV} **[kWh]**	V_m^{PV} **[m³]**	V_m^{grid} **[m³]**	WT_{day} **[h]**
January	3840	17155	7645	2
February	5927	26478	7122	3
March	12536	55999	6001	5
April	15686	70072	1928	6
May	21153	94495	4705	8
June	20860	93186	2814	8
July	21314	95216	3984	8
August	20565	91870	7330	8
September	16362	73094	10906	7
October	15227	68024	18776	7
November	11245	50234	21766	6
December	3655	16326	8474	2
Total	**168371**	**752148**	**101452**	
Pessimistic Scenario				
March	2516	11240	1160	1
April	10510	46951	1049	4
May	16148	72135	2265	6
June	15878	70931	1069	6
July	13466	60155	1845	5
August	10494	46880	2720	4
September	7155	31965	4035	3
October	6654	29725	7475	3
November	924	4128	1872	1
Total	**83746**	**374109**	**23491**	

Table 13 – Parameters of the simulation.

Parameter		**Value/ option**
Solar climate data		PVGIS
Real power vs nominal power [%]		96
DC/AC conversion [%]		95
Hydraulic part	**Motor-pump [%]**	72
	Filter [%]	80
	Cleaning and other [%]	90

3.3 Performance indices

The ratios defined in the case of Portugal will also be applied here. As a consequence of the electric hybridization, in this case, two differences should be mentioned. First, the *PVS* is only calculated with Eq. 3 substituting E_d by E_g (see Eq. 24).

$$PVS = \frac{E_{PV}}{E_{PV} + E_g} \quad \text{(Eq. 24)}$$

where E_g is the energy supplied by the grid.

Second, a minimum PV power to start pumping is not needed because with this type of hybridization the PV can be used from sunshine to sunrise and the grid will supply the remaining power in order to achieve the desired power level to guarantee the pressure set-point. As a consequence, Figure 15 should be modified and replaced by Figure 20, where G_{useful} is exploited since sun-shine being the only limitation the irradiance strictly required to keep P_{AC} stable to the power required by the pressure set-point. The *PR* equation and its components keep unchanged. It is worth noting that, due to the design of the system, the UR_{PVIS} will be higher than in the system of Portugal.

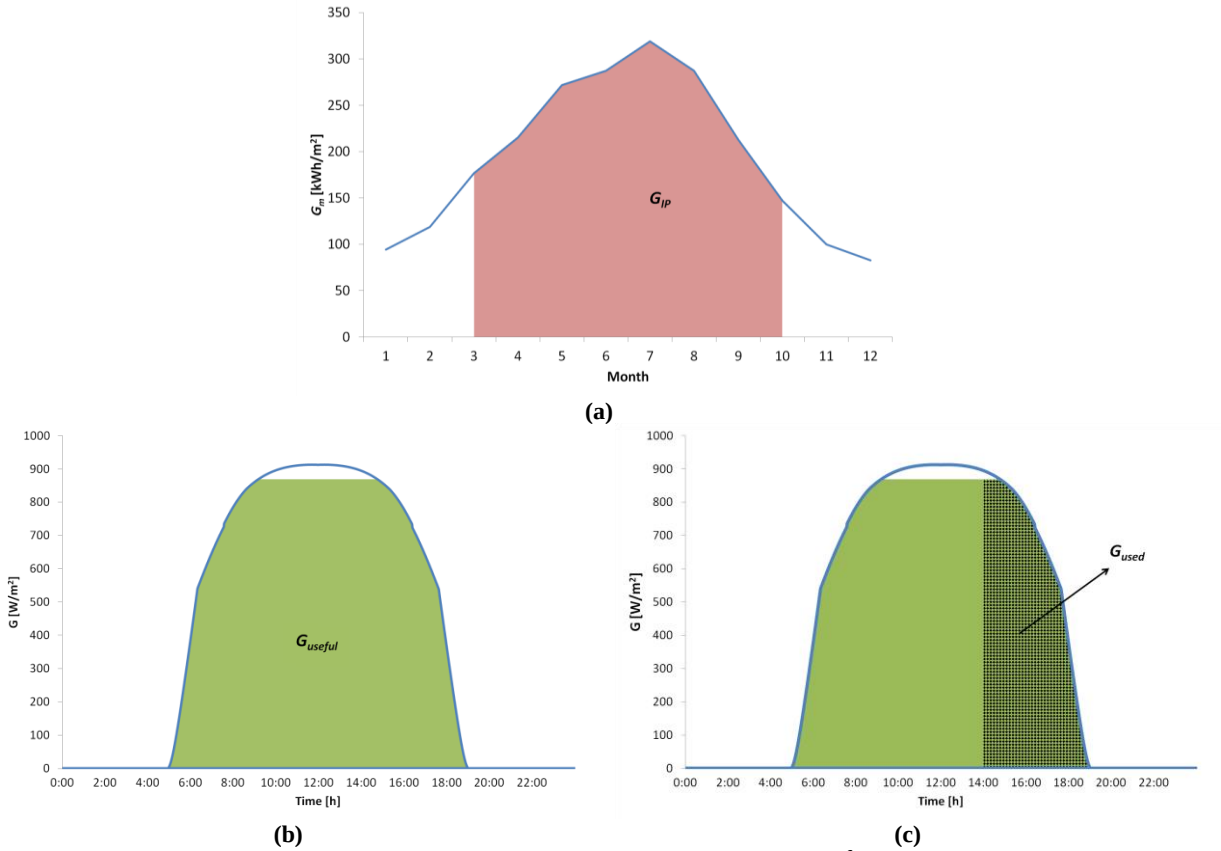

Figure 20 – Graphical representation of the different irradiations considered: (a) $\int G_{IP}$ is the irradiation during the irrigation period, (b) $\int G_{useful}$ is the useful irradiation during the IP determined by the design of the PV irrigation system; and (c) $\int G_{used}$ is the irradiation used effectively by the system.

3.3.1 Performance indices for the two scenarios

Table 14 shows the performance indices for the two scenarios. The annual *PVS* is 0.88 and 0.94 and the *PR* is 0.48 and 0.24 for the Optimistic and Pessimistic Scenarios respectively. The differences between the *PR* in both scenarios are due to lower values of UR_{IP} and UR_{EF} in the Pessimistic Scenario. UR_{IP} in the Optimistic Scenario is 1 because irrigation is done throughout the year, which does not happen in the Pessimistic Scenario. The lowest UR_{EF} is due to the low utilization of the system. It is interesting to note that the lowest values of UR_{PVIS} are observed in summer months because in this period there are moments of time in which the available irradiance is higher than the one strictly required to keep P_{AC} stable to the power required by the pressure set-point.

Table 14 – Simulated performance indices for the Optimistic and Pessimist scenarios.

Optimistic Scenario							
Month	***PVS***	***PR***	$\boldsymbol{PR_{PV}}$	$\boldsymbol{UR_{IP}}$	$\boldsymbol{UR_{PVIS}}$	$\boldsymbol{UR_{EF}}$	$\boldsymbol{\eta_{Hyd}}$
January	0.69	0.20	0.85	1.00	1.00	0.23	0.52
February	0.79	0.28	0.83	1.00	1.00	0.33	0.52
March	0.90	0.42	0.81	1.00	1.00	0.52	0.52
April	0.97	0.46	0.92	1.00	0.91	0.55	0.52
May	0.95	0.57	0.89	1.00	0.91	0.70	0.52
June	0.97	0.54	0.91	1.00	0.88	0.68	0.52
July	0.96	0.54	0.89	1.00	0.88	0.68	0.52
August	0.93	0.56	0.78	1.00	0.97	0.74	0.52
September	0.87	0.54	0.78	1.00	1.00	0.70	0.52
October	0.78	0.59	0.80	1.00	1.00	0.74	0.52
November	0.70	0.58	0.84	1.00	1.00	0.70	0.52
December	0.66	0.20	0.85	1.00	1.00	0.23	0.52
IP	**0.88**	**0.48**	**0.85**	**1.00**	**0.95**	**0.60**	**0.52**
Annual	**0.88**	**0.48**	**0.85**	**1.00**	**0.95**	**0.60**	**0.52**
Pessimistic Scenario							
March	0.91	0.08	0.80	1.00	1.00	0.11	0.52
April	0.98	0.31	0.94	1.00	0.91	0.36	0.52
May	0.97	0.44	0.91	1.00	0.91	0.53	0.52
June	0.99	0.41	0.93	1.00	0.88	0.51	0.52
July	0.97	0.34	0.89	1.00	0.88	0.43	0.52
August	0.95	0.29	0.77	1.00	0.97	0.38	0.52
September	0.89	0.24	0.77	1.00	1.00	0.31	0.52
October	0.80	0.26	0.79	1.00	1.00	0.33	0.52
November	0.69	0.05	0.83	1.00	1.00	0.06	0.52
IP	**0.94**	**0.29**	**0.87**	**1.00**	**0.94**	**0.35**	**0.52**
Annual	**0.94**	**0.24**	**0.87**	**0.83**	**0.94**	**0.35**	**0.52**

If ones compare these values with the ones obtained in Portugal, PR_{PV} is similar; UR_{PVIS} is higher in Morocco as a consequence of the electric hybridization instead of the hydraulic one (this system can use PV energy from sunrise to sunshine, i.e., a minimum PV power to start pumping is not needed); and UR_{EF} is lower in this case both due to the lower water needs of the plants and to the higher G_{useful} in this type of hybridization.

3.4 In-the-field performance

3.4.1 Commissioning of the system

The commissioning tests carried out in this system are the ones applied in Portugal. Table 15 summarizes the key results in comparison with the expectations established at the design phase. The losses in the PV generator are around 6% (higher than the value used in the simulations) and the ones of the motor-pumps plus filters are 27% lower than the expected values. We are also investigating this point further.

Table 15 – Expected and actual STC power of the PV generator and FCs and motor-pumps efficiencies.

	STC power [kW]		Efficiency		
	PV of FC 1	**PV of FC 2**	**FC 1 (electric)**	**FC 2 (electric)**	**Motor-pumps and filter (hydraulic)**
Expected	57.7 (-3.8% of nominal)		0.95		0.52
Actual	56.1 (-6.5% of nominal)	56.4 (-6.0% of nominal)	0.95	0.93	0.41

The system has been working since 2016, but full monitoring data are available from August 2017. Furthermore, in 2018, data are available from the months of February, March, April, July and August (in the end of April 2018 a storm damaged some electrical component and data was not recorded in the months of May and June).

3.4.2 Real performance in 2017

An analysis from August to November 2017 is presented. Table 16 and Table 17 show the results from the available real data of this year. This year was also very dry in Morocco (and water restrictions forced irrigation during night-time). The number of irrigation hours is between the values of the two scenarios presented in Table 11 – for example, in August, 8 hours, 4 hours and 6 hours in the Optimistic Scenario, Pessimist Scenario and 2017 respectively.

Table 16 – Real operational data in 2017.

Month	E_{PV} [kWh]	V_m^{PV} [m^3]	V_m^{grid} [m^3]	WT_{day} [h]
August	15938	44364	19942	6
September	14846	45372	13726	6
October	14784	15921	42400	5
November	13134	6023	46158	5
Total	**58703**	**111679**	**122227**	

The *PVS* of the system is 0.48, the *PR* is 0.24 and the η_{Hyd} is 0.41. Two completely different situations can be seen in these data: in the months of August and September irrigation was carried out mainly during the daytime, with *PVS* during IP of 0.69 and 0.77 respectively. On the other hand, in October and November water restrictions lead to irrigation during the night and the *PVS* decreases to 0.29 and 0.13 respectively. This effect is also seen in the *PR*, while in August and September it is 0.37 and 0.40 respectively, in October and November it decreases to 0.19 and 0.09 respectively. The *PR* is mainly influenced by UR_{EF}, which ranges from 0.10 in November to 0.52 in September. It is interesting to note that the UR_{PVIS} (the parameter related to the PV system design) keeps unchanged and that the PR_{PV} is lower in the hottest months (as expected due to the similarity of this parameter with the typical *PR* of a grid-connected PV system). Furthermore, the *PR* values are similar to the ones obtained in the Pessimistic Scenario.

Table 17 – Real performance indices from August to November 2017.

Month	*PVS*	*PR*	PR_{PV}	UR_{IP}	UR_{PVIS}	UR_{EF}	η_{Hyd}
August	0.69	0.37	0.74	1.00	0.99	0.50	0.43
September	0.77	0.40	0.77	1.00	1.00	0.52	0.41
October	0.29	0.19	0.82	1.00	1.00	0.24	0.40
November	0.13	0.09	0.83	1.00	1.00	0.10	0.40
IP	**0.48**	**0.24**	**0.77**	**1.00**	**1.00**	**0.32**	**0.41**

3.4.3 Real performance in 2018

Table 18 and Table 19 show the same information as Table 16 and Table 17 for 2018 data. As in 2017, the number of irrigation hours is in between the two scenarios considered.

Table 18 – Real operational data in 2018.

Month	E_{PV} [kWh]	V_m^{PV} [m^3]	V_m^{grid} [m^3]	WT_{day} [h]
February	12192	34230	14963	4
March	11946	34504	15323	4
April	12527	40085	32358	4
July	15767	41757	17928	5
August	16294	15835	44803	6
Total	**68726**	**166411**	**125374**	

The *PVS* is 0.55, the *PR* is 0.29 and the η_{Hyd} is 0.42. As expected, the *PR* is mainly influenced by the UR_{EF} that is between 0.41 and 0.45 from February to July and only 0.17 in August. The value of August is a consequence of the need to irrigate mainly during the night.

If ones compare the data from 2017 and 2018, both the *PVS* and the *PR* are higher in 2018 – the first one increases 0.07, while the second one increases 0.05. It is worth noting that the higher *PR* is linked to an increase of both PR_{PV} and UR_{EF}. The PR_{PV} is higher due to the influence of the spring months, while the increase in the UR_{EF} is a consequence of the higher use of the PV system, which can easily be seen in the higher *PVS*.

A comparison between 2018 and the scenarios shows that, in February, the average number of working hours per day was higher than the one supposed in the Optimistic Scenario (4 hours versus 3 in the scenario). For this reason, the *PR* is higher than initially expected (0.39 versus 0.28), mainly influenced by a higher UR_{EF} (0.44 versus 0.33). On the other hand, the number of irrigation hours in April and July is the one supposed in the Pessimist Scenario. Accordingly, the obtained *PR*s are quite similar to the expected ones (0.35 in April and 0.33 in July, versus 0.31 and 0.34 respectively).

Table 19 – Real performance indices from a period of 2018.

Month	*PVS*	*PR*	PR_{PV}	UR_{IP}	UR_{PVIS}	UR_{EF}	η_{Hyd}
February	0.70	0.39	0.89	1.00	0.99	0.44	0.43
March	0.69	0.39	0.89	1.00	0.98	0.44	0.47
April	0.55	0.35	0.86	1.00	0.97	0.41	0.39
July	0.70	0.33	0.73	1.00	1.00	0.45	0.40
August	0.26	0.13	0.77	1.00	1.00	0.17	0.41
IP	**0.55**	**0.29**	**0.81**	**1.00**	**0.99**	**0.36**	**0.42**

3.5 Economic analysis

This economic feasibility analysis is also carried out based on four different indicators: the *NPV*, the *IRR*, the *PBP* and the *LCOE*. These indicators are performed for 2 study cases similar to those used in Portugal.

The equations used in this section are the ones presented in section 2.5, where all the parameters previously related to the diesel are now changed by the values considering that electricity comes from the national grid. Table 20 includes the main economic data used in both study cases. The *IIC* of the system is 1.24 €/Wp and the $OPEX_0$ is 2100 €. The values for *h* [101] and *i* [102] are the average value along the last 10 years, *r* is calculated based on these two values and *s* is an estimated value based on information obtained from the different end-users.

Table 20 – Economic data for the Tamelalt PV-grid drip irrigation system.

	Values
***IIC* [€]**	148703.85
***IIC* per Wp [€/Wp]**	1.24
***$OPEX_0$* [€]**	2100
***h* [%]**	1.46
***i* [%]**	2.86
***r* [%]**	1.38
***s* [%]**	3

The obtained results are presented in Table 21. In case study A, the *NPV* is 638860 €, the *IRR* is 19% and the *PBP* is 7 years. In case study B these values are 510987 €, 15% and 8.1 years respectively. In what concerns the $LCOE_{CS}$, it is 0.07 in case study A and 0.08 in case study B. Since the $LCOE_{PE}$ was 0.16 €/kWh, savings of 66% and 61% are obtained in case studies A and B respectively.

Table 21 – Economic results of the Tamelalt PV-grid drip irrigation system.

Case study	**A**	**B**
***NPV* [€]**	638860	510987
***IRR* [%]**	19	15
***PBP* [years]**	7.0	8.1
***$LCOE_{CS}$* [€/kWh]**	0.07	0.08
Savings [%]	66	61

SECOND PART: CONTRIBUTIONS TO THE DESIGN OF PV IRRIGATION SYSTEMS

This second part includes other contributions to the design of large-power PVIS. These contributions are related to the PV generator structure, to the electrical design of the PV generator and to the selection of the best motor-pump for PVIS. So, a new type of structure called Delta that allows constant daily profiles of PV power is introduced in chapter 4; a detailed analysis of the PV energy losses in PVIS depending on the number of PV modules in series of the generator is shown in chapter 5; and finally a new pump selection method for large-power PVIS that considers that these systems work at a variable frequency is presented in chapter 6.

CHAPTER 4

PV ARRAYS WITH DELTA STRUCTURES FOR CONSTANT IRRADIANCE DAILY PROFILES

4.1 Introduction

The constancy of in-plane irradiance daily profiles represents a significant advantage for a number of PV applications [103], [104], [105]. In particular, when PV irrigation is concerned, this constancy allows the daily water extraction to be maximized when pumping from flow-limited boreholes, as well as optimizing PV performance with both constant pressure and water flow such as drip irrigation systems [49], [67], [78].

At first glance, the immediate solution for the constancy of irradiance profiles is to use North-South horizontal axis trackers [106], [107], [108]. This type of tracker is commonly used and has largely demonstrated its reliability in utility-scale PV plants [109]. Nevertheless, when smaller and isolated PV systems are concerned, trackers are still subject to reliability and cost issues suspects and static-structures used to be preferred [49], [110], [111], [112], [113]. However, the classic static structure oriented to the Equator does not fit the requirement of constant irradiance throughout the day [104].

In order to have these constant irradiance daily profiles without using solar trackers, this chapter proposes a new and different type of static structure, made up of two halves, one oriented to the East and the other to the West. In principle, both halves have an inclination of 60^0 with respect to the horizontal, which means that an equilateral triangle is made with the two halves and the ground. We refer to this structure as a “Delta structure” and this chapter aims at providing the knowledge about its constant profile and its operational performance, including the possible mismatch losses due to the different operating conditions of its two halves. The “Delta structure” provides constancy of irradiance at the price of reducing energy production with respect to an optimally tilted and Equator-oriented PV array. It is opportune to mention that instead of maximizing energy production, other objectives have been also addressed for grid-connected PV systems in other applications. In particular, the search for matching PV production with consumption in order to reduce transmission losses [114] and increase PV penetration [115]. Similarly, the Sacramento Municipal Utility District had promoted PV systems with other than Equator-orientated surfaces [116].

Furthermore, a new index is proposed to evaluate the constancy of the irradiance daily profile. For a given time series of N values, x_i, describing a general variable profile, a "constancy index", k_c, can be defined as:

$$k_c = 1 - \frac{\sigma}{\mu} \quad \text{(Eq. 25)}$$

where μ and σ are the mean and the standard deviation respectively

$$\mu = \frac{1}{N} \times \sum_{i=1}^{N} x_i \quad \text{and} \quad \sigma = \sqrt{\frac{1}{N} \times \sum_{i=1}^{N} (x_i - \mu)^2} \quad \text{(Eq. 26)}$$

Based on this new index, this chapter also sets out empirical evidence of the irradiance constancy provided by a Delta structure prototype installed on the roof of the Solar Energy Institute of the Universidad Politécnica de Madrid (IES-UPM) and compares it with those corresponding to a one-horizontal axis tracker and tilt-fixed structure oriented to the Equator.

Another important and unknown aspect related to the Delta structure is the possible electrical losses due to the different PV module operation temperatures of its two halves, leading to two different working points of maximum power. This work pays attention to evaluating these electrical mismatching losses when using just a single maximum power point tracker (MPPT).

Finally, an analysis of the electrical performance of the Delta structure when used for a PV grid-connected system and for a PV irrigation system, filling the knowledge gap of the behaviour of this new structure compared with the one-horizontal axis tracker and tilt-fixed structure is performed. This is made by means of an extended simulation exercise carried out in a representative location in Portugal.

4.2 The Delta structure

The Delta structure proposed is a static ground-mounted structure in which half of the PV array is oriented to the East and the other half to the West, both parts with the same tilt angle, β, (Figure 21). Hereinafter, this Delta structure will be denominated as $\Delta S(\beta)$. Note that in the case of $\beta=60^0$, the PV array surface seen by the Sun is equal at three moments of any day: in the morning when the Sun is perpendicular to the East-oriented surfaces, at Midday and in the afternoon when the Sun is perpendicular to the West-oriented surfaces. These moments occur about 4 hours before midday, at midday and 4 hours after midday. In-plane direct irradiance,

B, tends to be the same at these moments, which leads to in-plane global irradiance, *G*, reasonably approaching constancy for 8 hours per day.

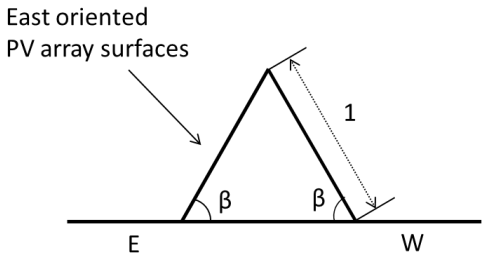

Figure 21 – The Delta structure, ΔS(*β*): The PV array is distributed in two halves. One half is oriented to the West while the other half is oriented to the East. For presentation clarity, the latter is not pointed out in the figure.

As a representative example, a ΔS(60), made up of two reference PV modules, has been installed on the roof of the IES-UPM. Figure 22 shows the in-plane irradiance observed on a clear day close to the Summer Solstice (23rd June). Subscripts "E" and "W" mean East- and West-oriented surfaces respectively, and "Δ" means the average. As expected, the East-oriented part receives more in-plane irradiance in the morning, while the West-oriented one gets more in the afternoon. The average on both surfaces is presented in red and it can be seen that constancy is almost achieved during the middle 8 hours of the day. The corresponding k_C value for just these 8 hours is 0.985. Despite they are not being shown in the figure, it is interesting to mention that the k_C values for the horizontal irradiance and for the in-plane irradiance over a 41^0 tilted and South oriented surface during the same period are 0.837 and 0.787 respectively.

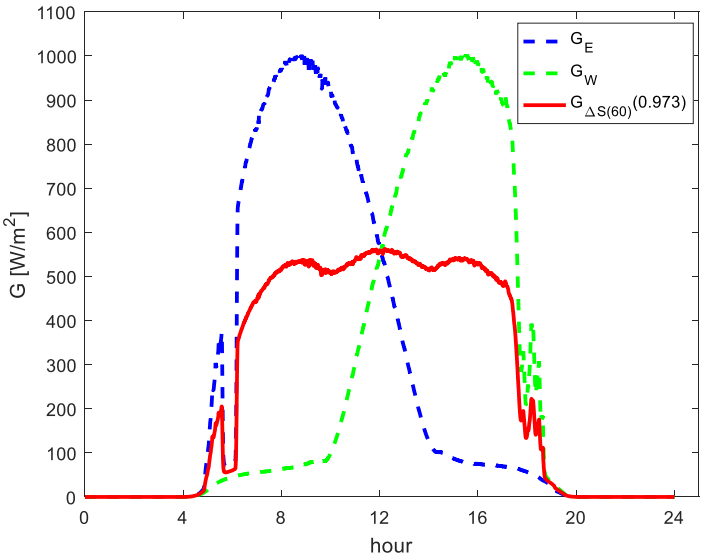

Figure 22 – The in-plane global irradiance over a ΔS(60) measured on a clear day close to the Summer Solstice (23rd June 2017) at IES-UPM. In-plane global irradiance in the East- and West-oriented halves of the ΔS(60) are presented in blue and green respectively. The average value is in red. It is seen that constancy is almost achieved during the middle 8 hours of the day. Variations near 8 h and 20 h are due to shadows from surrounding objects.

This $\Delta S(\beta)$ has been incorporated in SISIFO [75], a PV system simulation tool able to deal with different PV array static and tracking structure possibilities. As a representative case, we have used this tool to analyse the performance of a PV grid-connected system and of a PV irrigation system located in Figueirinha, Silves, Portugal. For comparison purposes, we have considered the $\Delta S(60)$ proposed here and two representative cases of the current state-of-art: a static structure oriented to the South and tilted 25^0, S(25), and a single North-South horizontal axis tracker, 1xh, with the rotation angle limited to 60^0 and capable of backtracking [117], [118].

The energy and water pumping performance depend extensively on the particularities of the inverter and motor-pump (power limitation and efficiency curves) and of the borehole and irrigation system (water flow limitation, irrigation period and pressure requirements), and will be analysed in the next section. Here, we will only present the aspects which are intrinsic to the $\Delta S(60)$: the constancy of the irradiance profile, the ground cover ratio and the electric losses due to the division of the PV array into two halves subject to different operating conditions.

4.2.1 Irradiance profiles

The monthly mean daily horizontal irradiation values, $G_{dm}(0)$, have been obtained from PVGIS [90] in Figueirinha (37.941 N, 7.998 W) and corresponding daily irradiance profiles have been derived using SISIFO, by selecting the Erbs model [119] for decomposition of monthly global values in direct and diffuse components, the Collares-Pereira and Rabl model [120] for deriving instantaneous irradiance from daily irradiation values, and the Perez model [121] for transposition from horizontal to in-plane diffuse irradiances. Soiling and ground reflectance have been established at 2% and 0.3, respectively, and, finally, the simulation time step has been set to 1 minute.

Figure 23 shows the in-plane global irradiance evolution on the Summer and Winter Solstices, as well as the Spring Equinox. This is obtained as the weighted average of the in-plane global irradiance on each half of the Delta, the instantaneous power of each half being the weighting factor. Table 22 gives the values of k_C between 8 am and 4 pm for these 3 days, together with that corresponding to S(25) and to 1xh. Irradiance constancy provided by the $\Delta S(60)$ is nearly as good as that provided by the 1xh (and the best in the Winter Solstice) and much better than that corresponding to the S(25). It is worth recognizing that, due to irradiance fluctuations caused by passing clouds, irradiance constancy on some real days would be lower than that

suggested by the k_C values in this table. However, cloud effect is essentially independent of the PV array structure, so that the good constancy features of the Delta in comparison with the other structures would remain the same.

Table 22 – Constancy index values, for three representative days and for three different PV array structures.

Structure	Summer Solstice	Spring Equinox	Winter Solstice
ΔS(60)	0.974	0.971	0.839
S(25)	0.800	0.756	0.628
1xh	0.976	0.979	0.834

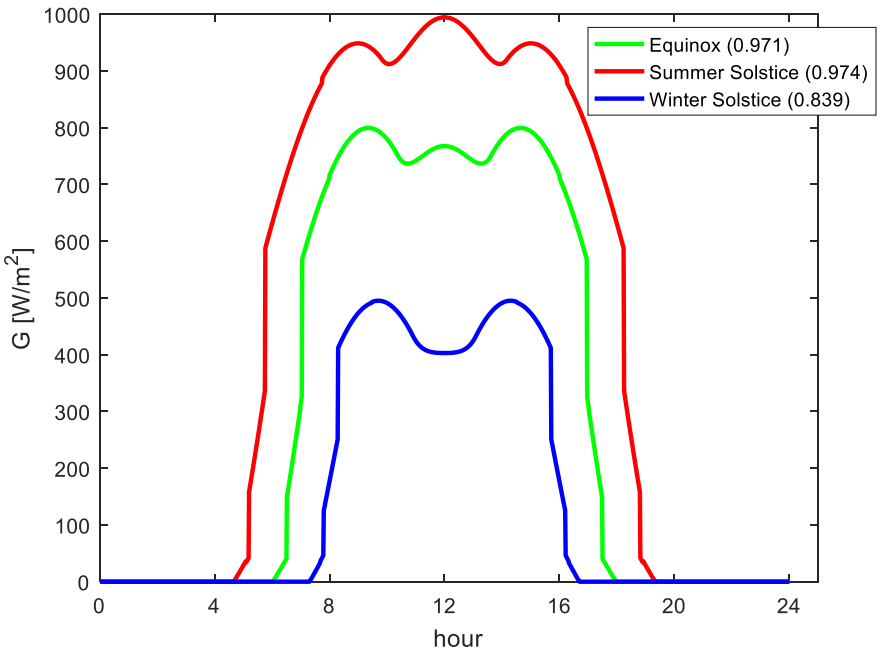

Figure 23 – The in-plane global irradiance evolution during the Spring Equinox (green), the Summer Solstice (red), and the Winter Solstice (blue) days at Figueirinha, Silves, Portugal. The highest constancy index is obtained during the Summer Solstice (0.974), followed by the Spring Equinox (0.971), the lowest value being obtained during Winter Solstice (0.839).

Figure 24 details the evolution of yearly irradiation and k_C versus β. The yearly irradiation corresponding to the S(25) is also detailed. This helps to explain that the good constancy of the ΔS(60) is at the price of yearly irradiation losses of about 25% as regards the S(25).

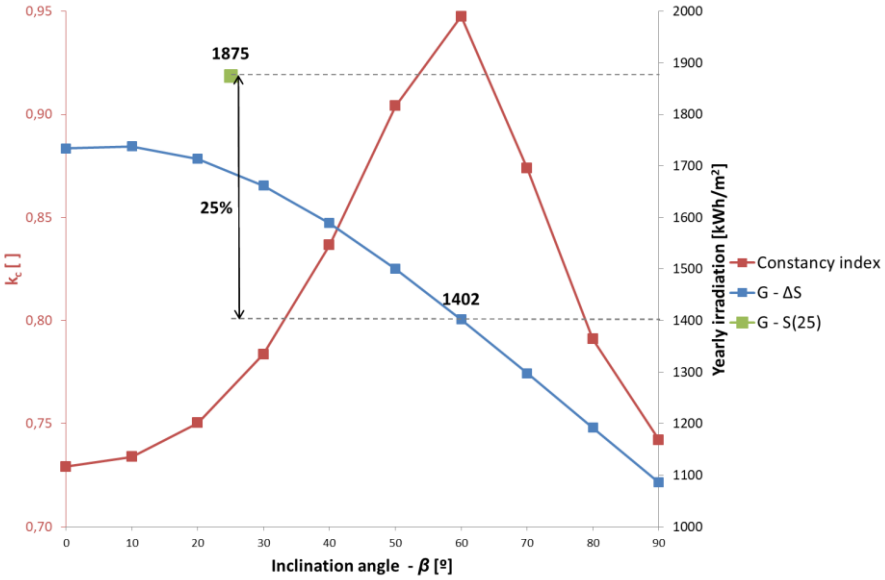

Figure 24 – The constancy index and yearly irradiation for different angles of inclination (from 0 to 90^0) for the ΔS(β). As expected, the maximum constancy index is obtained for an inclination of 60^0 (0.948). The green point represents the yearly irradiation for S(25).

4.2.2 Ground Cover Ratio

The expressions of the Ground Cover Ratio equations [108], *GCR*, for the three structures in this study are shown in Figure 25. Figure 26 shows the yearly energy yield versus *GCR*. The impact of shade has been analyzed by selecting the Martinez model [122] in SISIFO, which essentially considers this impact as being directly proportional to the PV module surface fraction protected by a diode and affected by shade. Additional details of this model are irrelevant in the context of this analysis.

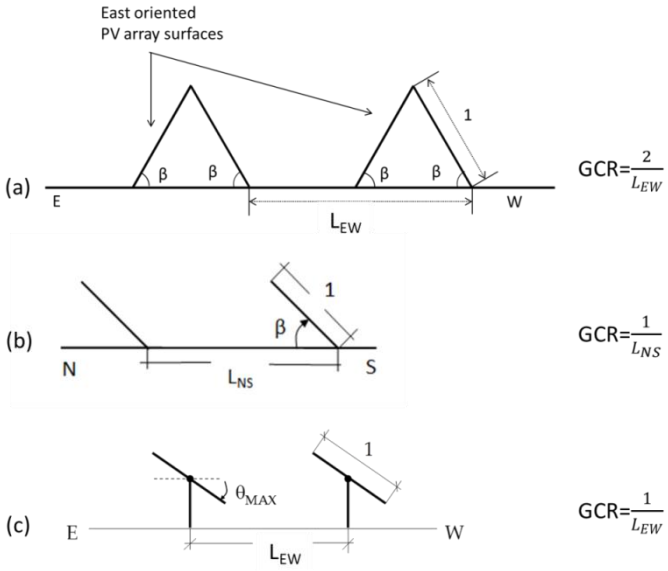

Figure 25 – Spacing between adjacent rows in ΔS(β) (a), S(β) (b), and 1xh (c).

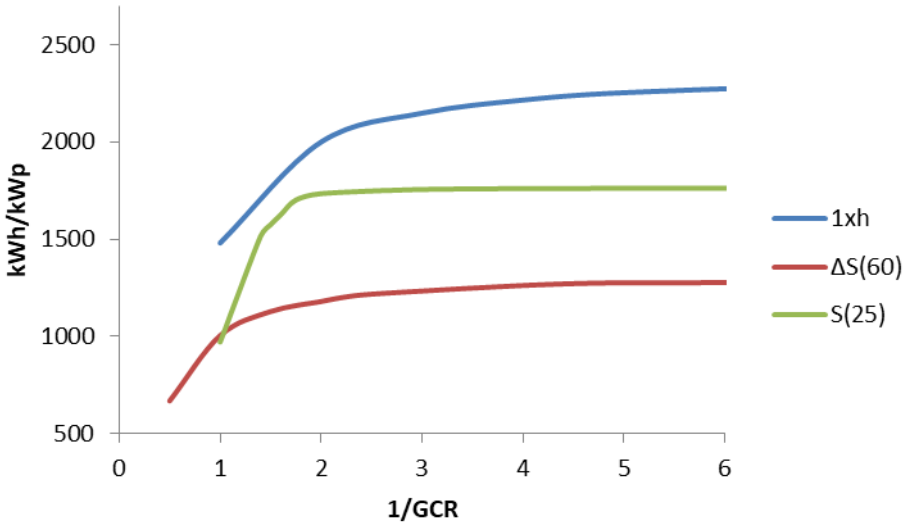

Figure 26 – The evolution of yearly energy yield in Figueirinha for the three structures considered.

The typical row separation for 1xh is L_{EW} equal to 3, which leads to yearly energy losses of 11% due to backtracking. To achieve the same losses in the ΔS(60) due to shadowing, L_{EW} increases to 4.5, while that for S(25) is 1.5, leading to the *GCR* values detailed in Table 23.

Table 23 – The separation between structures (*L*) and 1/*GCR* for the three structures in the study.

Structure	ΔS(60)	S(25)	1xh
L	4.5	1.5	3
1/*GCR*	2.25	1.5	3

4.2.3 Electrical losses

Because the operating conditions (incident irradiance, *G*, and solar cell temperature, T_C) differ between the two halves of the ΔS(β), the corresponding PV array must be accommodated in such a way that all of the PV modules of a same string are installed on the same half. Following the nomenclature of [123] and assuming that the two halves of the PV array are operated at the maximum power point, MPP, the DC power delivered by each half, P_i, is given by:

$$P_i = P_i^* \times \frac{G}{G^*} \times [1 + \gamma(T_C - \mathrm{T_C^*})] \qquad \text{(Eq. 27)}$$

where the subscript "i" can be either the East or West Delta side, the superscript "*" means Standard Test Conditions ($G^* = 1000\ \mathrm{W/m^2}$; $T_C^* = 25^{\circ}\mathrm{C}$) and γ is the power temperature coefficient of the PV modules.

According to [123] and [124] this model properly combines simplicity and accuracy.

The total power delivered by the full ΔS(β), P_{Δ}, is just:

$$P_{\Delta} = P_E + P_W \quad \text{(Eq. 28)}$$

Since the MPP voltage varies both with irradiance and cell temperature, the MPP voltage of the two PV array halves is different. Coupling this PV array to a single inverter requires two different maximum power point trackings, MPPTs, one for each half. A cheaper alternative, attractive in practice, consists of using only one MPPT. Then, electrical mismatching losses appear and Eq. 27 must include the corresponding correction. For that, it is reasonable to assume that the MPP voltage of the whole Delta structure, V_{MPP}^{Δ}, is given by the weighted average of the corresponding values of the two halves, the power being the weighting factor:

$$V_{MPP}^{\Delta} = \frac{V_{MPP}^{E} P_E + V_{MPP}^{W} P_W}{P_E + P_W} \quad \text{(Eq. 29)}$$

On the other hand, the MPP voltage of each half, V_{MPP}^{i}, is calculated through the following equation [125], [126]:

$$V_{MPP}^{i} = V_{MPP}^{*} \times N_s \times [1 - \beta_c(T_C - T_C^{*})] + V_t \times N_s \times ln\left(\frac{G}{G^{*}}\right) \quad \text{(Eq. 30)}$$

where N_s is the number of modules in series, β_C is the voltage temperature coefficient of the PV modules and V_t is the thermal voltage of a module.

Because the irradiance at the two halves is asymmetric, the resulting $V_{MPP}^{\Delta}$is slightly lower than the V_{MPP} of the more illuminated half, so the power corresponding to this voltage can simply be calculated by linear approximations of the P-V curves. That is:

$$P_i\left(V_{MPP}^{\Delta}\right) = P_i\left(V_{MPP}^{i}\right) \times [1 - abs(\frac{V_{MPP}^{\Delta} - V_{MPP}^{i}}{V_{MPP}^{i}})] \quad \text{(Eq. 31)}$$

when the total power of the Delta structure with only one MPPT (P_{MPP}^{Δ}) is obtained as the sum of both surfaces (as in Eq. 28). So, the electrical mismatching losses (F_{ML}) are obtained as the difference between the power obtained with two and one MPPT – Eq. 32.

$$F_{ML} = \frac{P_{\Delta} - P_{MPP}^{\Delta}}{P_{\Delta}} \times 100 \quad \text{(Eq. 32)}$$

It is interesting to point out that electrical mismatching losses are higher in the less illuminated half of the Delta, which contributes less to the instantaneous available PV power.

As a representative example, Figure 27 shows the DC power considering one and two MPPTs over a typical day of June (in blue) as well as the electrical mismatching losses during the same period (in orange). Mismatching losses at midday are null since the operation conditions are equal on both sides of the ΔS(60). As we move away from noon, the difference in operating conditions increase and the electrical mismatching losses also increase.

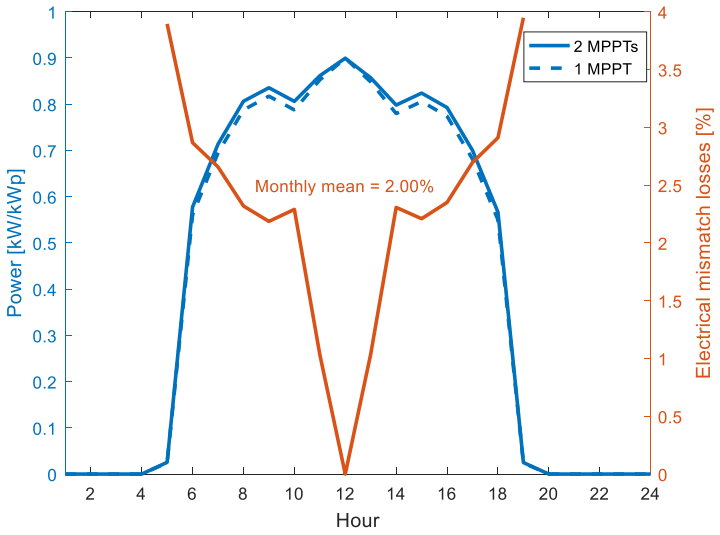

Figure 27 – DC power with 1 and 2 MPPTs, as well as electrical mismatching losses over a typical day of June. The monthly mean of electrical mismatching losses is 2%.

Figure 28 shows the monthly electrical mismatching losses throughout a typical year, the yearly mean being 2.4%. The minimum value, 1.9%, is achieved in July, while the maximum is in December, 3.5%. It is worth underlining that, in applications such as PV irrigation systems, the losses are lower than the yearly mean because they usually work from May to September.

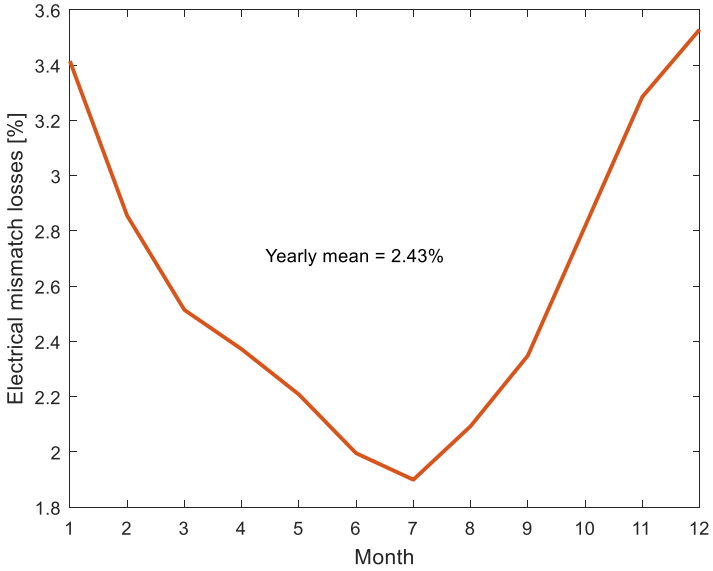

Figure 28 – Electrical mismatching losses over a typical year. The yearly mean value is 2.4%.

4.3 Comparative performance analysis

This section compares the performance of the structure proposed here, the ΔS(60), with the traditional ones, S(25) and 1xh, within the framework of two different PV applications also characterized by different constancy requirements: grid connection (PVGCS) and irrigation (PVIS). The grid connection performance is assessed in terms of yearly energy delivered to the grid while the irrigation performance is assessed in terms of pumped water over two different periods: the whole year and from May to September, which is a typical irrigation period for many crops.

For this reason, we have extended the Figueirinha simulation exercise to a 40 kWp PV generator mounted on 1xh. 40 kW is also the nominal power of the inverter (for PVGCS) and of the frequency converter (for PVIS), and both have identical efficiency and just one single MPP tracker. Their efficiency is calculated using the Schmid model [127], which is based on three different parameters: K_0 (no-load losses), K_1 (linear losses), and K_2 (Joule losses). For this simulation, the values of Schmid parameters for both the inverter and the frequency converter are K_0= 0.0115, K_1= 0.0015, and K_2=0.0438, which lead to a European efficiency value of 94.3%. The SISIFO models mentioned in section 4.2.1 are also selected here, and the separation between the rows for the three PV array structures are those stated in section 4.2.2.

The losses scenario includes a soiling degree of 2%, wiring losses of 1.5 and 3% for DC and AC, respectively, and a ratio between real and nominal power of the PV generator of 0.96 due to initial degradation and mismatching losses.

In the case of the PVIS, a stand-alone PV irrigation system pumping into a water pool is studied. The pumping head of the system is 50 m and the nominal frequency of the pump is 50 Hz, it being able to work from 38 to 55 Hz. The pump and system curves are shown in Figure 29 and the main characteristics of the PVIS are summarized in Table 24.

Table 24 – Characteristics of the PV irrigation system.

Parameter	Value
Type of PV irrigation system	Stand-alone
Type of pumping	Water pool
Pumping head [m]	50
Working flow [m^3/h]	Variable

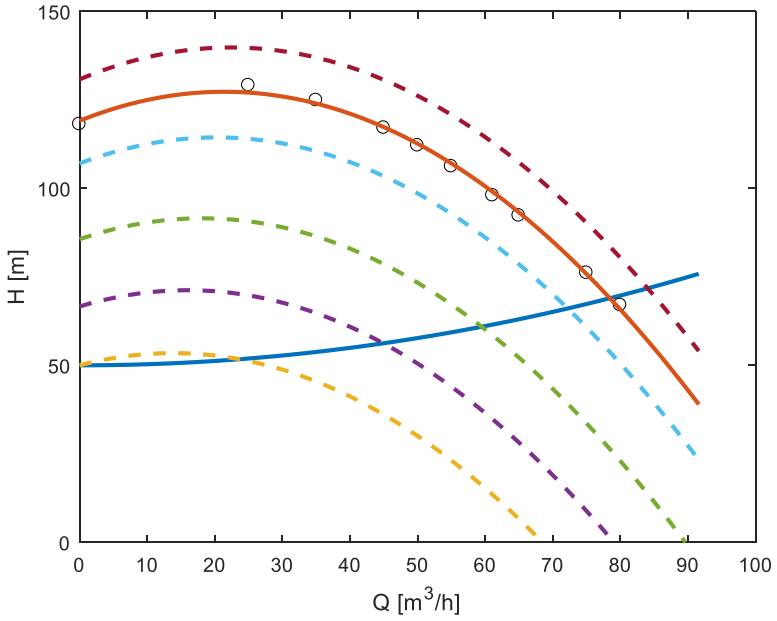

Figure 29 – System (blue solid line) and pump curves (orange solid line represents 50 Hz and the points marked with circles have been obtained from manufacturer information, the remaining dashed lines corresponds to frequencies different from 50 Hz).

Table 25 presents the AC energy (E_{AC}) produced for PVGCS and the water volume for PVIS by a 40 kWp 1xh. Yearly values are presented for both cases, while the water volume is also presented for the typical irrigation period.

Table 25 – AC energy for a PVGCS and water volume for a PVIS for a 40 kWp 1xh. NA means not applicable.

	PVGCS	**PVIS**
	E_{AC} [kWh/kWp]	**Water volume [m^3/kWp]**
Yearly	2148	6289
Irrigation period	NA	3308

The PV peak power (P^*) needed for ΔS(60) and S(25) to deliver the same AC energy (E_{AC}) and water volume than the 40 kWp 1xh are shown in Figure 30 and Figure 31. The AC energy, water volume and peak power are normalized by the values corresponding to the 40 kWp 1xh detailed in Table 25 and known here as E_{AC1xh}, $Water\ volume_{1xh}$ and P^*_{1xh}.

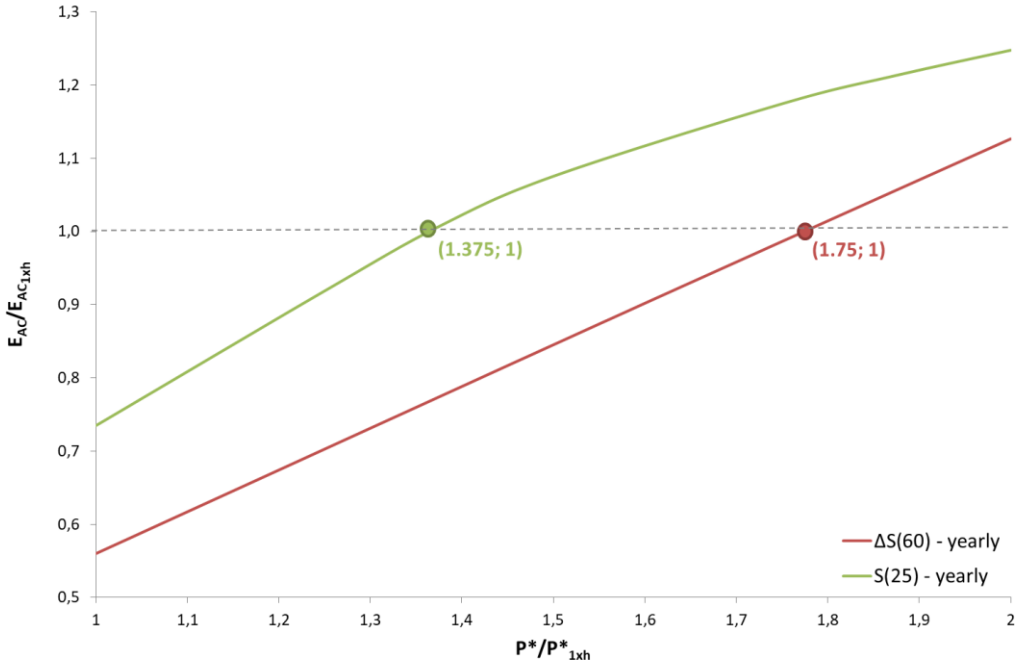

Figure 30 – The yearly AC energy produced by a PVGCS with ΔS(60) and S(25) normalized by the AC energy produced by a 40 kWp 1xh (E_{AC}/E_{AC1xh}) as a function of its PV peak power normalized by the 40 kWp peak power of 1xh (P^*/P^*_{1xh}). The two points with E_{AC}/E_{AC1xh} =1 represent the required oversizing of ΔS(60) and S(25) PV peak power to equal the performance of the 40 kWp 1xh.

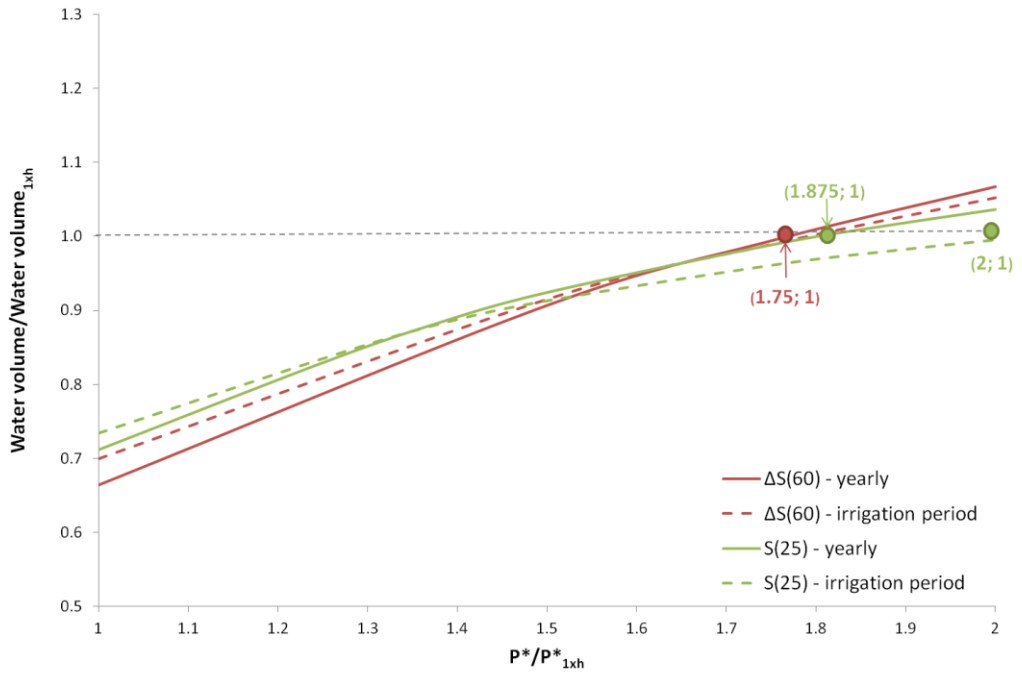

Figure 31 – Water volume pumped by a PVIS with ΔS(60) and S(25) normalized by the water volume pumped by a 40 kWp 1xh (Water volume/Water volume$_{1xh}$) as a function of its PV peak power normalized by the 40 kWp peak power of 1xh (P^*/P^*_{1xh}). The continuous lines represent yearly values and dashed lines show the water volume pumped during the irrigation period. The points with *Water volume/Water volume*$_{1xh}$ =1 represent the required oversizing of ΔS(60) and S(25) PV peak power to equal the performance of the 40 kWp 1xh.

From these figures, it is possible to conclude that to guarantee the same yearly energy and water volume for the ΔS(60), it is necessary to install 1.75 times the peak power of the 1xh, while, in the case of S(25), it is necessary to install 1.37 times for PVGCS and 1.87 times for PVIS (2 times if we consider just the irrigation period). These values are summarized in Table 24.

It is worth highlighting that the relative peak power needed in the PVIS is higher than that needed in PVGCS for S(25), which can be explained because in the case of a PVIS the system only starts in the morning when the AC power is higher than the minimum needed to pump the water from the borehole to the tank (in this case 7 kW). This occurs earlier in the morning in ΔS(60) than in S(25), working more hours a day in the first case. Symmetrically, a similar behaviour occurs at the end of the day. Therefore, due to the shorter pumping period, to equal the volume of water pumped during the irrigation period, the peak power of S(25) must be doubled.

Table 26 – PV generator size needed to guarantee the same yearly AC energy (for a PVGCS) or water volume (for a PVIS) than a 40 kWp 1xh

Period		ΔS(60) P^*/P^*_{1xh}	S(25) P^*/P^*_{1xh}
PVGCS – AC energy	**Annual**	1.75	1.37
PVIS – Water volume	**Annual**	1.75	1.87
	Irrigation period	1.75	2

Figure 32 (a) and (b) show the AC power of the PVGCS and water flow of the PVIS, respectively, on a characteristic day of June for the calculated PV generators. At first glance, 1xh and ΔS(60) have a much more constant profile than S(25). Even so, it is easy to see that, due to the inverter/frequency converter saturation, the constancy of the S(25) is achieved 100% for a small central time interval. In order to quantify this, the constancy index is applied to the middle 8 hours of the day (from 8 am to 4 pm) for a whole year and the yearly mean values are presented in Table 27.

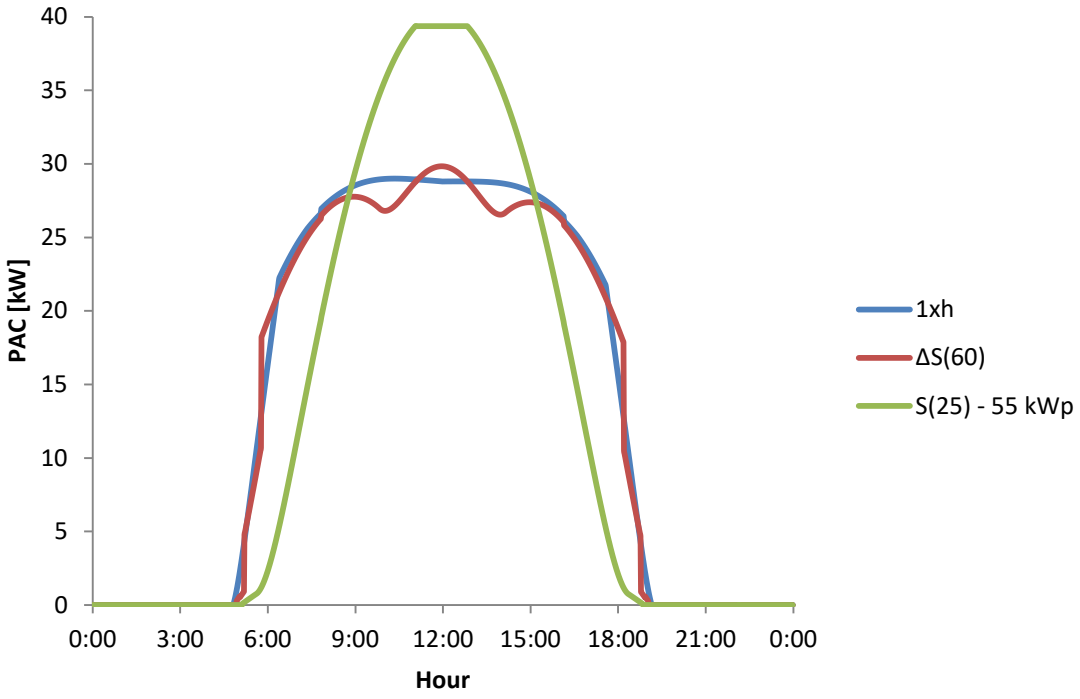

(a)

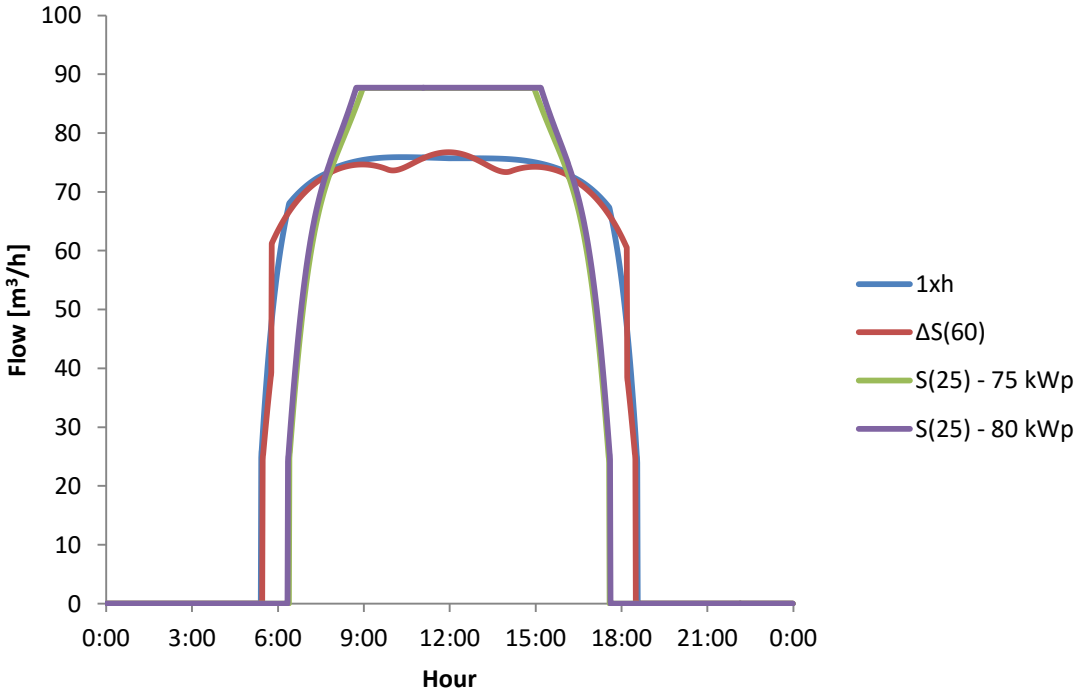

(b)

Figure 32 – AC power of PVGCS (a) and water flow of PVIS (b) for a characteristic day of June for the three structures in the study.

Table 27 – Yearly mean of the constancy index (k_C) applied to AC power of a PVGCS and to water flow for PVIS for the three structures in the study.

	ΔS(60)	S(25)			1xh
		55 kWp	75 kWp	80 kWp	
PVGCS Yearly mean	0.947	0.743			0.951
PVIS Yearly mean	0.954		0.844		0.956
PVIS Irrigation period	0.987			0.965	0.992

Some interesting results can be elicited from the previous table:

- The values of the ΔS(60) and of the 1xh are very similar for both cases, PVGCS and PVIS, and higher than the values of S(25).
- The constancy index during the irrigation period is always higher than the yearly mean, which is very interesting from the point of view of a PVIS.

It is also important to note that S(25) is the one which presents the best improvement from PVGCS to PVIS. This happens because the peak power in the second case is so high that the frequency converter works in saturation (55 Hz) for most of the day, i.e., delivering its maximum power constantly. This is also another reason in favour of ΔS(60): with a similar k_C than S(25) (0.987 versus 0.965), ΔS(60) does not expose the borehole to the stress of working continuously at maximum flow.

CHAPTER 5

ON THE NUMBER OF PV MODULES IN SERIES FOR LARGE-POWER IRRIGATION SYSTEMS

5.1 Introduction

The electrical compatibility between the PV generator and the FC limits the number of PV modules in series because the maximum input voltage of the FC is normally around 800 V [128], [129]. This can have consequences both in terms of PV production losses and that of the water pumped for two main reasons:

- As the most used electrical centrifugal pumps in large-power irrigation systems are 400 V_{AC} three-phase, the FC needs at its DC bus at least 540 V_{DC} to deliver the voltage needed by the pump at its output. A stand-alone PV irrigation system to a water pool at a variable frequency extracts the maximum power from the PV generator through a maximum power point tracker (MPPT) algorithm in the frequency converter that establishes a voltage in the DC bus that is just the maximum power point voltage, V_{MPP}, of the PV generator. This V_{MPP} depends basically on the number of PV modules in series and on the cell temperature of the PV generator under certain operating conditions, T_C. If the required V_{MPP} is less than $V_{DC_{BUS\_PUMP}}$=540 V_{DC}, the PV generator will not work at its maximum power point, MPP, to supply the required voltage to the pump and, therefore, an energy loss will occur in terms of PV electricity regarding that which could be delivered if this limitation did not exist.
- In the case of large-power PV irrigation systems hybridized with the 400 V_{AC} three-phase grid, the voltage of the DC bus established by the grid ($V_{DC_{BUS\_GRID}}$) is 565 V. Again, if the V_{MPP} is less than $V_{DC_{BUS\_GRID}}$, energy losses brought about by not following the MPP will occur.

In fact, there are some products on the market that include electronic devices to change the number of PV modules in series in this kind of application depending on T_C (a greater number of PV modules when T_C is high and less as the T_C decreases), but they have disadvantages such as the more complexity of the system and the reduction of the reliability. This

complexity is not justified because an in-depth analysis of the actual impact of these losses has never been carried out.

This chapter analyses and quantifies the PV energy losses in large-power PV irrigation systems depending on the number of PV modules in series, it discusses whether they are relevant or not and proposes simple design solutions for those cases in which they are relevant. The analysis is carried out by taking several factors into account: two different applications (stand-alone and hybrid PVIS), two the different locations with different ambient temperatures (Villena and Marrakech), and the different AC voltages required by the pump (from 400 to 430 V) or supplied by the grid (from 400 to 415 V).

A detailed description of the limitation of the number of the PV modules in series and its effects on the PV energy losses is made in section 5.2, and the actual impact on the PV production depending on the number of PV modules is analysed in depth in section 5.3. The results are discussed in section 5.4 and finally, section 5.5 shows a design of a simple solution to avoid these losses when it is relevant.

5.2 Limitation of the number of PV modules in series and impact in the PV irrigation system performance

As a starting point, it is important to answer two main questions: Why is not possible to install more than a certain number of PV modules in series in large-power PV irrigation systems? How does this limitation affect PV production?

As regards the former, the root of the limitation is that, in the current state of the art of the most used FCs, the maximum input voltage that they accept is 800 V [128], [129]. If this voltage is surpassed, the FC can be damaged and, in any case, the product guarantee is lost.

The open circuit voltage of a PV module under standard test conditions (STC), V^*_{OC}, is typically 36 V or 43 V for 60 solar cells or 72 solar cells PV modules respectively. This V^*_{OC} depends on the temperature of the solar cell, T_C, according to the following equation:

$$V_{OC} = V^*_{OC}[1 + \beta_c(T_C - T^*_C)] \quad \text{(Eq. 33)}$$

where T^*_C is the temperature of the solar cell at STC (25ºC), β_c is the coefficient of variation in the voltage with the temperature of the solar cell and V_{OC} is the open circuit voltage under certain ambient conditions.

It is significant to observe that, if we consider that a minimum T_C in a certain location can reach -10ºC at sunrise and a value of β=-0.31%/ºC, the corresponding open circuit voltage is $V_{OC(60cells)}$= 39.9 V and $V_{OC(72cells)}$= 47.7 V, which leads to a maximum number of PV modules in series of N_S(60 cells)= 20 and N_S(72 cells)= 16. To surpass this number of PV modules means that the maximum open circuit voltage can be higher than the maximum input voltage of the FC at certain moments of the year.

The second question is how this limitation can affect the PV production in large-power PVIS. The most used pumps in this kind of application are three-phase centrifugal ones with 400 V nominal voltage. The equation that relates the output AC voltage ($V_{AC_{PUMP}}$) and the DC bus voltage ($V_{DC_{BUS\_PUMP}}$) in an FC is [130]:

$$V_{DC_{BUS\_PUMP}} = \sqrt{1 + \frac{3 \cdot \sqrt{3}}{2\pi}} \cdot V_{AC_{PUMP}} \quad \text{(Eq. 34)}$$

So, the required DC bus voltage is $V_{DC_{BUS\_PUMP}} = 540$ V.

However, if there is an extensive length of wires between the FC and the pump and/or there are filters between them, the voltage drop must be compensated to allow 400 V at the motor-pump input, which means that higher voltages at the FC output are needed. Table 28 details the required values of $V_{DC_{BUS\_PUMP}}$ depending on the $V_{AC_{PUMP}}$.

Table 28 – The required values of $V_{DC_{BUS\_PUMP}}$ depending on $V_{AC_{PUMP}}$.

$V_{AC_{PUMP}}$ [V]	$V_{DC_{BUS\_PUMP}}$ [V]
400	540
415	561
430	581

So, in the case of a stand-alone PV irrigation system pumping to a water pool at a variable frequency, it will be able to track the MPP whenever the corresponding MPP voltage (V_{MPP}) is higher than the $V_{DC_{BUS\_PUMP}}$ values set out in Table 28. But if $V_{DC_{BUS\_PUMP}} > V_{MPP}$, the DC bus voltage will remain at $V_{DC_{BUS\_PUMP}}$ and will not be that corresponding to the MPP and some potential PV energy will be wasted.

In the case of large hybrid PV-grid systems, both the PV generator and the three-phase 400 V grid are connected to the FC input. The grid imposes the DC bus voltage, $V_{DC_{BUS\_GRID}}$, in accordance with the following equation [131]:

$$V_{DC_{BUS\_GRID}} = \sqrt{2} \cdot V_{AC_{GRID}} \quad \text{(Eq. 35)}$$

where $V_{AC_{GRID}}$ is usually 400 V but it can vary depending on the tuning of the transformer. In particular, hybrid PV-grid irrigation systems located at the beginning of the grid line can have higher $V_{AC_{GRID}}$values. Table 29 sets out the $V_{DC_{BUS_GRID}}$values corresponding to different $V_{AC_{GRID}}$.

Table 29 – $V_{DC_{BUS_GRID}}$values corresponding to different $V_{AC_{GRID}}$.

$V_{AC_{GRID}}$ [V]	$V_{DC_{BUS\_GRID}}$ [V]
400	566
415	587

If the PV generator is able to supply enough power to feed the pump at a certain frequency without the support of the grid and with a V_{MPP} higher than that imposed by the grid, $V_{MPP} > V_{DC_{BUS\_GRID}}$, all of the energy will be provided by the PV generator and the voltage of the DC bus will be V_{MPP}, absorbing the maximum PV energy available. If $V_{MPP} < V_{DC_{BUS\_GRID}}$, then the PV generator will work outside of its MPP, wasting some PV energy.

Finally, in the case of direct pumping at constant pressure and water flow (and therefore, constant power, $P_{p=cte}$) with both stand-alone or hybrid PV-grid irrigation systems, the previous analysis is valid just by substituting V_{MPP} by $V_{p=cte}$ where $V_{p=cte}$ is the PV generator voltage needed to deliver $P_{p=cte}$.

5.3 Energy losses versus number of PV modules in series

5.3.1 Methodology

The PV energy losses due to the mechanisms described in the previous section depend on the number of PV modules in series, the temperature of the solar cell and the values of $V_{DC_{BUS\_PUMP}}$ or $V_{DC_{BUS\_GRID}}$, but other aspects can also have an influence, such as the configuration of the PV irrigation system (stand-alone or hybrid). So, the PV energy losses will be calculated for two main applications: a stand-alone PV irrigation system pumping to a water pool and a hybrid PV-grid irrigation system working at constant power. The characteristics of both PV irrigation systems are detailed in Table 30 and are based on two real demonstrators developed within the framework of a real project [74], [132], [133]. Both systems will be simulated at two locations – Villena (Spain) and Marrakech (Morocco) – with

different mean maximum and minimum ambient temperatures (T_{Mm}, T_{mm}) [90] as shown in Table 31.

Table 30 – PV generator size, frequency converter and pumping characteristics of the stand-alone and hybrid PVIS.

Parameter	Stand-alone	Hybrid
PV generator size [kWp]	360	60
Nominal power of the FC [kW]	315	45
Type of pumping	Water pool	Constant pressure
Static head [m]	270	0
Friction losses at rated flow [m]	18	15
Working pressure [bar]	Variable	40
Working flow [m3/h]	Variable	200

Table 31 – Maximum and minimum monthly mean ambient temperatures (T_{Mm}, T_{mm}) in Villena and Marrakech.

	T_{Mm}		T_{mm}	
Month	**Villena**	**Marrakech**	**Villena**	**Marrakech**
January	8.2	19.5	2.5	6.5
February	9.7	20.1	2.1	7.5
March	13.3	24.2	3.9	10.1
April	16.0	26.9	6.2	12.6
May	20.2	30.9	9.6	16.0
June	25.2	35.0	13.6	19.3
July	28.6	39.3	15.9	22.5
August	28.1	39.2	15.2	22.8
September	24.3	33	12.6	19.9
October	18.8	29.8	9.6	17.0
November	11.6	23.4	5.7	12.1
December	8.4	20.7	2.8	8.2
Yearly	17.7	28.5	8.3	14.5

So, the methodology used to analyse the relationship between the PV energy losses and the number of PV modules in series is based on using the typical meteorological years (TMY) of both locations and calculating the hourly power generated throughout the irrigation period (from May to September) by both PV irrigation configurations mounted on a North-South

horizontal axis tracker. So, for the two typical series of power, the PV energy losses are calculated as follows.

In the case of the stand-alone PVIS to a water pool, the PV energy losses are calculated by integrating the difference in the maximum power that could be generated by the system and the power that is really being produced due to the limitation of $V_{DC_{BUS\_PUMP}}$, as shown in Figure 33. The losses will be calculated for 20, 21 and 22 PV modules in series with 60 solar cells and $V_{DC_{BUS\_PUMP}}$ will take the values set out in Table 28.

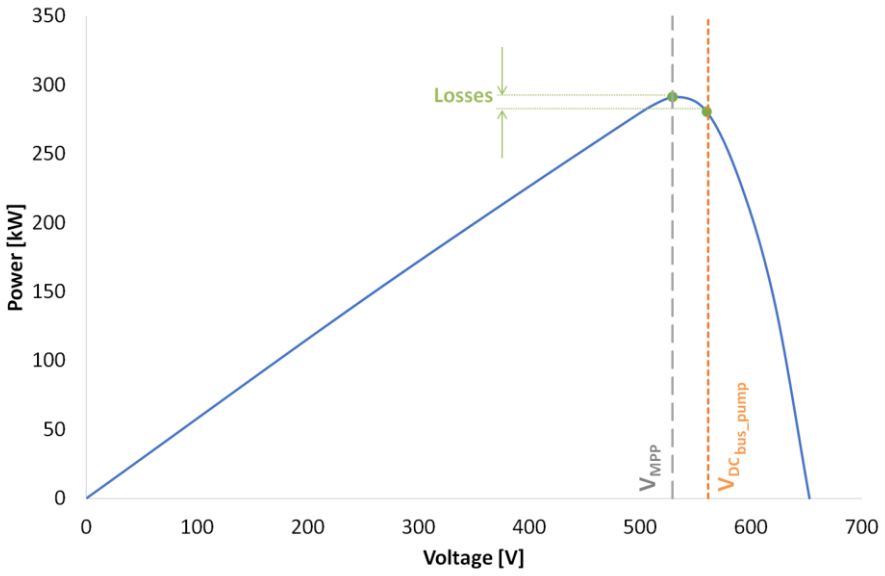

Figure 33 – P-V curve of the stand-alone PV irrigation system to a water pool. The PV energy losses are calculated integrating along the whole irrigation period the difference of the maximum power that could be generated by the system and the power that is really producing due to the limitation of $V_{DC_{BUS\_PUMP}}$.

In the case of the hybrid PV-grid irrigation systems, two different types of loss may take place. The first one is when the PV-power available (P_{MPP}) is higher than the constant power required by the pump ($P_{p=cte}$) but the PV generator voltage needed is less than $V_{DC_{BUS\_GRID}}$. In this case, the PV generator will only produce the corresponding power at $V_{DC_{BUS\_GRID}}$ and the rest of the power will be supplied by the grid. The PV energy losses are calculated by integrating the difference between $P_{p=cte}$ and the PV power at $V_{DC_{BUS\_GRID}}$, as shown in Figure 34 (a).

The second type of loss occurs when the PV-power available is less than $P_{p=cte}$. In this case, the grid is always supplying power and, therefore, imposing the $V_{DC_{BUS\_GRID}}$. So, the PV

energy losses are calculated by integrating the difference between P_{MPP} and the PV power corresponding to $V_{DC_{BUS\_GRID}}$, as shown in Figure 34 (b).

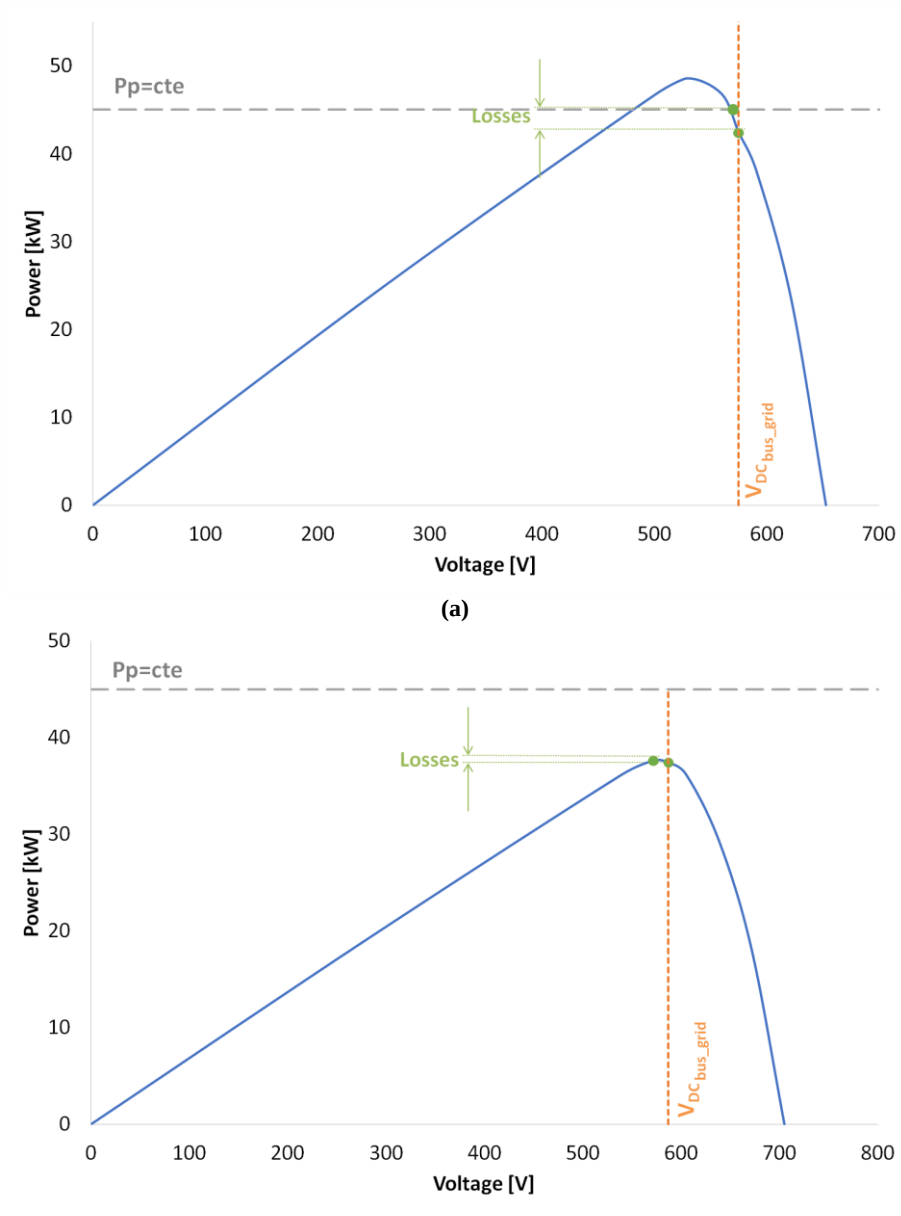

Figure 34 – P-V curve of the hybrid PV-grid system. The PV energy losses are calculated integrating the difference between $P_{p=cte}$ and the PV power corresponding to $V_{DC_{BUS\_GRID}}$: (a) $P_{MPP} \geq P_{p=cte}$; (b) $P_{MPP} < P_{p=cte}$.

The total losses will be the addition of both types of loss throughout the year and will also be calculated for 20, 21 and 22 PV modules in series with 60 solar cells. $V_{DC_{BUS\_GRID}}$ will take the values set out in Table 29.

5.3.2 Losses for the stand-alone PV irrigation system to a water pool

Table 32 shows the PV energy losses of the stand-alone PV irrigation system in Villena (Vi) and Marrakech (Ma) for 20 to 22 PV modules in series and for the three values of $V_{DC_{BUS\_PUMP}}$ in Table 28.

Table 32 – PV energy losses of the stand-alone PV irrigation system in Villena (Vi) and Marrakech (Ma) for 20 to 22 PV modules in series and for the three values of $V_{DC_{BUS\_PUMP}}$.

	Losses [%]					
Number of PV modules	**20**		**21**		**22**	
$V_{DC_{BUS\_PUMP}}$ **[V]**	**Vi**	**Ma**	**Vi**	**Ma**	**Vi**	**Ma**
540	0.00	0.29	0.00	0.00	0.00	0.00
561	0.59	2.15	0.00	0.08	0.00	0.00
581	2.88	6.21	0.17	1.25	0.00	0.00

These results show that, if the output of the FC is 400 V (i.e. $V_{DC_{BUS\_PUMP}}$ = 541 V), the losses for both Villena and Marrakech are negligible and do not justify any further action. In the case of 415 V ($V_{DC_{BUS\_PUMP}}$ = 561 V), the losses are solved with 21 PV modules in series. For 430 V ($V_{DC_{BUS\_PUMP}}$ = 581 V), the losses are practically eliminated with 21 PV modules in Villena and completely solved in Marrakech with 22 PV modules.

Apart from the losses, another interesting result is the analysis of the occurrence of PV generator voltages of more than the maximum 800 V allowed at the input of the FC. Figure 35 shows the frequency of occurrence of a *V*oc greater than this value per hour of the day during the daytime in the tracker. As expected, most occurrences happen in the morning as a consequence of the lowest cell temperature at these moments. It is interesting to note that for 22 modules in the coldest place (Villena) there are some days in which the overvoltages do not disappear.

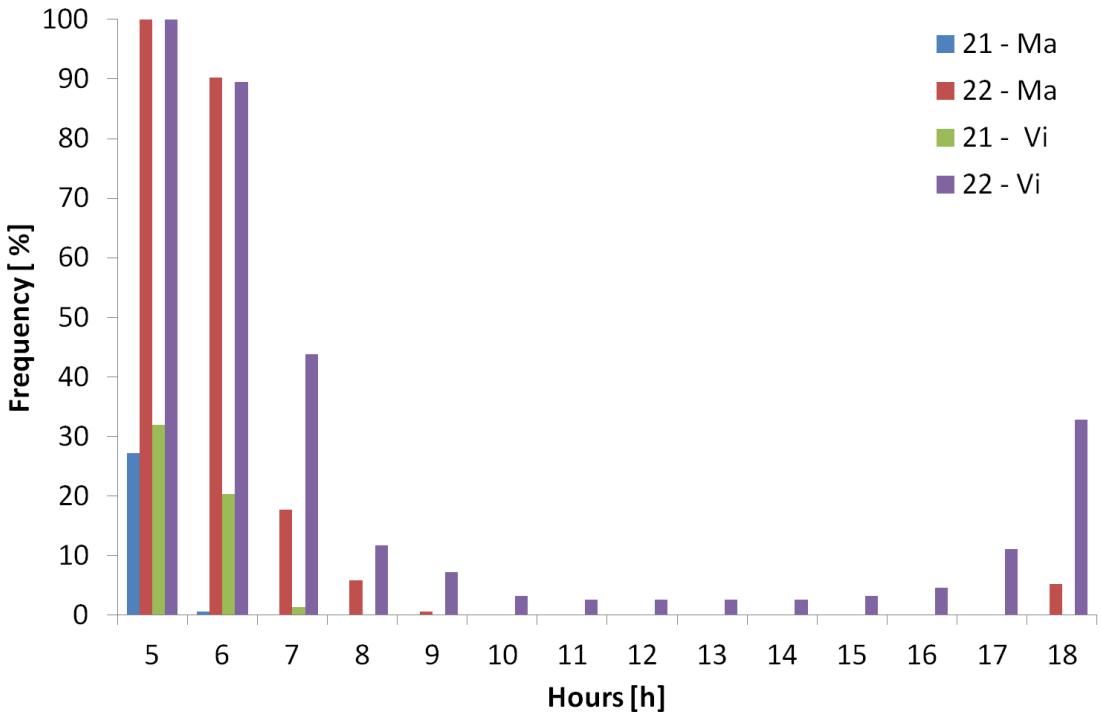

Figure 35 – Frequency of occurrences of hourly V_{oc}>800 V in the N-S structure.

5.3.3 Losses for the hybrid PV-grid irrigation system at constant power

Table 33 shows the PV energy losses of the hybrid PV-grid irrigation system at constant power in Villena (Vi) and Marrakech (Ma) for 20 to 22 PV modules in series and for the two values of $V_{DC_{BUS\_GRID}}$ in Table 29.

Table 33 – PV energy losses of the hybrid PV-grid irrigation system at constant power in Villena (Vi) and Marrakech (Ma) for 20 to 22 PV modules in series and for the two values of $V_{DC_{BUS\_GRID}}$.

	Losses [%]					
Number of PV modules	**20**		**21**		**22**	
$V_{DC_{BUS\_GRID}}$ [V]	**Vi**	**Ma**	**Vi**	**Ma**	**Vi**	**Ma**
566	0.77	0.88	1.89	1.10	2.52	1.70
587	1.30	4.07	0.87	0.56	2.23	1.03

The results show that, if the grid supplies 400 V (i.e.$V_{DC_{BUS\_GRID}}$= 566 V) for both Villena and Marrakech, the lowest losses correspond to 20 PV modules in series. In the case of 415 V (i.e. $V_{DC_{BUS\_GRID}}$=587 V), the losses are reduced, but not eliminated, with 21 PV modules in series. It is worth noting that the losses increase if the number of PV modules in series increases to 22. These results may seem surprising and will be discussed in section 4.

As the hourly frequency of the open-circuit voltage is the same as in the previous case, the number of occurrences of overvoltages at the input of the FC will also be very low here because the optimum configurations are restricted to 20 and 21 PV modules in series.

5.4 Discussion of the results

5.4.1 Stand-alone PV irrigation system to a water pool

The relationship between the PV energy losses and the number of PV modules in series in this application (Table 32) is as expected:

- For the same location, the losses are reduced when increasing the number of PV modules in series.
- For the same number of PV modules in series, the losses increase with the increase in the temperature of the location.

The most outstanding result is that, if between the FC and the motor-pump there is neither a long distance nor any filter, that means a voltage drop and the FC output is 400 V (i.e. $V_{DC_{BUS\_PUMP}}$ = 540 V), the PV energy losses are negligible even in locations with very high temperature such as Marrakech.

If we establish a reasonable allowable value for the losses at 1.25%, the losses are only relevant when the FC output is 415 V or 430 V (i.e. $V_{DC_{BUS\_PUMP}}$ equal to 561 V or 581 V respectively) and they are solved just by increasing the number of PV modules in series to 21 in both sites.

The solution of 21 PV modules does not merit more action in Marrakech because, as it has been shown in Figure 35, the number of occurrences of open-circuit voltages of more than 800 V is negligible. In the case of 21 PV modules in Villena, an action to protect the FC input against overvoltage is necessary, as there are occurrences of open-circuit voltages of more than 800 V during the irrigation period. A simple and reliable possible solution is described in section 5.

5.4.2 Hybrid PV-grid irrigation system at constant power

The results regarding hybrid PV-grid systems at constant pressure are not so evident and deserve an explanation. It was already mentioned that the PV energy losses in this system result from two different mechanisms, depending on whether the P_{MPP} available is higher than the constant power required by the irrigation system ($P_{p=cte}$) or not.

If $P_{MPP}>P_{p=cte}$, the losses will occur when the PV generator voltage for $P_{p=cte}$, $V_{DC_{PV\_p=cte}}$, is less than $V_{DC_{BUS\_GRID}}$, as shown in Figure 36 (a). It can be noted that these losses can be eliminated by increasing the number of PV modules in series because $V_{DC_{PV\_p=cte}} > V_{DC_{BUS\_GRID}}$.

If $P_{MPP}<P_{p=cte}$,the grid is constantly supplying power and, therefore, imposing the voltage of the FC DC bus ($V_{DC_{BUS\_GRID}}$). So, the losses will be the difference between the P_{MPP} and the power that the PV generator is able to deliver at $V_{DC_{BUS\_GRID}}$. These losses depend on the difference between $V_{DC_{BUS_GRID}}$and $V_{DC_{PV\_p=cte}}$ and can be reduced as well as being increased when varying the number of PV modules in series, as shown in Figure 36 (b).

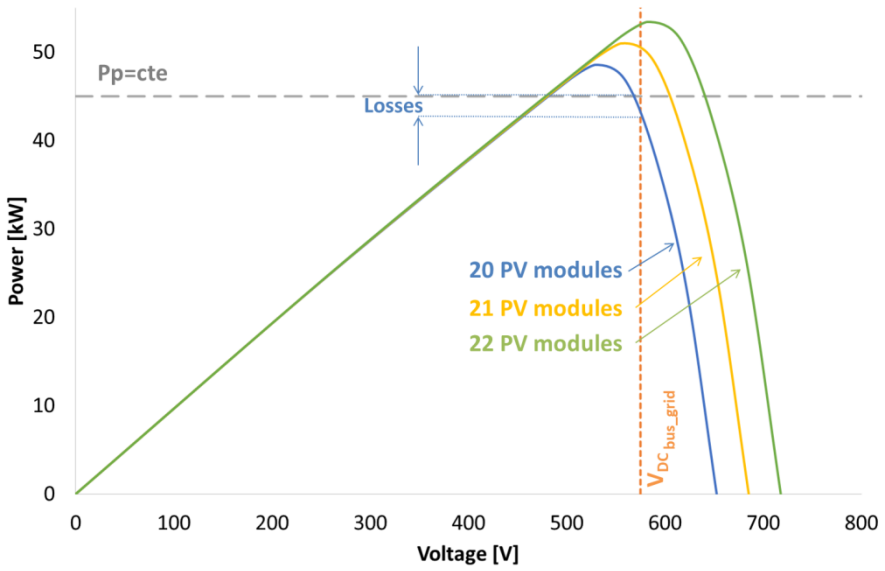

(a)

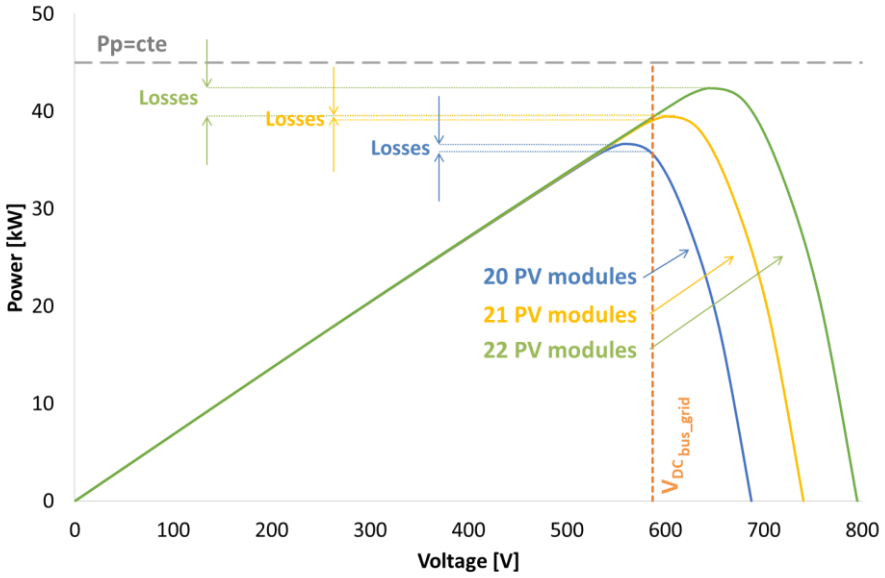

(b)

Figure 36 – PV energy losses: (a) Losses when $P_{MPP}>P_{p=cte}$ occur if the PV generator voltage for $P_{p=cte}$, $V_{DC_{PV\_p=cte}}$, is less than $V_{DC_{BUS\_GRID}}$, and they can be eliminated increasing the number of PV modules in series; (b) Losses when $P_{MPP}<P_{p=cte}$ depend on the difference between $V_{DC_{BUS\_GRID}}$ and $V_{DC_{PV\_p=cte}}$ and can be reduced but also increased when varying the number of PV modules in series.

To illustrate this, Table 34 shows the breakdown of the losses in these two mechanisms for the case of $V_{DC_{BUS\_GRID}} = 587$ V in Marrakech when increasing the number of PV modules.

Table 34 – PV energy losses of the hybrid PV-grid irrigation system at constant power in Marrakech (Ma) for 20 to 22 PV modules in series.

Number of PV modules in series	Losses $P_{MPP}> P_{p=cte}$ [%]	Losses $P_{MPP}< P_{p=cte}$ [%]	Total losses [%]
20	2.34	1.73	4.07
21	0.03	0.53	0.56
22	0.00	1.03	1.03

It is confirmed that the losses corresponding to $P_{MPP}> P_{p=cte}$ are reduced with the number of PV modules in series. However, in the case of $P_{MPP}< P_{p=cte}$ the losses are reduced when increasing the number to 21 PV modules but increase again with 22 PV modules. This behaviour is reflected in the total losses.

For a better understanding, Figure 37 shows the evolution of the losses throughout the irrigation period for this case depending on the number of PV modules in series. It can be clearly observed that while the losses associated to the temperature of the solar cell decreases with the number of PV modules in series (losses during the hottest months, July and August, decrease), the losses associated to the $V_{DC_{PV\_p=cte}}$ is further away from the $V_{DC_{BUS\_GRID}}$ increase (May, June and September).

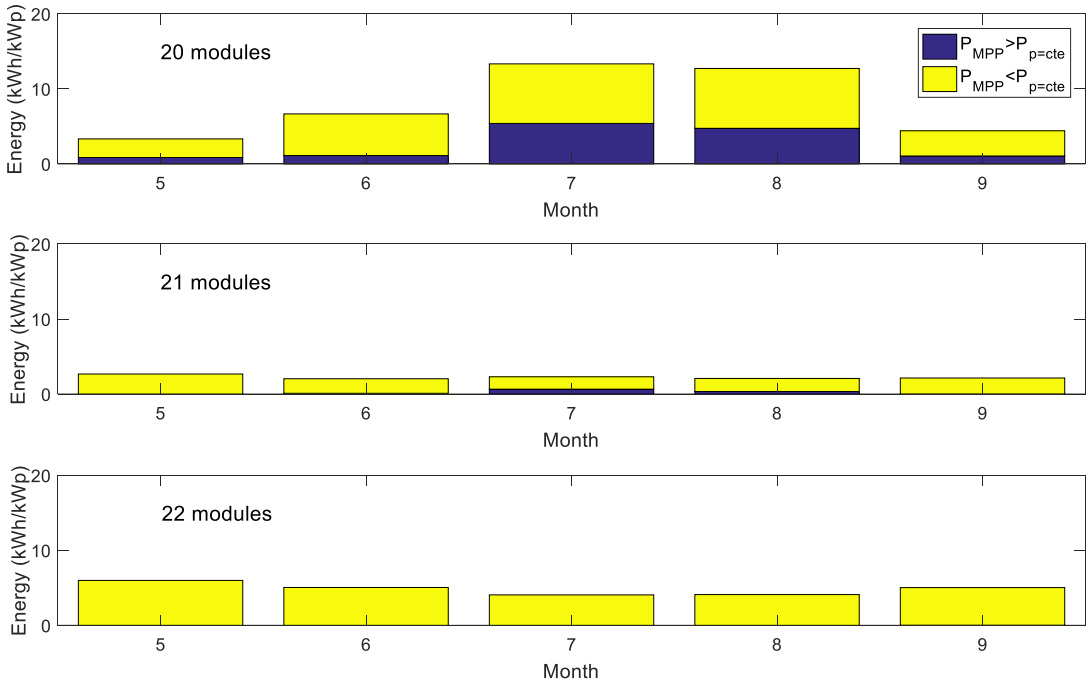

Figure 37 – Evolution of the losses along the year for the case of $V_{DC_{BUS\_GRID}}$ = 587 V for a hybrid PVIS at constant pressure in Marrakech and depending on the number of PV modules.

In conclusion, if the grid supplies 400 V (i.e. $V_{DC_{BUS\_GRID}}$= 566 V), the lowest losses correspond to 20 PV modules in series, so it makes no sense to increase the number of PV modules in series. When the grid supplies 415 V (i.e. $V_{DC_{BUS\_GRID}}$= 587 V), the losses are minimized with 21 PV modules in series.

5.4.3 Summary and generalization of results

In summary, the cases in which it is necessary to reduce the PV energy losses by increasing to 21 PV modules in series are detailed in Table 35 and Table 36 for the stand-alone and hybrid PV-grid irrigation systems respectively.

Table 35 – Optimum number of PV modules in series to reduce the losses at the FC input for the stand-alone PV irrigation system to a water pool.

	Number of PV modules	
$V_{DC_{BUS\_PUMP}}$ [V]	Vi	Ma
540	20	20
561	20	21
581	21	21

Table 36 – Optimum number of PV modules in series to reduce the losses at the FC input for the hybrid PV-grid irrigation at constant power.

$V_{DC_{BUS\_GRID}}$ [V]	Number of PV modules	
	Vi	**Ma**
566	20	20
587	21	21

In order to generalize the previous results, the dependency of the losses with the temperature of the location and with $V_{DC_{BUS\_GRID}}$ and with $V_{DC_{BUS\_PUMP}}$ has been analysed.

Figure 38 shows the losses in a stand-alone PV irrigation system to a water pool for $V_{DC_{BUS\_PUMP}}$ = 561 V depending on the temperature. The abscissa axis is expressed in terms of a temperature offset regarding the yearly mean maximum temperature in Villena (17.7ºC, see Table 31). As can be seen, a configuration of 21 PV modules in series does not show any losses until the temperature is increased in 7ºC.

Figure 39 shows the losses again for a stand-alone PV irrigation system to a water pool in Villena depending on $V_{DC_{BUS\_PUMP}}$. The figure shows that the losses start with $V_{DC_{BUS\_PUMP}}$ values of 550 V and 580 V for 20 and 21 PV modules in series respectively.

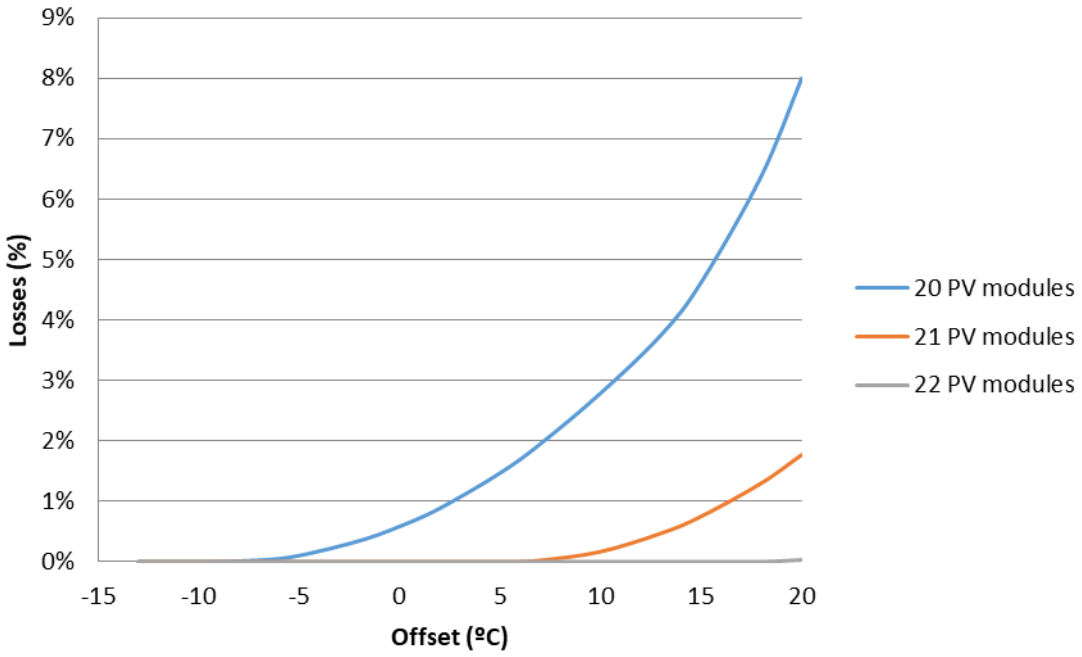

Figure 38 – Losses depending on the temperature of the location for a stand-alone PVIS to a water pool. The abscissa axis is expressed in terms of a temperature offset regarding the yearly mean maximum temperature in Villena.

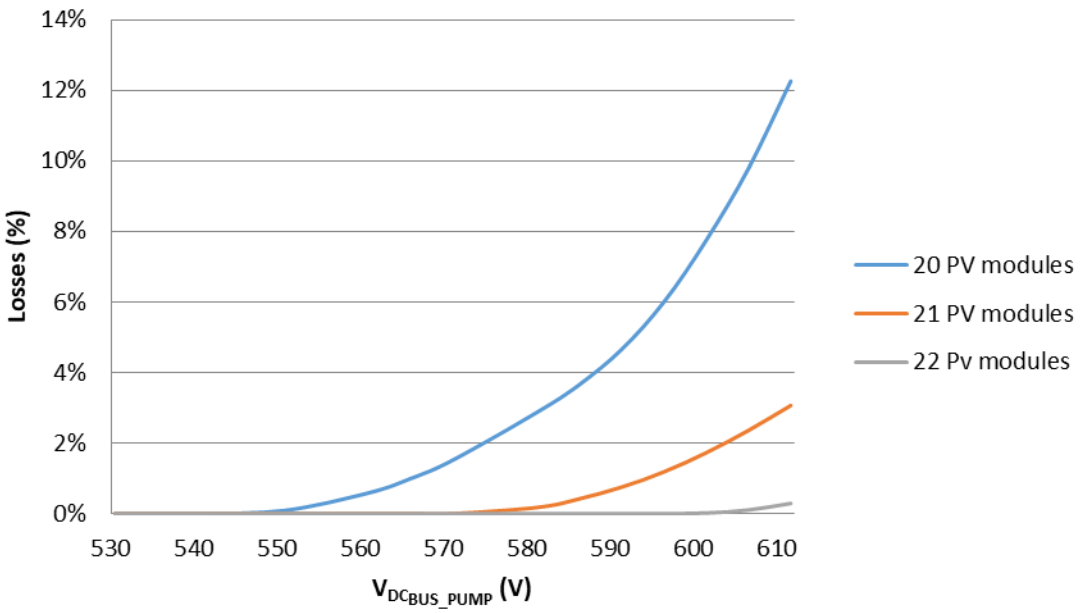

Figure 39 – Losses depending on $V_{DC_{BUS\_PUMP}}$ for a stand-alone PVIS to a water pool.

In a similar way, Figure 40 shows the losses in a hybrid PV-grid irrigation system at constant power depending on the temperature. As can be seen, the minimum losses with the different configurations of PV modules in series show a minimum that corresponds to an offset in the yearly mean maximum temperature regarding Villena of 2ºC for 20 PV modules and 18ºC for 21 PV modules. This figure can be seen as a tool for selecting the best configuration of PV modules in series depending on the yearly mean maximum temperature of a certain location where the system is going to be installed.

Figure 41 shows the losses again for a hybrid PV-grid irrigation system at constant power in Villena depending on $V_{DC_{BUS\_GRID}}$. The figure shows that the minimum losses with the different configurations of PV modules in series correspond to $V_{DC_{BUS\_GRID}}$ values of 575 V and 607 V for 20 and 21 PV modules respectively. So, this figure can be seen as a tool for selecting the best configuration of PV modules in series depending on the grid voltage to which the hybrid system is going to be connected.

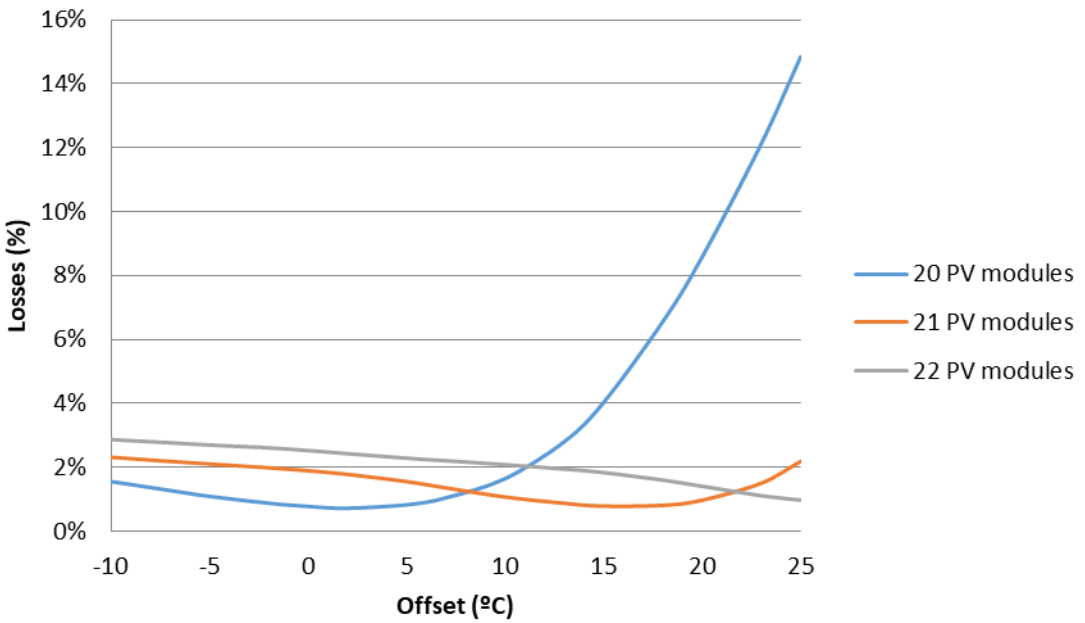

Figure 40 – Losses in a hybrid PV-grid irrigation system at constant power depending on the temperature. The abscissa axis is expressed in terms of a temperature offset regarding the yearly mean maximum temperature in Villena.

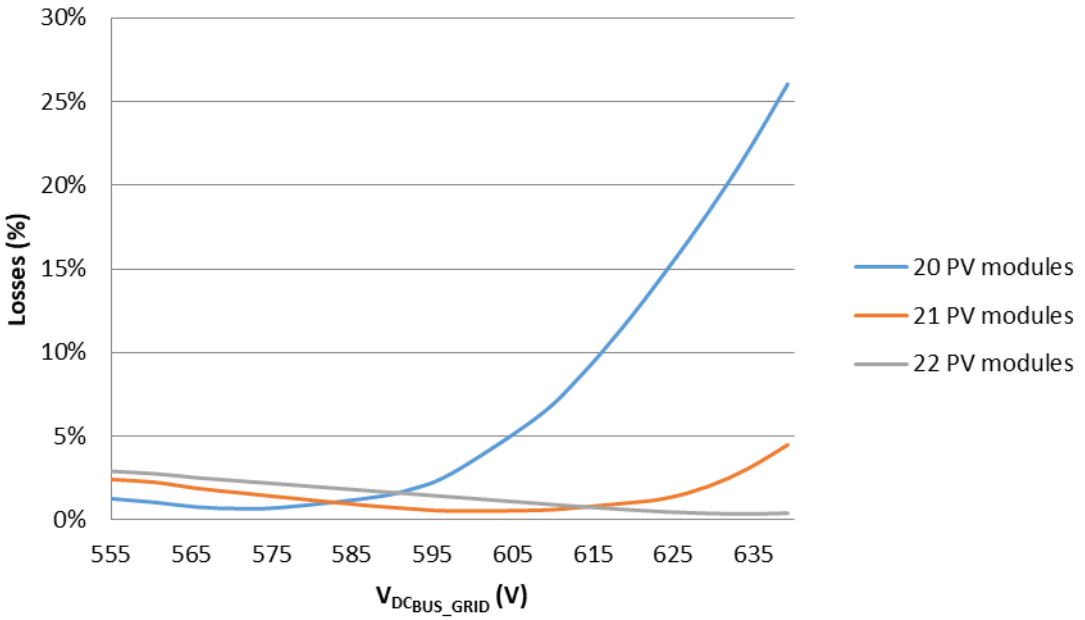

Figure 41 – Losses for a hybrid PV-grid irrigation system at constant power in Villena depending on $V_{DC_{BUS\_GRID}}$.

5.5 Design of solutions to avoid energy losses

Obviously, the best design solution would be to install the required number of PV modules in series together with an FC that allows higher voltages at its input, but it is not easy to find this kind of FC in the market.

Taking into account that the most voltages of more than 800 V are at sunrise, when the V_{OC} is higher but the PV-power available is very small, a simple, robust and reliable solution could be to avoid the PV generator being in open circuit by installing a small-power load from the sunrise till the V_{OC} is less than 800 V. Figure 42 shows a schematic of the solution.

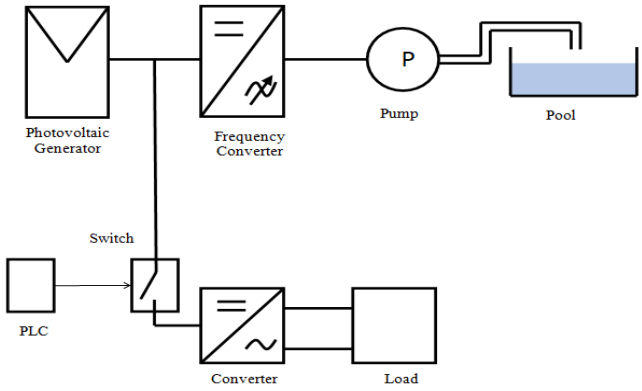

Figure 42 – Proposal of design to avoid overvoltages at the FC input when it is necessary to use 21 PV modules in series.

The concept is that a Programmable Logic Controller, PLC, evaluates the V_{OC} and the PV-power available, P_{MPP}. From the sunrise, when P_{MPP} is less than that needed to start pumping and the V_{OC} is more than 800 V, the PLC closes the switch to power the load. This load has typically 1% of the power of the pump but it is enough to establish an operating voltage of less than 800 V. Once there is incident irradiance on the PV generator that elevates the solar cell temperature, the V_{OC} decreases to less than 800 V, and the switch can be opened.

The main advantage of this solution is that it is very reliable and it is not dispersed throughout the PV generator that, in large sizes, can cover a great area with the associated difficulties in maintenance. Furthermore, this load could be the air-conditioning system that usually already exists to control the temperature of the FC box.

CHAPTER 6

A NEW PUMP SELECTION METHOD FOR LARGE-POWER PV IRRIGATION SYSTEMS AT A VARIABLE FREQUENCY

6.1 Introduction

The traditional way of selecting the appropriate pump is just to look for the pump that shows the highest efficiency just at this duty point (usually at 50 or 60 Hz) [134]. The objective of the pump selection procedure is to maximize the efficiency, i.e. that the duty point and the point of maximum efficiency are as close as possible. In fact, professional irrigator communities, in their maintenance tasks, periodically extract the pump from the well after a certain number of hours of operation and refurbish the impellers and/or diffusers or replace them with new ones, in order to increase the efficiency at the duty point even if this means reducing efficiency at other working points that are not used.

However, this usual way of selecting is not valid for PVIS because they work at different frequencies [135] and therefore at different working points [48], [54].

This chapter proposes a new way of selecting a pump suitable for PV irrigation applications at a variable frequency that is based on considering not only the efficiency at the maximum operating frequency but in the whole range of operating frequencies. This new method also allows considering pumps that widen the range of operating frequencies and, therefore, enlarge the daily number of hours of irrigation and increase the volume of water pumped during low irradiation periods.

As it influences the performance of the system, it not only describes the new method but also shows how it affects the final performance. For this, the yearly water pumped by two pumps selected with the traditional method [134] and with the new method proposed here has been simulated for three locations with different climatic conditions, showing the improvement in the performance associated to this new pump selection method.

The impact of the way of selecting a pump on the performance of the system is shown for PV irrigation systems pumping into a water pool but it can also be applied to direct pumping to

the irrigation network, which usually is carried out with sprinklers, pivots or drip systems. Direct pumping requires constant pressure and water flow which also means constant power. But the reality is that one single irrigation network includes several sectors with different values of constant pressure and water flow [135]. So, different powers are needed but, in this case, it does not depend on the instantaneous PV-power available but on the sector being irrigated [136]. In any case, the pump must also work at different frequencies and working-points.

This new method has been implemented in SISIFO [75] and this is also shown.

6.2 The traditional pump selection method

The following items need to be considered to select the appropriate pump for an irrigation system:

- The total manometric head (*HMT*) against which the pump must operate. The *HMT* is the addition of the static level of water in the well (H_{st}), the drawdown of the water level at a certain water flow, the friction losses in the pipes ($H_{friction}$)and the height of the water tank (H_{pool}) (see Figure 43). H_{st} is the level at which the free water surface is positioned in the well at zero pump flow. Frequently, H_{st} plus drawdown is called the dynamic level of water in the well (H_{dyn}). H_{dyn} is the level at which the water is positioned in the well at a determined flow. The relationship between H_{st} and H_{dyn} is a characteristic of each well and is mainly a function of the nature of the soil and the water veins contained therein.

- The maximum flow rate. This value is usually determined by the well and/or by the diameter of the pipes of the existing irrigation network.

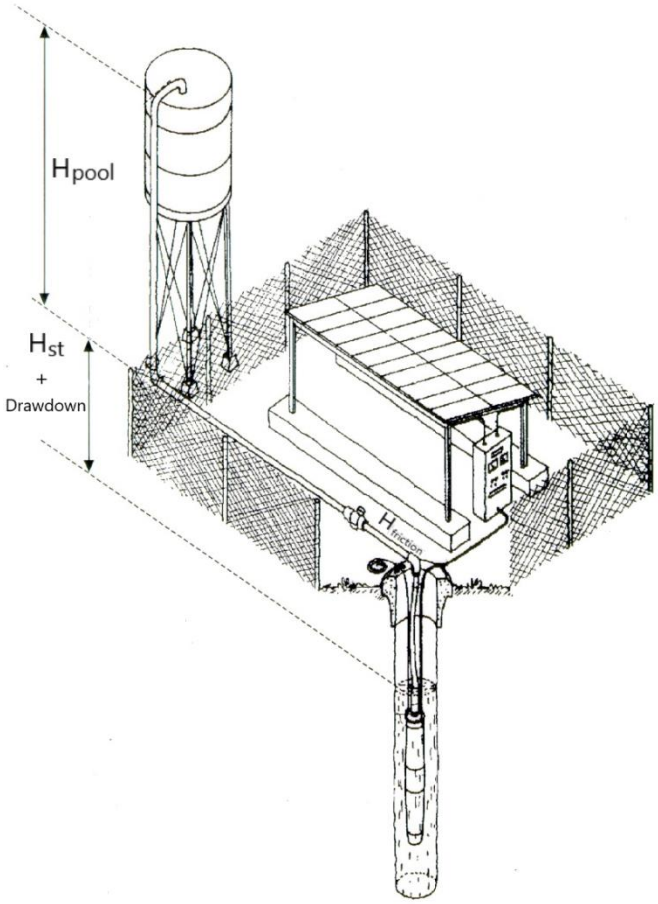

Figure 43 – PV pumping system from a well to a water tank. The figure illustrates the static head (H_{st}), the drawdown and the head of the water tank, (H_{pool}). The total manometric head is the addition of H_{st}, drawdown, H_{pool} plus the friction losses.

This information allows the system curve and the duty point to be identified. The "system curve" is a graphical representation of the relationship between the pumping head, taking into account the friction losses in the pipes of the irrigation system, and the flow rate. It is completely independent of the pump characteristics and its basic shape is parabolic. If H_{st} is zero, it will start at the point zero water flow (Q) and zero pumping head (H); otherwise the curve will be vertically offset from the zero to H_{st}. In a generic system curve this point is called the “geodetic head” and it represents the height between the water withdrawal point and the ground.

The duty point is the intersection between the *H-Q* curve of the pump and the system curve. Also referred to as the “operating point”, it indicates the values of H and Q that will be obtained at stationary operation with the respective speed-related pump *H-Q* curve and it is defined to be that point in the *H-Q* curve system for which a pump is to be selected.

In the traditional pump selection method, the objective is to minimize the deviation between the specified and the actual duty points, and to choose a pump with the best efficiency point

(BEP) as close as possible to the duty point (see Figure 44). BEP corresponds to the water flow which the hydraulic passages in the pump were designed for, where the speed of the fluid most closely matches the geometries of the impeller and the casing, where the pressure distribution around the impeller(s) is symmetrical and where hydraulic passage entry and exit are the smoothest.

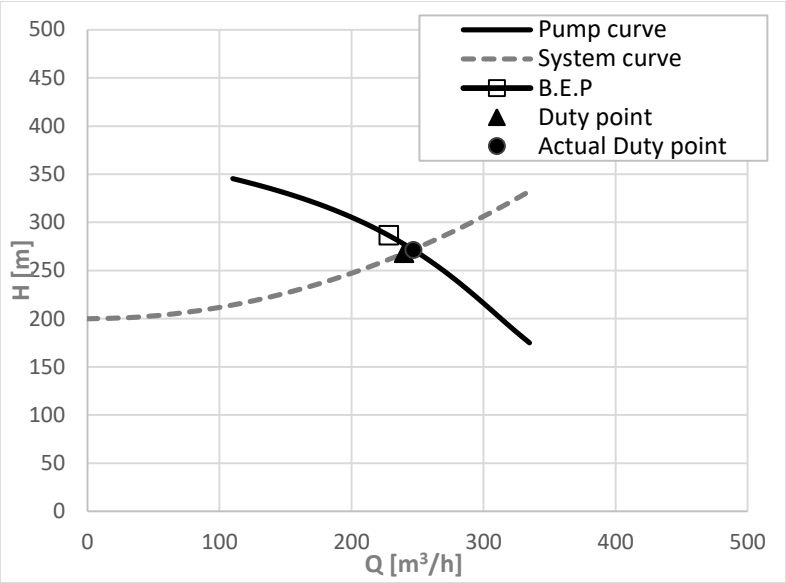

Figure 44 – System curve, *H-Q* pump curve and characteristic points to select a pump.

It is usually possible to find several pumps suitable for a specific duty point but, while the "correct selection" has its BEP in the proximity of the duty point, the other pumps may have it too far to the "right" or to the "left" of the duty point (see Figure 45).

According to the traditional pump selection method, pump B in Figure 45 is to be preferred because the BEP is close to the duty point. This pump should always be selected so that it operates predominantly close to the BEP in the so-called "preferred operating region" (Figure 46). This mode of operation is apt to bring about the lowest energy and maintenance cost and to reduce the risk of system problems since hydraulic excitation forces and cavitation risk attain a minimum close to the BEP [137]. Operating away from BEP moves the speed profiles away from this ideal, leading to compromised flow, inevitable turbulence and recirculation [138]. In the pump selection documentation provided by a pump manufacturer, normally, only the "Allowable operating region" is generally indicated while the "Preferred operating region" is generally derived from the efficiency of the BEP minus five points.

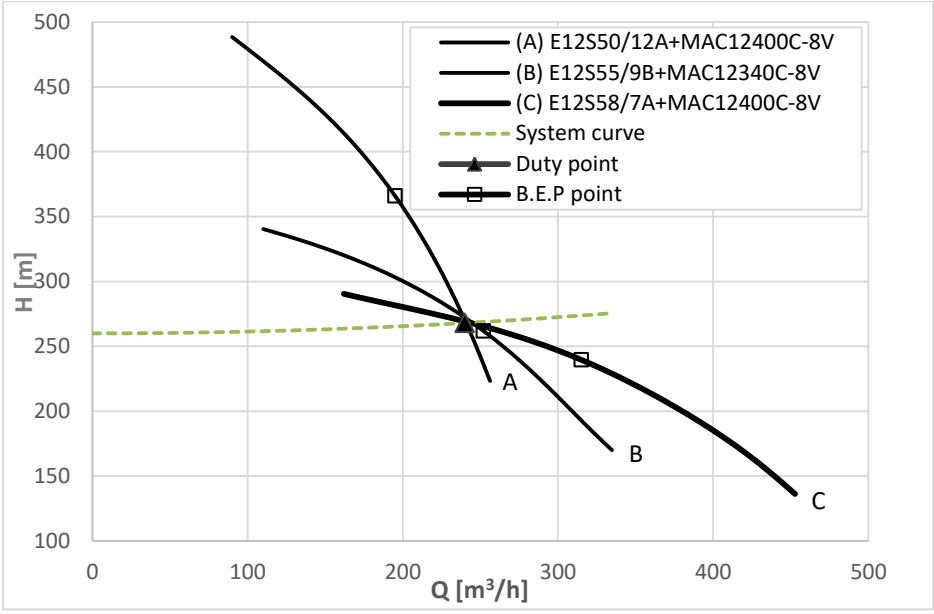

Figure 45 – Three possible pumps for a certain duty point. Pump A has its BEP too far to the left in respect to the duty point; Pump C has its BEP too far to the right in respect to the duty point. Pump B has the BEP close to the duty point and the pump would be the selected according to the traditional pump selection method.

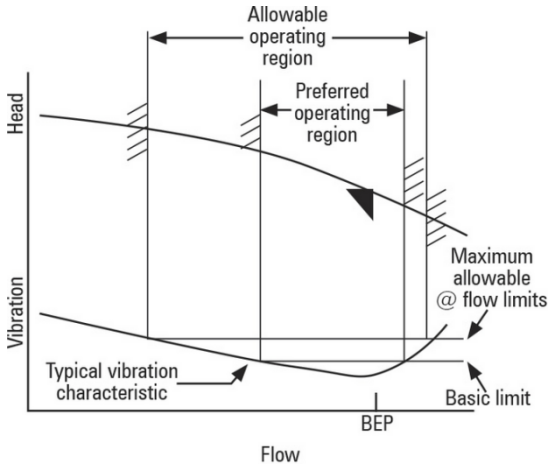

Figure 46 – Preferred operating region to bring about the lowest energy and maintenance cost and to reduce the risk of system problems since hydraulic excitation forces and cavitation risk attain a minimum close to the BEP [137].

A pump selected with the duty point in a low water-flow rate range (Pump C) may have problems due to increased internal turbulence, recirculation, increased pressure fluctuations and vibrations, increased axial and radial thrust, and rise in temperature due to the high internal energy loss. On the other hand, pump selected in proximity to the maximum allowable water-flow rate (Pump A) may have problems of cavitation.

To illustrate this method, let us imagine a case in which it is necessary to pump a water flow of Q= 227 m^3/h from a deep well to a water pool with a total manometric head of 288 m (H_{st}= 270 m and drawdown plus friction losses of 18 m).

The next step is to use any of the tools that the different pump manufacturers offer to select the most suitable pump for this duty point. We will use the PumpTutorNG tool, offered by Caprari [134] but the procedure would be similar with any other tool.

Once the *H*-*Q* duty point is introduced, the tool presents the possible pumps that could work at this point. It can be observed in Figure 47 that the tool itself presents the list of suitable pumps ordered according to their efficiency, which shows that this is the main criteria when selecting a pump. In this case, the pump with the best efficiency at this duty point (79.3%) is the E12S55/9B+MAC12340C-8V model. Figure 48 shows the *H*-*Q* curves of the different possible pumps, in which the one with the best efficiency is highlighted.

Pump	Model	Code	Speed [1/min]	Frequency [Hz]	DNm [mm]	Efficiency [%]	P2 max [kW]	M.E.I.
	E12S55/9B+MAC12340C-8V	823597	2900	50		79,3	232,8	
	E12S55/9Q+M14330-8V	823299	2900	50		79,3	240	
	E10S55/15A+MAC12340C-8V	823593	2900	50		78,8	224,5	
	E12S42/6P+MAC12340C-8V	823604	2900	50		78,3	231,8	
	E12S42/6P+M14330-8V	822775	2900	50		77,6	235,3	
	E12S50/11A+MAC12340C-8V	823595	2900	50		76,1	227,2	
	E12S58/8AB+M14380-8V	823304	2900	50		74,8	278,2	
	E12S58/8AB+MAC12400C-8V	823637	2900	50		74,3	275,9	
	E14SE50/6W+M14430-8V	822784	2900	50		68,3	312,8	
	E14SE50/6W+MAC12475C-8V	823613	2900	50		68,2	308,7	

Figure 47 – List of the suitable pumps offered by PumpTutorNG tool for the duty point *H*= 288 m and *Q*= 227 m^3/h.

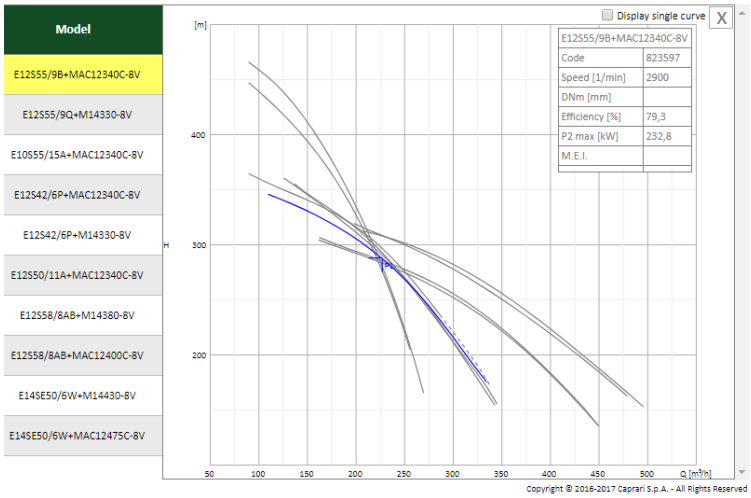

Figure 48 – H-Q curves of the pumps offered by PumpTutorNG tool for the duty point *H*= 288 m and *Q*= 227 m^3/h.

There is another pump model with the same high efficiency, E12S55/9Q+M14330-8V but it demands slightly more power, so from a technical point of view, the final selected pump

would be the E12S55/9B+MAC12340C-8V leaving the final decision down to economic aspects.

6.3 The new selection method for PV irrigation systems at a variable frequency

When working with PVIS at a variable frequency, by means of a frequency converter, it is possible to vary the rotation speed of the pump by adjusting the operating frequency according to the PV-power available. So, it must be assured that, first, the selected pump is able to work at a wide range of frequencies for a certain irrigation system and, second, between a range of high efficiencies. These conditions are satisfied if the pump has an H-Q curve with a high slope to allow a wide range of intersection points between the system curve and the H-Q curves of the pump at different frequencies. So, the new pump selection method would have the following four steps:

a. To select the pumps with an *H-Q* curve at 50 Hz with the greatest slopes from those that can work at a certain duty point.
b. To select the pumps (from the previous ones) in which the duty point is in the "right-hand third" of the *H-Q* curve. The duty point at this position, together with its great slope, will allow a wide range of operating frequencies.
c. To identify the lowest operating frequency at which the pump is able to elevate water into the pool. It will be defined by the *H-Q* curve with the lowest frequency that intersects with the system curve. The pumps with the lowest frequencies will be preferable, as they will allow a wider range of operating frequencies.
d. To select the pump with the best efficiency between those fulfilling the previous steps.

Let us illustrate this method by applying it to the example set out in the previous section.

a) To select the pumps with an H-Q curve at 50 Hz with the greatest slopes

The two pumps with the greatest slopes from among those that cover the duty point are those marked in blue in Figure 49. They are the models E10S55/15A+MAC12340C-8V and E12S50/11A+MAC12340C-8V. Observe that, in the first one, the ratio between the lowest (200 m) and the highest pumping head (460 m) is 2.3, while in the second one is 2.0 (from 215 m to 430 m).

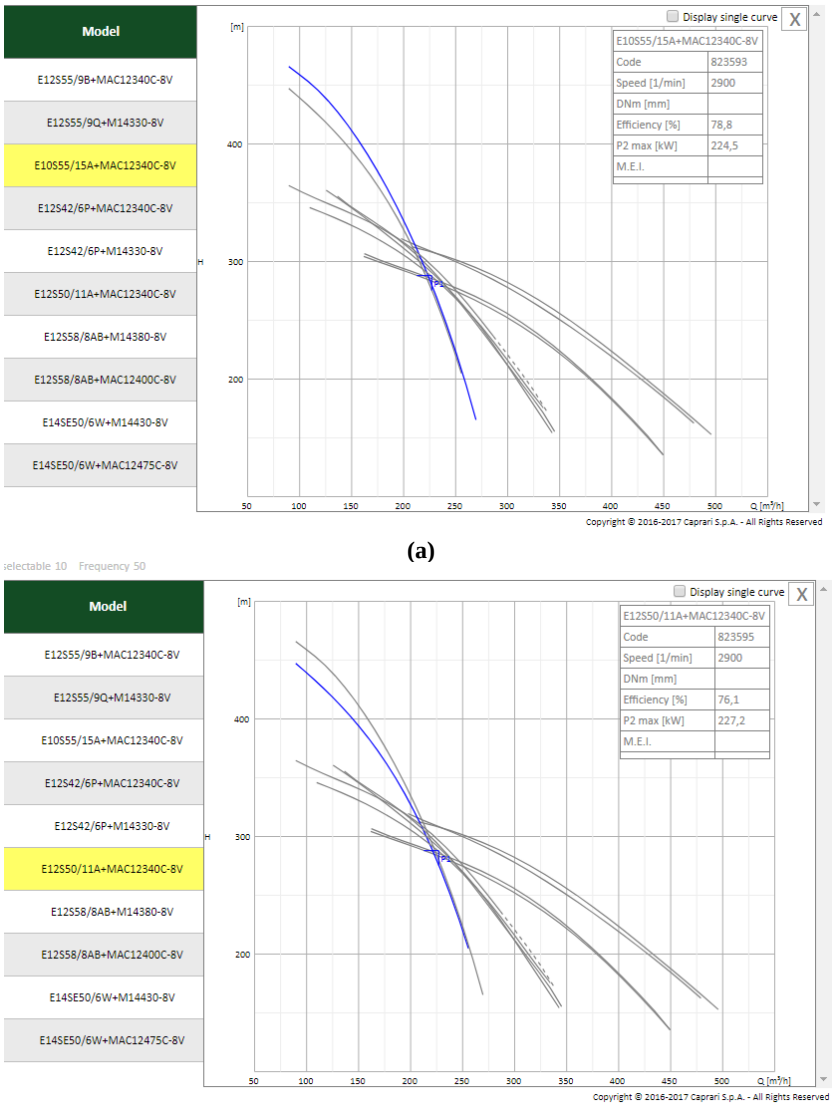

Figure 49 – Pumps with the highest slope. The E10S55/15A+MAC12340C-8V (a) and E12S50/11A+MAC12340C-8V (b) models show the ratio between the lowest and the highest head of 2.3 and 2.0 respectively.

b) To select the pump with the duty point in the right-hand third of the H-Q curve

Figure 50 shows the *H-Q* curve of both pumps in detail. They differ slightly in the slope and the efficiency curve but both of them have the duty point (marked as P1 in Figure 50) in the right-hand third of the *H-Q* curve.

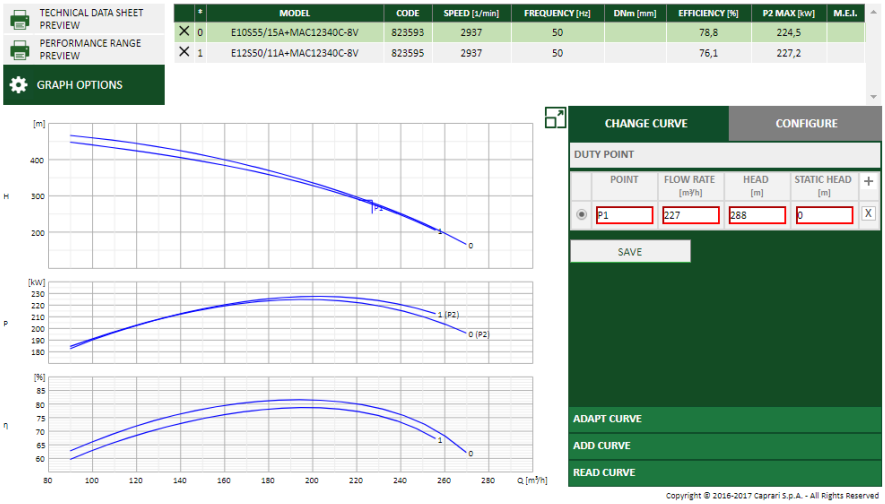

Figure 50 – Detail of the H-Q, power-Q and efficiency-Q of both pumps. In both cases, the duty point is in the right-hand third of the H-Q curve.

c) To identify the lowest operating frequency at which the pump is able to elevate water into the pool

The procedure for finding the lowest frequency that allows pumping with a certain pump consists of drawing the system curve together with the pump H-Q curve at different frequencies. The pump *H-Q* curves crossing the system curves correspond to frequencies that allow pumping. The lowest operating frequency is that whose H-Q curve is tangent to the system curve.

The minimum frequency for pumping in the case of E10S55/15A+MAC12340C-8V is 38 Hz, as shown in Figure 51 (a), while in the case of E12S50/11A+MAC12340C-8V it is 39 Hz, as shown in Figure 51 (b).

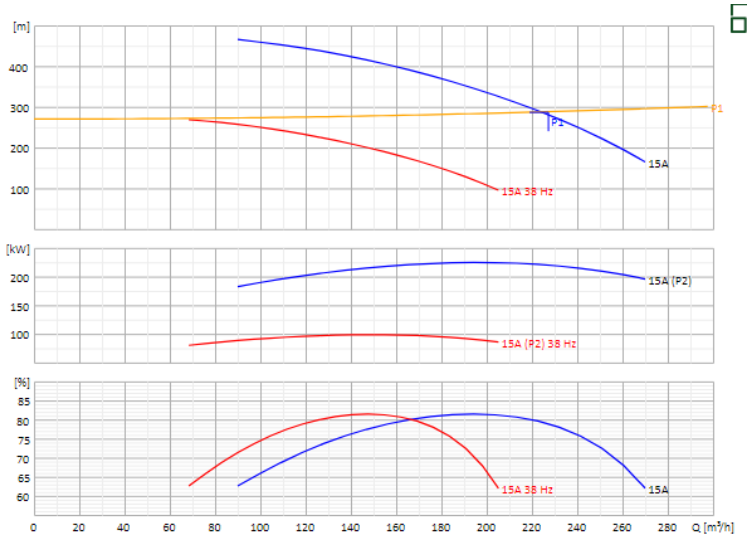

(a)

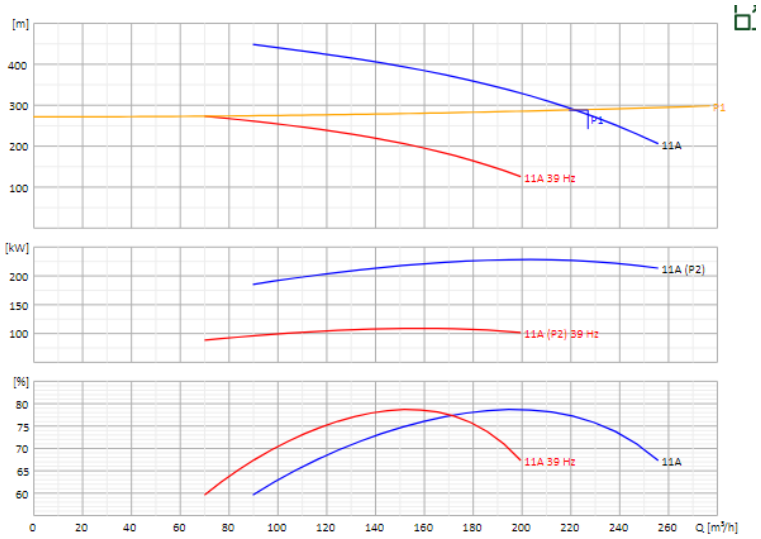

(b)

Figure 51 – Determination of the lowest operating frequency for the E10S55/15A+MAC12340C-8V pump (a) and the E12S50/11A+MAC12340C-8V pump (b). The values are 38 Hz and 39 Hz respectively.

d) To select the pump with the best efficiency

The efficiency of a pump depends on the operating frequency. So, in order to analyse the efficiency, it is necessary to evaluate its values at different frequencies. Obviously, in the design stage, the necessary data to evaluate the energy efficiency are not available. So, for design purposes, we will evaluate the power efficiency at four different operating frequencies (maximum, η_{max}, minimum, η_{min}, and two intermediate frequencies, η_{int1} and η_{int2}) and we define an energy "Irrigation efficiency", EFF_{IRR}, in accordance with the following equation:

$$EFF_{IRR} = 0.125\,\eta_{min} + 0.125\,\eta_{int1} + 0.25\,\eta_{int2} + 0.50\,\eta_{max} \qquad \text{(Eq. 36)}$$

Figure 52 (a) and (b) shows the efficiency curves at the aforementioned frequencies for both pumps. Only the efficiency values for 50 Hz are shown but the procedure is similar for the rest of the frequencies. By applying Eq. 36, the resulting EFF_{IRR} for both pumps are shown in Table 37.

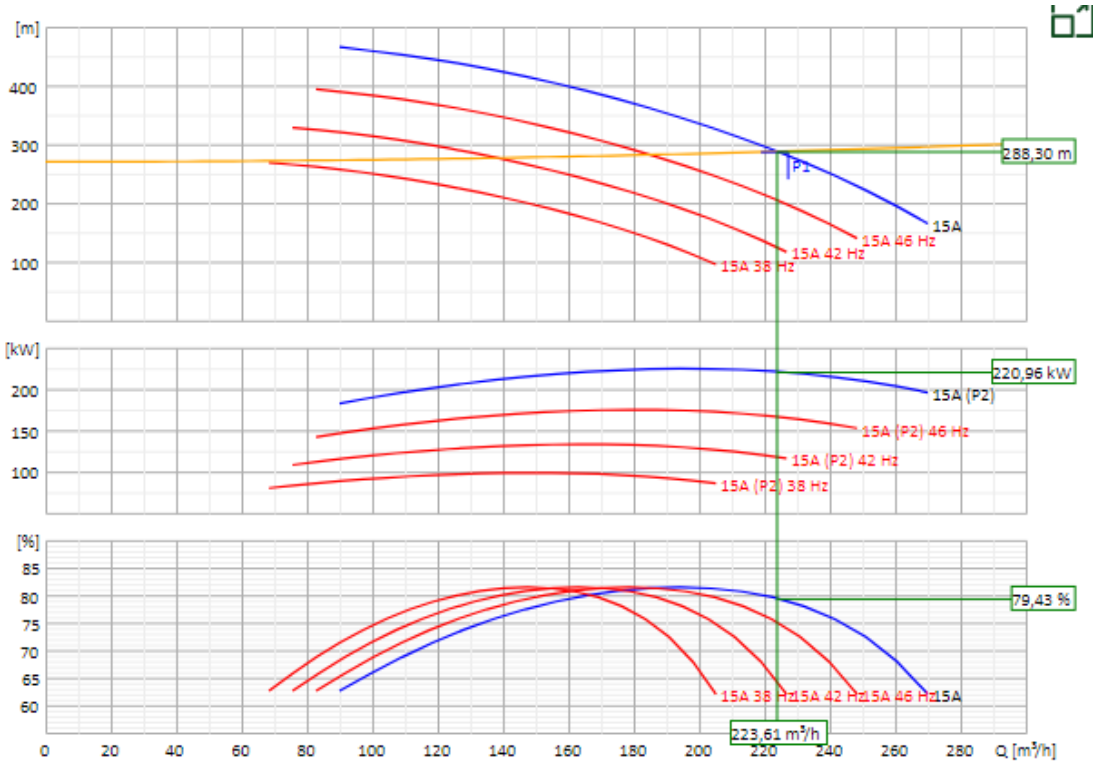

(a)

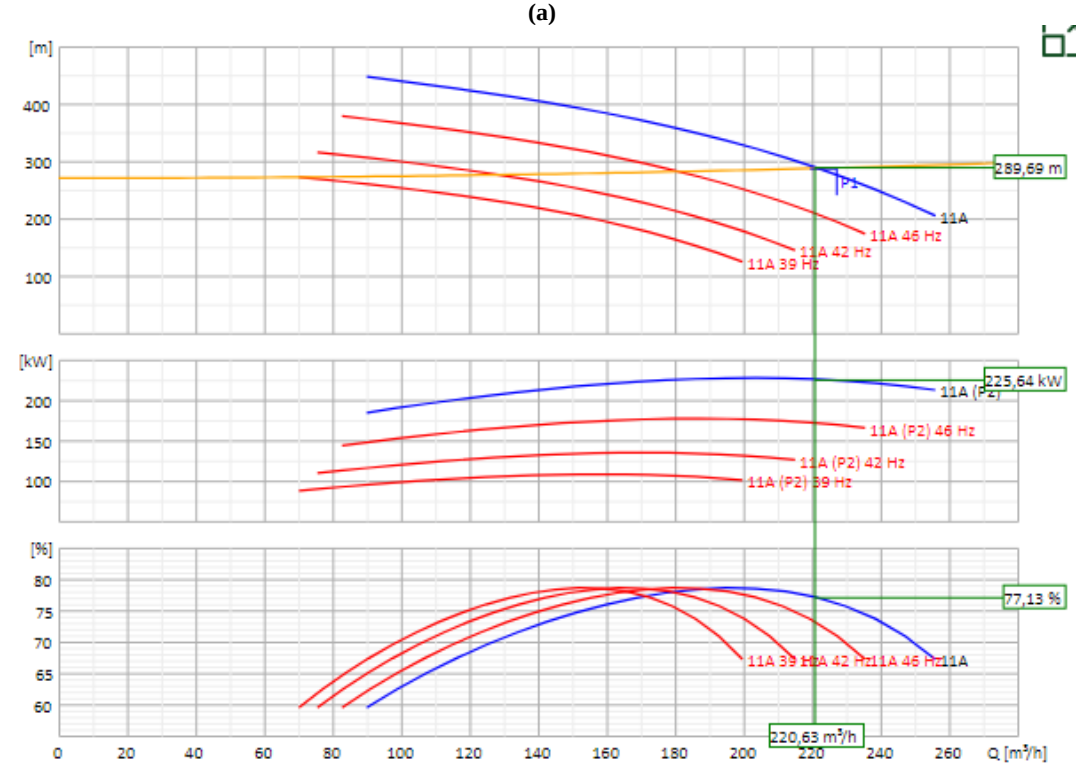

(b)

Figure 52 – H-Q, power-Q and efficiency-Q curves at the frequencies used to calculate EFF_{IRR} for the E10S55/15A+MAC12340C-8V pump (a) and the E12S50/11A+MAC12340C-8V pump (b). Only the efficiency values for 50Hz are shown but the procedure is similar for the rest of the frequencies.

Table 37 – Values of the pump efficiency at the four frequencies used to calculate EFF_{IRR}.

	E10S55/15A+MAC12340C-8V	**E12S50/11A+MAC12340C-8V**
η_{max} [%]	79.43	77.13
η_{int2} [%]	81.29	78.53
η_{int1} [%]	79.93	74.87
η_{min} [%]	63.18	60.36
EFF_{IRR} [%]	**77.93**	**75.10**

According to the results, the selected pump would be the E10S55/15A+MAC12340C-8V with a EFF_{IRR} of 77.93% and a frequency range from 38 Hz to 50 Hz.

It is interesting to note that the efficiency of the pump selected with the traditional method (E12S55/9B+MAC12340C-8V) is EFF_{IRR} = 75.01% and the frequency range is from 44 Hz to 50 Hz.

Accordingly, with the new proposed method, the range of working frequencies is higher than that of the traditional one, and the EFF_{IRR} is also better. Although the pump may work in a low water-flow region further away from the BEP, the low water-flow problems highlighted in section 2 are not expected to happen because this condition only occurs for limited periods at a low rotation speed, at a lower power and with a lower pump operating pressure than at the duty point. Furthermore, although the duty point in this new method is in the right-hand third of the pump H-Q curve and, therefore, working at a high-water flow, it is far from the maximum allowable water flow limit and still within the preferred region of operation. So, cavitation is not likely to occur. Moreover, the selection of the duty point to the right of the BEP allows the pump to work at a high efficiency even at reduced frequencies, working at low efficiency only at extremely low frequencies that occur just for a limited time, in the start-up phase at sunrise and in the shutdown phase at sunset.

6.4 Pump selection method and PV irrigation system performance

The comparison of the performance of the same PV irrigation system with the two pumps selected with both the traditional and the proposed method is carried out using the SISIFO tool [75] with irradiation values for Madrid from the PVGIS database [90].

The main characteristics of the components of the system are summarized in Table 38 together with the main information of the hydraulic system curve. For the PV generator, we have used the M Prime 3R PLUS of 250 Wp PV modules mounted on a North-South

horizontal axis tracker with backtracking to avoid mutual shadows, a ground cover ratio of 1/3 and a maximum rotation angle of 45°.

Table 38 – PV generator size, inverter and pumping characteristics.

Parameter	Value/ option
PV generator size [kWp]	360
Nominal power of the FC [kW]	315
Type of PV irrigation system	Stand-alone
Type of pumping	Water pool
Static head [m]	270
Friction losses at rated flow [m]	18
Working flow [m^3/h]	227

Table 39 details the results of the performance of both pumps, in terms of volume of water per kWp of nominal power of the PV generator and in terms of the annual efficiency of the pump. Figure 53 shows the monthly volume of water pumped with both pumps.

Table 39 – Performance and annual efficiency of both pumps, that selected with the new method proposed here and that selected with the traditional method.

Parameter	Proposed method E10S55/15A+MAC12340C-8V	Traditional method E12S55/9B+MAC12340C-8V
Performance [m^3/kWp]	1779	1476
Annual pump efficiency [%]	78.54	75.27

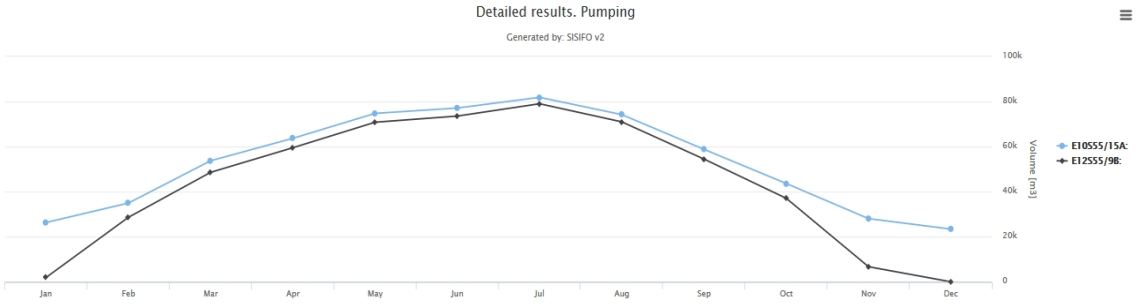

Figure 53 – Monthly yield with both the proposed pump and the traditional one.

The results show that the proposed pump selection method translates into an increase in the performance of 20.5%. This increase is basically due to the wider range of operating frequencies that allows the daily hours of pumping to be expanded and the increase in the pump efficiency of 4.3%. To illustrate this, Table 40 shows the comparison of the time and water flow of both pumps at the start, at the duty point and at the end during the characteristic days of the months of May, June and July. It can be observed that the E10S55/15A+MAC12340C-8V (Pump A in Table 40) has a longer period of pumping and higher daily volume of water pumped due to its wider range of operating frequencies.

Table 40 – Performance comparison of the pumps selected with the new (Pump A: E10S55/15A+MAC12340C-8V) and the traditional method (Pump B: E12S55/9B+MAC12340C-8V) in the characteristic days of the months of May, June and July.

Charac-teristic day	Pump	Start		Duty point		End		ΣQ
		h [hh:mm]	Q [m³/h]	h [hh:mm]	Q [m³/h]	h [hh:mm]	Q [m³/h]	[m³]
May	A	5:57	91	9:01 – 11:11	219-220	17:59	91	**2412**
	B	6:14	111	9:15 – 10:42	219-220	17:41	111	**2287**
June	A	5:39	91	8:28– 14:40	219-224	18:16	91	**2571**
	B	5:57	111	8:35 – 14:22	219-224	17:58	111	**2452**
July	A	5:41	91	7:55 – 15:31	219-231	18:14	91	**2641**
	B	5:57	111	8:00 – 15:24	219-233	17:58	111	**2552**

Pump B requires a higher power threshold to start pumping and, therefore, in the one hand, pump A has a longer daily period of pumping as seen in Table 40, and in the other hand pump A pumps more water in the winter months with less mean irradiation, as seen in Figure 53. This is the main reason why pump B has less annual energy efficiency (75.27%) than pump A (78.54%) even when their power efficiency at the maximum operating frequency are more similar (pump B: 77.13 % and pump A: 79.43%). These similar efficiency values of at the maximum operating frequency are also the reason for having similar water flows at the duty point.

A similar simulation has been performed for Marrakech (Morocco) and Nice (France), two different locations in terms of latitude, total annual solar radiation and ambient temperature, both in the Mediterranean zone. The comparative results between pump A and pump B show an increase in the pumped water of 7.2% for Marrakech and 21.0% for Nice as well as an increase in the pump efficiency of 4.3% for Marrakech and 5.3% for Nice. These differences are presented in Table 41 and the variation in the performance is mainly due to the latitude: the higher the latitude, the higher the increase in the performance. This is due to the North-South tracker used in large-power PVIS that performs better in winter for latitudes closer to the equator. This way, the power threshold to elevate water with Pump B is reached more frequent in winter months in Marrakech but, even in this case, the increased volume of pumped water is 7.2%.

Table 41 – Increase in the pumped water and efficiency obtained with the pump selected with the new method proposed here for to other locations: Marrakech and Nice.

Parameter	Marrakech (Morocco)	Nice (France)
Increase in the pumped water [%]	7.2	21.0
Increase in the pump efficiency [%]	4.3	5.3

The previous results illustrate the advantages of the new pump selection method for PV irrigation applications, but it is worth highlighting that a totally correct pump selection from all points of view also requires other factors to be considered that generally contribute to the selection: type of pump, construction materials, type of water to be pumped, characteristics of the well and of the irrigation system. The most important one is the resistance to wear in case of water with silt/sand. Only a skilled pump technician can identify the most suitable pump in these cases. Another important factor for submersible pumps is the variability with time of the water table in the well: if the water table decreases every year, for example, due to overexploitation of the well, it will be necessary to consider the current hydraulic conditions to select the pumps as well as future ones. In conclusion, this new pump selection method means an alternative basis for the correct design of PVIS but it will not substitute the validation of an expert pumping technician.

6.5 Implementation in SISIFO

This new pump selection method has already been implemented in the SISIFO tool. Once the duty point is defined, it allows the user to opt for the tool to show just the pumps with a high slope, all pumps that work at the duty point or just specific pump models introduced by the user. In any case, SISIFO shows the *H-Q* curves of the shown pumps for the user to check their slope and the relative position of the duty point. Thus, the user will be able to apply the pump selection method proposed here (see Figure 54).

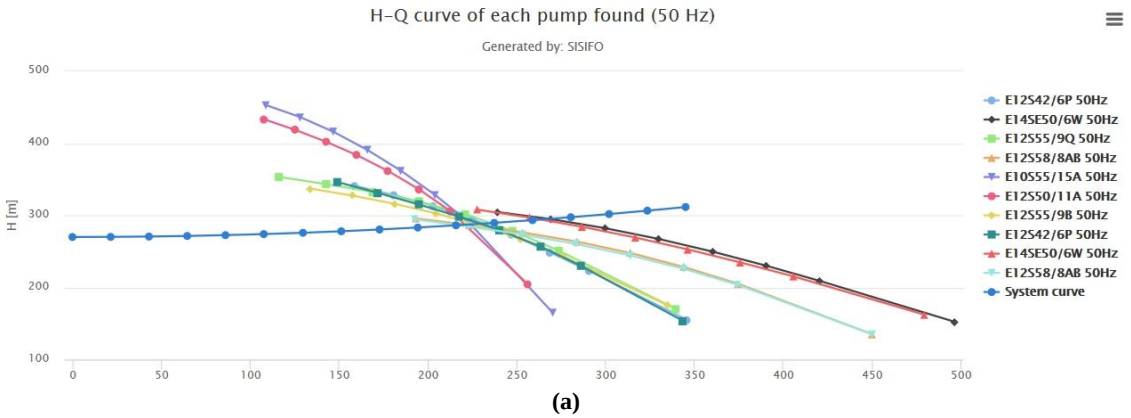

(a)

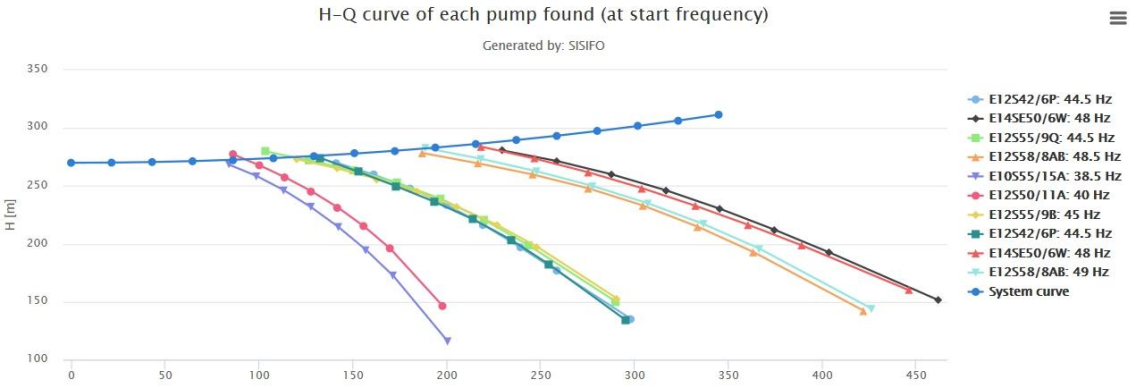

(b)

Figure 54 – Comparison of the H-Q curves of several possible pumps for a certain duty point as shown by SISIFO – curves at 50 Hz are shown in (a), while the ones at start frequency are in (b). The system curve is also included.

Moreover, SISIFO allows the simulation of the whole PVIS in a certain location with just the selected pump or with a set of possible pumps for comparing their performance. SISIFO delivers the total volume of water as output during the whole year or during an irrigation period defined by the user. It also allows the monthly, daily or hourly water pumped in the characteristics days of the months of interest to be compared (Figure 55). Thus, from the base of the proposed pump selection method, fine-tuning of the selection is possible.

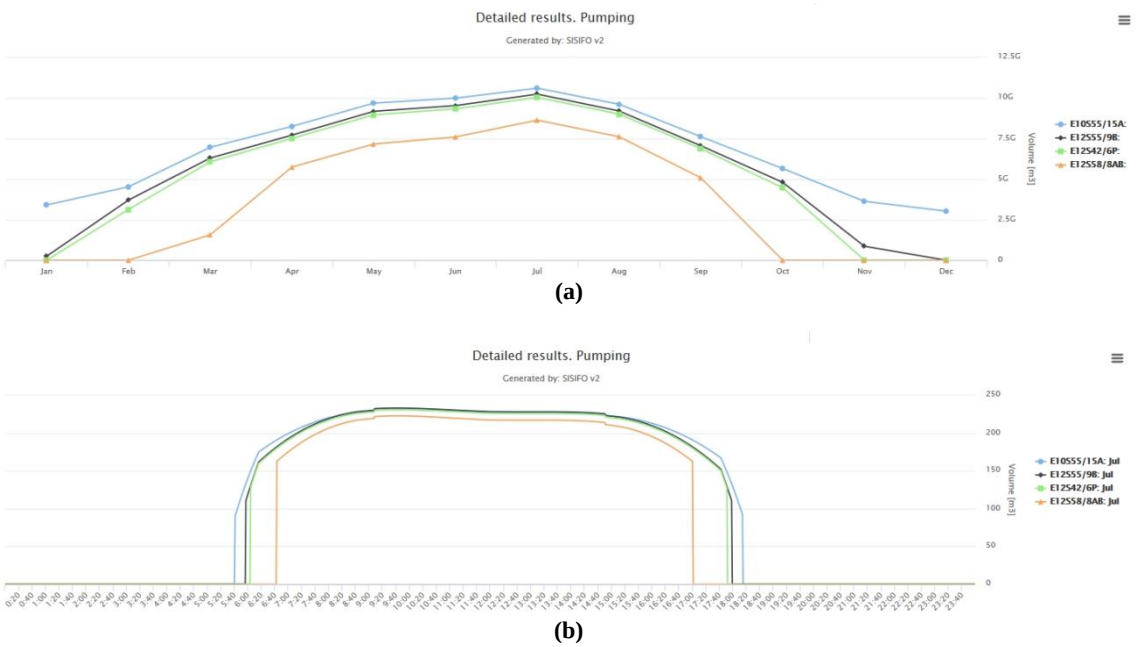

(a)

(b)

Figure 55 – Comparison of the volume of water pumped by four possible pumps during (a) the twelve months of a year and (b) during the pumping hours of the characteristic day of July.

The implementation of this method in SISIFO integrates the usefulness of the traditional tools for selecting pumps, usually offered by pump manufacturers, and the possibility of simulating the performance of PV irrigation systems by considering the variable water-flow depending on the PV-power available.

CHAPTER 7

CONCLUSIONS AND FUTURE RESEARCH LINES

7.1 Conclusions

The aim of this thesis was the development of technical solutions for the reliable and efficient performance of large-power PV irrigation systems (PVIS). These technical solutions have been applied to the design and implementation of two real-scale large-power hybrid PV drip irrigation systems – a 140 kWp hybrid PV-diesel system in Alter do Chão (Portugal) and a 120 kWp hybrid PV-grid in Tamelalt (Morocco). Both systems were installed in pre-existing irrigation facilities of ELAIA, which is part of Sovena Group, one of the biggest producers of olive oil in the world and that has all of the value chain form the cultivation of olive trees till the commercialization of the olive oil. Accordingly, the systems represent the complexity of the irrigation infrastructures of modern agro-industries.

The main technical solutions developed included:

- a way to solve the problems associated with PV-power intermittences – in the case of Portugal through tuning procedures in the frequency converter, in the case of Morocco with the electric hybridization;
- the match of PV production and irrigation needs with the use of a North-South horizontal axis tracker in both systems;
- the integration of the PV system into the pre-existing irrigation system – this meant that a deep understanding of the irrigation system was needed for the correct design of the system. For example, in Portugal, the irrigation network was designed in such a way that the number of irrigation hours per day is higher than the number of sun hours during some months of the year which meant that the best solution is the use of a hybrid system.

A description of the previous and current systems is carried out for both systems, which can currently work in three different operating modes: “Only PV”; “Hybrid”; and “Only-Diesel”/“Only-Grid”. Then, a performance analysis of two simulated Scenarios (an Optimistic and a Pessimistic) is performed. The hybrid systems have been in routine operation since 2016 and two years (2017 and 2018) of full monitoring data are available. These data allowed

the development of new performance indices in the PV field specifically designed to the specific characteristics of a PVIS, as well as a technical and economic validation of these particular systems and of the solution of large-power hybrid PVIS in general.

The following set of indices to evaluate the design and operation of hybrid PV systems were proposed: the PV share (*PVS*), the PV performance ratio (*PR*), and the hydraulic efficiency (η_{Hyd}). Regarding the *PVS*, a hybrid diesel ratio is defined and a new *PVS*, the PVS^{H}, is calculated with the objective of knowing the PV share considering only the "Only PV" and "Hybrid" modes.

In what concerns the *PR*, the typical *PR* of a grid-connected PV system does not allow a full understanding of a PV irrigation system. This happens since the performance of a PVIS is not only influenced by the technical quality of the PV system components and by the efficient use of the available irradiation but by the characteristics of the irrigation system and also external circumstances influencing a PVIS. For example, the power threshold to start pumping can be seen as a factor which is a consequence of the irrigation system, while the availability of water can be seen as an external circumstance.

So, the typical *PR* is kept but it is factorized in 4 different indicators (PR_{PV}, UR_{IP}, UR_{PVIS}, UR_{EF}) in order to distinguish the losses corresponding to four different reasons. The first one, the PR_{PV}, is the one which considers only losses strictly related to the PV system itself. The UR_{IP} is intrinsic to a given crop and gives an idea of the losses associated with the irrigation period. The UR_{PVIS} is intrinsic to the PVIS design (depends on the type of irrigation, the ratio between the needed and peak power, and on the PV generator structure). Finally, the UR_{EF} gives an idea of the use of the system (it is influenced by the irrigation scheduling in each month and by the availability of water in the source).

The previous indices were calculated to the two hybrid PV drip irrigation systems. In the case of Portugal, two external circumstances affect the performance of the system in the full irrigation campaign of 2017 and in a huge part of the 2018 irrigation campaign. In 2017, a huge lack of water only allows 94 days of irrigation along the whole irrigation period and mainly during the night. So, the *PVS* achieved is 0.49 and the *PR* during the irrigation period is 0.16 due to the low UR_{EF} (0.29). In 2018, the use of the diesel was higher than initially expected due to a problem in the fertirrigation system. This problem was solved only in August and it is interesting to verify that in this month the system worked, on average, 16

hours a day (with almost 7 and half hours only with PV, close to the Optimistic Scenario). The *PR* during this month was 0.56.

In the case of Morocco, the lack of water affects both years under analysis. The real irrigation hours were in between the two simulated scenarios. Full data in 2017 was only available from August to November and the main conclusion is that the *PR* is lower than expected due to the lower UR_{EF}. In 2018, data is available from February to April and then from July to August. During this year, and even with the huge lack of water, the *PVS* is 0.55 and the *PR* achieves 0.29, with PR_{PV}=0.81, UR_{IP}=1, UR_{PVIS}=0.99, UR_{EF}=0.36.

By comparing the real performance of both systems, it is very interesting to verify the effect of the type of hybridization in the UR_{PVIS}. In the case of Portugal (hydraulic hybridization), the UR_{PVIS} during the irrigation period ranges from 0.59 to 0.75. On the other hand, in the case of Morocco (electric hybridization), this indicator is higher than 0.97 in all situations. This happened because the design of the system in the case of the electric hybridization allows the use of PV energy from sunrise to sunset.

Finally, the economic results of the systems are also very promising: the initial investment cost of both systems is around 1.2 €/Wp; the payback period is 8.8 years in Portugal and 7 in Morocco; and the Levelized Cost of Energy is 0.13 €/kWh in Portugal and 0.07 €/kWh in Morocco, leading to savings in the electricity cost of 61% and 66% respectively.

Furthermore, other contributions to the design of large-power PVIS were developed regarding the PV generator structure, the electrical design and the selection of the motor-pump: a new type of structure called Delta was proposed and simulated, the PV energy losses in a PVIS as a consequence of the number of PV modules in series was quantified, and finally a new pump selection method for PVIS was developed and applied to a study case.

The main objective of Delta was to achieve constant in-plane irradiance profiles without using trackers. The electrical mismatching losses were calculated and a yearly mean loss of 2.4% was obtained. This solution is particularly interesting for PV irrigation systems since it requires a peak power of less than that needed with the typical static structure oriented to the Equator: in order to achieve the same water volume than the North-South horizontal axis tracker, the Delta needs 1.75 the peak power of the tracker, while the static structure oriented to the Equator requires twice this tracker peak power. Furthermore, the value of a new

proposed constancy index is as good as that obtained with the tracker – the yearly value achieves 0.95, reaching 0.99 during the irrigation period.

In what concerns the influence of the number of PV modules in series in large-power PVIS, the PV energy losses were calculated for strings of 20, 21 and 22 PV modules (for modules of 60 cells), for two different applications (a stand-alone PV irrigation system to a water pool and hybrid PV-grid system at constant pressure), two different locations (Villena, Spain and Marrakech, Morocco), and for different AC voltages required by the pump or supplied by the grid. In the case of the stand-alone system, if there is no AC voltage drop between the FC and the motor-pump, the losses are null in Villena and negligible in Marrakech. As this voltage drop increases, the percentage of losses also increases. If it is possible to put more than 20 PV modules in series these losses can be eliminated but this is limited by the range of voltages accepted at the FC input. In the case of the hybrid system, the losses cannot be eliminated but they can be minimized – the best solution is 20 modules in series for a grid voltage of 400 V and 21 for 415 V. Finally, a generalization of these results is performed through an analysis of the dependency of the losses with the temperature of the location and with the voltage needed in the DC bus voltage of the FC. For example, in the case of the stand-alone PVIS with strings of 20 modules, losses will appear if the DC bus voltage is equal to or higher than 550 V. It is also important to mention that if more than 20 PV modules in series need to be installed, a specific design has been proposed to avoid that the voltage at the FC input surpass its maximum allowed value (800 V).

Regarding the new pump selection method, the traditional way of selecting it just chooses the one that shows the highest efficiency at 50 or 60 Hz at a certain duty point. This procedure is not the best one in the case of PVIS working at different frequencies and duty points. So, in this work, a new pump selection method for large-power PV irrigation is proposed. This procedure was implemented in SISIFO and a comparison with the pump selected with the new and the traditional selection method is carried out for three different places in the Mediterranean zone: Madrid, Marrakech and Nice. The results show an increase in the yearly volume of water pumped in the range of 7.3-20.5% and an increase in pump efficiency in the range of 4.3-5.3%.

7.2 Future research lines

Finally, some future research lines are proposed: ones related to the proposed indices, others to the frequency converters and finally some about SISIFO tool.

The new performance indices were proposed and defined to distinguish the losses due to the different aspects that affect a PVIS. Then, they were applied to the two hybrid systems under analysis in this document. Results seem promising and conclusions can be drawn from the obtained values. Although, these indices should be applied to more PV irrigation systems to obtain typical values and to allow an easy interpretation of the overall performance of PVIS. For example, in the case of a grid-connected PV system, the expected *PR* is higher than 0.75. As more and more PV irrigation systems are installed we should be able to have this kind of values for each one of the indices proposed here.

In what concerns the FCs, two main issues deserve attention. First, since each FC has its own programming language, it is difficult to have an updated version of the new developments in different languages. Accordingly, a high-level programming language, regardless of the manufacturer, should be developed. Second, the traditional way of auto-tuning the PID parameters of the FC does not work in PVIS due to the high influence of the dynamic of the water source and the characteristics of the irrigation network. So, there is the need to find a way to do the auto-tuning in this kind of application.

Regarding SISIFO, its current version includes the possibility of simulating PV irrigation systems both to a water pool and direct pumping. However, it does not allow the simulation of more than one pump at a time. This is quite important and should be one priority since the use of only one PV generator to fed more than one pump is being used in many installations (as in the case of the demonstrator of Portugal).

Another drawback that can be seen as future research line is the integration in SISIFO of hybrid PVIS. Currently, SISIFO only simulates stand-alone PVIS. As it can be seen during this work, an important part of the market of large-power PVIS will be hybrid ones. Accordingly, SISIFO should be able to do hybridizations both in the electric and hydraulic part of the systems, as well as with the national grid and diesel generators. It should be pointed out that this also means that the irrigation scheduling needs to be added as a new input in SISIFO. This would open the door to the automatic calculation of the new performance indices proposed for PVIS.

CHAPTER 8

PUBLICATIONS

8.1 International peer reviewed journals

1) L. Narvarte, **R.H. Almeida**, I.B. Carrêlo, L. Rodriguez, L.M. Carrasco, F. Martínez-Moreno, *On the number of PV modules in series for large-power irrigation systems*, submitted to Energy Conversion and Management.
2) **R. H. Almeida**, I. B. Carrêlo, E. Lorenzo, L. Narvarte, J. Fernández-Ramos, F. Martínez-Moreno, L.M. Carrasco, *Large-power hybrid PV irrigation: a 140 kW PV-diesel representative case*, submitted to Energies.
3) Giuseppe Todde, Lelia Murgia, Paola A Deligios, **Rita Hogan**, Isaac Carrêlo, Antonio Pazzona, Luigi Ledda, Luis Narvarte, *Energy and Environmental Performances of Hybrid Photovoltaic Irrigation Systems in Mediterranean Intensive and Super-Intensive Olive Orchards*, Science of the Total Environment 651, Part 2, 2514-2523, 15 February 2019. DOI: 10.1016/j.scitotenv.2018.10.175
4) **R. H. Almeida**, J. R. Ledesma, I. B. Carrêlo, L. Narvarte, G. Ferrara, L. Antipodi, *A new pump selection method for large-power PV irrigation systems at a variable frequency*, Energy Conversion and Management, Volume 174, 874-885, 15 October 2018. DOI: 10.1016/j.enconman.2018.08.071
5) L. Narvarte, J. Fernández-Ramos, F. Martínez-Moreno, L.M. Carrasco, **R.H. Almeida**, I.B. Carrêlo, *Solutions for adapting photovoltaics to large power irrigation systems for agriculture*, Sustainable Energy Technologies and Assessments, Volume 29, 119-130, October 2018. DOI: 10.1016/j.seta.2018.07.004
6) **R. H. Almeida**, L. Narvarte, E. Lorenzo, *PV arrays with delta structures for constant irradiance daily profiles*, Solar Energy, Volume 171, 23-30, September 2018. DOI: 10.1016/j.solener.2018.06.066
7) Giuseppe Todde, Lelia Murgia, Isaac Carrêlo, **Rita Hogan**, Antonio Pazzona, Luigi Ledda, Luis Narvarte, *Embodied Energy and Environmental Impact of Large-Power Stand-Alone Photovoltaic Irrigation Systems*, Energies, Volume 11, Issue 8, August 2018. DOI: 10.3390/en11082110
8) C. Lorenzo, **R. H. Almeida**, M. Martínez-Núñez, L. Narvarte, L. M. Carrasco, *Economic assessment of large power photovoltaic irrigation systems in the ECOWAS*

region, Energy, Volume 155, 992-1003, 15 July 2018. DOI: 10.1016/j.energy.2018.05.066

8.2 Conference proceedings

1) **R. H. Almeida**, I.B. Carrêlo, C. Lorenzo, L. Narvarte , *Economic validation of large power PV irrigation systems*, 35th EU PVSEC, 24-28 September 2018, Brussels, Belgium.
2) **R. H. Almeida**, I.B. Carrêlo, L. Narvarte, J. Fernández-Ramos, F. Martinez-Moreno, L. M. Carrasco, *Main final results of MASLOWATEN - the H2020 project for market uptake of large power PV irrigation systems*, 35th EU PVSEC, 24-28 September 2018, Brussels, Belgium.
3) **R. H. Almeida**, I. B. Carrêlo, L. Narvarte, E. Lorenzo, *Delta structure for constant daily power profile in PV irrigation systems*, 35th EU PVSEC, 24-28 September 2018, Brussels, Belgium.
4) I. B. Carrêlo, **R. H. Almeida**, L. Narvarte, *Performance of a 40 kWp PV Irrigation Demonstrator Combining Variable and Constant Pressure Pumping*, 35th EU PVSEC, 24-28 September 2018, Brussels, Belgium.
5) **R. H. Almeida**, L. García, L. Narvarte, I. B. Carrêlo, F. Martinez-Moreno, L. M. Carrasco, *Sobre el número de módulos fotovoltaicos en serie para aplicaciones de riego*, XVI Congresso Ibérico & XII Congresso Iberoamericano de Energia Solar, 20-22 June 2018, Madrid, Spain.
6) **R. H. Almeida**, I. B. Carrêlo, L. Narvarte, E. Lorenzo, *Estrutura Delta para sistemas de irrigação PV*, XVI Congresso Ibérico & XII Congresso Iberoamericano de Energia Solar, 20-22 June 2018, Madrid, Spain.
7) I. B. Carrêlo, **R. H. Almeida**, L. Narvarte, L. M. Carrasco, F. Martinez-Moreno, *Viabilidade técnica de dois sistemas de irrigação fotovoltaica de alta potência em Espanha*, XVI Congresso Ibérico & XII Congresso Iberoamericano de Energia Solar, 20-22 June 2018, Madrid, Spain.
8) C. Lorenzo, **R. H. Almeida**, M. Martínez-Nuñez, L. Narvarte, L. M. Carrasco, *Viabilidad Económica de Sistema de Riego Fotovoltaico de Alta Potencia en la Región de ECOWAS*, XVI Congresso Ibérico & XII Congresso Iberoamericano de Energia Solar, 20-22 June 2018, Madrid, Spain.

9) **R. H. Almeida**, I.B. Carrêlo, L.M. Carrasco, F. Martinez-Moreno & L. Narvarte, *Large-scale hybrid PV-Grid irrigation system*, 33rd EU PVSEC, 25-29 September 2017, Amsterdam, Netherlands. DOI: 10.4229/EUPVSEC20172017-6BV.1.26
10) **R. H. Almeida**, I.B. Carrêlo, F. Martinez-Moreno, L.M. Carrasco & L. Narvarte, *A 140 kW hybrid PV-Diesel Pumping system for constant-pressure irrigation*, 33rd EU PVSEC, 25-29 September 2017, Amsterdam, Netherlands. DOI: 10.4229/EUPVSEC20172017-6BV.1.27
11) I.B. Carrêlo, **R. H. Almeida**, F. Martinez-Moreno, L.M. Carrasco & L. Narvarte, *A 160 kWp constant pressure PV Irrigation system in Spain*, 33rd EU PVSEC, 25-29 September 2017, Amsterdam, Netherlands. DOI: 10.4229/EUPVSEC20172017-6BV.1.25
12) I.B. Carrêlo, **R. H. Almeida**, L.M. Carrasco, F. Martinez-Moreno & L. Narvarte, *A 360 kWp PV Irrigation system to a water pool in Spain*, 33rd EU PVSEC, 25-29 September 2017, Amsterdam, Netherlands. DOI: 10.4229/EUPVSEC20172017-6BV.1.24

8.3 Patents

1) J. Fernández-Ramos, L. Narvarte-Fernández, **R. Hogan Teves de Almeida**, I. Barata Carrêlo, L. M. Carrasco Moreno, E. Lorenzo Pigueiras, *ES2607253B2 - Procedimiento y dispositivo de control para sistemas de bombeo fotovoltaico*, 01/03/2018.
2) J. Fernández-Ramos, L. Narvarte-Fernández, **R. Hogan Teves de Almeida**, I. Barata Carrêlo, L. M. Carrasco Moreno, E. Lorenzo Pigueiras, *ES2619555B2 - Sistema de riego por bombeo fotovoltaico hibridado eléctricamente*, 19/10/2017.
3) J. Fernández-Ramos, L. Narvarte-Fernández, **R. Hogan Teves de Almeida**, I. Barata Carrêlo, L. M. Carrasco Moreno, E. Lorenzo Pigueiras, *ES2608527B2 - Sistema de bombeo fotovoltaico hibridado hidráulicamente con la red eléctrica o con grupos diésel para aplicaciones de riego*, 24/07/2017.

8.4 Other publications during the doctorate not related to the thesis

1) V. Reis, **R. H. Almeida**, J. A. Silva, M. C. Brito, *Demand aggregation for photovoltaic self-consumption*, accepted in Energy Reports.

2) **R. H. Almeida**, M. C. Brito, *A review of technical options for solar charging stations in Asia and Africa*, AIMS Energy, Volume 3, 428-449, 2015. DOI: 10.3934/energy.2015.3.428
3) C. Augusto, **R. H. Almeida**, S. Mandelli, M.C. Brito, *Evaluation of potential of demand side management strategies in isolated microgrids*, 6th International Conference on Clean Electrical Power, 27-29 June 2017, Santa Margherita Ligure, Italy. DOI: 10.1109/ICCEP.2017.8004840
4) **R. H. Almeida**, I. B. Carrêlo, J. Maia Alves, *Intelligent Stand Alone Solar Street Light*, 4th Symposium on Small PV Applications, 9-10 June 2015, Munich, Germany.

CHAPTER 9

REFERENCES

[1] IRENA, “Renewable Power Generation Costs in 2017,” International Renewable Energy Agency, Abu Dhabi, 2018.

[2] IRENA, “Renewable capacity statistics 2018,” International Renewable Energy Agency, Abu Dhabi, 2018.

[3] FAO & GIZ, Prospects for solar-powered irrigation systems (SPIS) in developing countries, Rome, 2015.

[4] Eurostat, “Agricultural census 2010 - main results,” Eurostat, [Online]. Available: https://ec.europa.eu/eurostat/statistics-explained/index.php?title=Agricultural_census_2010_-_main_results. [Accessed 24 09 2018].

[5] D. Zilberman, T. Sproul, D. Rajagopal, S. Sexton and P. Hellegers, “Rising energy prices and the economics of water in agriculture,” *Water Policy,* vol. 10, no. 1, pp. 11-21, 2008.

[6] J. Nuncio and C. Arranja, “Regadio: binómio água e energia,” *Recursos Hídricos,* vol. 38, pp. 17-23, 2017.

[7] J. M. Tarjuelo, J. A. Rodriguez-Diaz, R. Abadía, E. Camacho, C. Rocamora and M. A. Moreno, “Efficient water and energy use in irrigation modernization: Lessons from Spanish case studies,” *Agricultural Water Management,* vol. 162, p. 67*77, 2015.

[8] Instituto para la Diversificación y Ahorro de la Energía (IDAE), “Ahorro y Eficiencia Energética en Agricultura de Regadío,” Instituto para la Diversificación y Ahorro de la Energía, Madrid, 2005.

[9] I. Fernández García, P. Montesinos, E. Camacho Poyato and J. A. Rodríguez Días, “Energy cost optimization in pressurized irrigation networks,” *Irrigation Science,* vol. 34, no. 1, pp. 1-13, 2016.

[10] B. Werner and R. Collins, “Towards efficient use of water resources in Europe,” European Environment Agency, Copenhagen, 2012.

[11] Institute for European Environmental Policy, London; Polytechnical University of Madrid; and University of Athens, “The environmental impacts of irrigation in the European Union - A report to the Environment Directorate of the European Commission,” 2000.

[12] Eurostat, “Agricultural census in Spain,” Eurostat, [Online]. Available: https://ec.europa.eu/eurostat/statistics-explained/index.php/Agricultural_census_in_Spain.

[Accessed 25 09 2018].

[13] Eurostat, “Agricultural census in Portugal,” Eurostat, [Online]. Available: https://ec.europa.eu/eurostat/statistics-explained/index.php/Agricultural_census_in_Portugal. [Accessed 25 09 2018].

[14] Eurostat, “Share of irrigated areas in UAA by NUTS 2 regions, EU-28 and Norway, 2013,” Eurostat, [Online]. Available: https://ec.europa.eu/eurostat/statistics-explained/images/c/c7/Share_of_irrigated_areas_in_UAA_by_NUTS_2_regions%2C_EU-28_and_NO%2C_2013_%28%25%29.png. [Accessed 24 09 2018].

[15] Eurostat, "Share of irrigable and irrigated areas in UAA, 2013 (%)," Eurostat, [Online]. Available: https://ec.europa.eu/eurostat/statistics-explained/index.php?title=File:Share_of_irrigable_and_irrigated_areas_in_UAA,_2013_(%25).png. [Accessed 24 09 2018].

[16] Secretaría General Técnica, Subdirección General de Estadística, Ministerio de Agricultura y Pesca, Alimentación y Medio Ambiente, “Encuesta sobre superficies y rendimientos de cultivos: informe sobre regadíos en España,” Ministerio de Agricultura y Pesca, Alimentación y Medio Ambiente, Madrid, 2017.

[17] I. Fernández García, P. Montesinos, E. Camacho and J. A. Rodriguez Dias, “Medidas para la mejora de la eficiencia energética en el suministro de agua de riego,” in *La gestión integrada de los recursos hídricos en Andalucía y norte de Marruecos*, 2015, pp. 133-151.

[18] FENACORE - Federación Nacional de Comunidades de Regantes de España, “Federación Nacional de Comunidades de Regantes - Dossier de prensa 2017,” FENACORE, Madrid, 2017.

[19] FAOSTAT, “FAOSTAT - Energy - Percentage of total energy used/production in agriculture and forestry,” 2009. [Online]. Available: http://www.fao.org/faostat/en/#data/EE. [Accessed 24 09 2018].

[20] Secretaría de Estado de Energía - Ministerio para la Transición Energética, “Estadística de la Industria de la Energía Eléctrica (datos provisionales a 14/06/2018),” Ministerio para la Transición Energética, Madrid, 2016.

[21] J. Corominas, “Agua y Energía en el riego, en la época de la sostanibilidad,” *Ingeniería del Agua,* vol. 17, no. 3, 2010.

[22] M. Abu-Aligah, “Design of Photovoltaic Water Pumping System and Compare it with Diesel Powered Pump,” *Jordan Journal of Mechanical and Industrial Engineering,* vol. 5, no. 3, pp. 273-280, 2011.

[23] R. Langarita, J. Sánchez Chóliz, C. Sarasa, R. Duarte and S. Jiménez, “Electricity costs in irrigated agriculture: A case study for an irrigation scheme in Spain,” *Renewable and Sustainable Energy Reviews,* vol. 68, pp. 1008-1019, 2017.

[24] FENACORE, “September Bulletin,” FENACORE, Madrid, 2013.

[25] I. Martins and C. Arranja, “Água e energia no regadio - perspetiva do setor,” 4 12 2014. [Online]. Available: http://pagina-web.arbcas.pt/images/DOCUMENTOS/FENAREG_custo_energ_agricultura.pdf. [Accessed 21 9 2018].

[26] FENAREG (Press Release), “Regantes pedem apoios ao investimento em energias limpas - FENAREG,” 21 05 2018. [Online]. Available: http://www.fenareg.pt/wp-content/uploads/NOTA-DE-IMPRENSA_FENAREG_21_Maio_2018.pdf. [Accessed 25 09 2018].

[27] J. Nuncio and C. Arranja, “Regadio: água e energia,” in *VI Congresso Nacional de Rega e Drenagem*, Beja, 2016.

[28] J. Carroquino, R. Dufo-López and J. L. Barnal-Augustin, “Sizing of off-grid renewable energy systems for drip irrigation in Mediterranean crops,” *Renewable Energy,* no. 76, pp. 566-574, 2015.

[29] IRENA, “Solar pumping for irrigation: Improving livelihoods and sustainability,” The International Renewable Energy Agency, Abu Dhabi, 2016.

[30] FENACORE, “Las tarifas eléctricas del regadío. Cronología, problemática y soluciones,” FENACORE, 2017.

[31] L. Narvarte, J. Fernández-Ramos, F. Martínez-Moreno, L. M. Carrasco, R. H. Almeida and I. B. Carrêlo, “Solutions for adapting photovoltaics to large power irrigation systems for agriculture,” *Sustainable Energy Technologies and Assessments,* vol. 29, pp. 119-130, 2018.

[32] FAOSTAT, “Total area equipped for irrigation,” FAOSTAT, 2011.

[33] W. Palz, “The French Connection: The rise of the PV water pump,” *Refocus: The International Renewable Energy Magazine,* vol. 2, no. 1, pp. 46-47, 2001.

[34] R. Barlow, B. Mc Nelis and A. Derrick, "Solar pumping: an introduction and update on the technology, performance, costs, and economics (World Bank technical paper number 168)," World Bank, Washington DC, 1993.

[35] R. V. Enochian, "Solar- and Wind-Powered Irrigation Systems," United States Department of Agriculture, Washington D.C., 1982.

[36] W. Halcrow, "Small-scale solar-powered irrigation pumping systems - technical and economical review," World Bank, 1981.

[37] M. N. Bahadori, "Solar Water Pumping," *Solar Energy,* pp. 307-316, 1978.

[38] M. C. Fedrizzi and I. L. Sauer, “Bombeamento Solar Fotovoltaico, histórico, características e projectos,” in *Encontro de Energia no Meio Rural*, Campinas, 2002.

[39] B. van Campen, D. Guidi and G. Best, “Solar photovoltaics for sustainable agriculture and rural development,” FAO, Rome, 2000.

[40] M. A. Galdino, “PRODEEM - The Brazilian Programme for Rural Electrification Using Photovoltaics,” in *World Climate & Energy Event*, Rio de Janeiro, 2002.

[41] M. C. Fedrizzi, Sistemas fotovoltaicos de abastecimento de água para uso comunitário: lições apreendidas e procedimentos para potencializar sua difusão, São Paulo: Tese (Doutorado) - Programa Interunidades de Pós-Graduação em Energia da Universidade de São Paulo, 2003.

[42] M. R. Borges Neto and P. C. M. Carvalho, “Energia solar fotovoltaica no semi-árido: estudo de caso sobre a atuação do prodeem em Petrolina-PE,” in *Proceedings of the 6. Encontro de Energia no Meio Rural*, Campinas, 2006.

[43] Centro de Pesquisa de Energia Elétrica - Cepel, “Energia para as Comunidades Isoladas - PRODEEM,” Centro de Pesquisa de Energia Elétrica, Brasilia.

[44] A. D. Cota Espericueta, R. E. Foster, M. P. Ross, C. Hanley, V. P. Gupta, O. Montúfar Avilez and A. R. Paredes Rubio, “Ten-year reliability assessment of photovoltaic water pumping systems in Mexico,” in *Solar 2004, American Solar Energy Society*, Portland, Oregon, 2004.

[45] E. Lorenzo Pigueiras, F. Poza Sauro, L. Narvarte Fernández, M. C. Fedrizzi, R. Zilles, M. Aandam and S. Zaoui, “Boas práticas na implantação de sistemas de bombeamento fotovoltaico,” Instituto de Energía Solar, Universidad Politécnica de Madrid, Madrid, 2005.

[46] L. Narvarte, F. Poza and E. Lorenzo, “Specification and Testing of PV Pumps for a Moroccan Project,” *Progress in Photovoltaics: Research and Applications,* vol. 14, pp. 733-741, 2006.

[47] L. Narvarte and E. Lorenzo, “Sustainability of PV water pumping programmes: 12-years of successful experience,” *Progress in Photovoltaics: Research and applications,* vol. 18, pp. 291-298, 2010.

[48] M. A. Abella, E. Lorenzo and F. Chenlo, "PV Water Pumping Systems Based on Standard Frequency Converters," *Prog. Photovolt: Res. Appl.,* vol. 11, pp. 179-191, 2003.

[49] H. Hartung and L. Pluschke, “The benefits and risks of solar-powered irrigation - a global overview,” Food and Agriculture Organization of the United Nations and Deutsche Gesellschaft für Internationale Zusammenarbeit, 2018.

[50] MASLOWATEN, "Technical Specifications for Photovoltaic Irrigation Systems," 2017.

[51] C. Lorenzo, R. H. Almeida, M. Martínez-Núñez, L. Narvarte and L. M. Carrasco, “Economic assessment of large power photovoltaic irrigation systems in the ECOWAS region,” *Energy,*

vol. 155, pp. 992-1003, 2018.

[52] P. E. Campana, H. Li and J. Yan, “Techno-economic feasibility of the irrigation system for the grassland and farmland conservation in China: Photovoltaic vs. wind power water pumping,” *Energy Conversion and Management,* vol. 103, pp. 311-320, 2015.

[53] X. Gao, J. Liu, J. Zhang, J. Yan, S. Bao, H. Xu and T. Qin, “Feasibility evaluation of solar photovoltaic pumping irrigation system based on analysis of dynamic variation of groundwater table,” *Applied Energy,* vol. 105, pp. 182-193, 2013.

[54] A. U. Brito and R. Zilles, “Systematized Procedure for Parameter Characterization of a Variable-speed Drive Used in Photovoltaic Pumping Applications,” *Progress in Photovoltais: Research and Application,* vol. 14, pp. 249-260, 2006.

[55] L. R. Valler, T. A. Melendez, M. C. Fedrizzi, R. Zilles and A. M. de Moraes, “Variable-speed drives in photovoltaic pumping systems for irrigation in Brazil,” *Sustainable Energy Technologies and Assessments,* vol. 15, pp. 20-26, 2016.

[56] Z. Gao, Y. Zhang, L. Gao and R. Li, "Progress on Solar Photovoltaic Pumping Irrigation Technology," *Irrigation and Drainage,* vol. 67, pp. 89-96, 2018.

[57] G. Li, Y. Jin, M. W. Akram and X. Chen, "Research and current status of the solar photovoltaic water pumping system - A review," *Renewable and Sustainable Energy Reviews,* vol. 79, pp. 440-458, 2017.

[58] I. Odeh, Y. G. Yohanis and B. Norton, “Economic viability of photovoltaic water pumping systems,” *Solar Energy,* vol. 80, pp. 850-860, 2006.

[59] IRENA, “Solar pumping for irrigation: Improving livelihoods and sustainability,” The International Renewable Energy Agency, Abu Dhabi, 2016.

[60] A. Tiwari and V. Kalamkar, “Effects of total head and solar radiation on the performance of solar water pumping system,” *Renewable Energy,* vol. 118, pp. 919-927, 2018.

[61] PoweringAg, “Powering Agriculture: An Energy Grand Challenge for Development (Fact Sheet),” PoweringAg, 2016.

[62] S. S. Chandel, M. N. Naik and R. Chandel, "Review of performance studies of direct coupled photovoltaic water pumping systems and case study," *Renewable and Sustainable Energy Reviews,* vol. 76, pp. 163-175, 2017.

[63] S. M. Wazed, B. R. Hughes, D. O´Connor and J. K. Calautit, "A review of sustainable solar irrigation systems for Sub-Saharan Africa," *Renewable and Sustainable Energy Reviews,* no. 81, pp. 1206-1225, 2018.

[64] V. C. Sontake and V. R. Kalamkar, “Solar photovoltaic water pumping system - A comprehensive review,” *Renewable and Sustainable Energy Reviews,* vol. 59, pp. 1038-1067,

2016.

[65] L. E. Jones and G. Olsson, "Solar Photovoltaic and Wind Energy Providing Water," *Global Challenges,* vol. 1, no. 5, 2017.

[66] K. Y. Lau, M. F. M. Yousof, S. N. M. Arshad, M. Anwari and A. H. M. Yatim, "Performance analysis of hybrid photovoltaic/diesel energy system under Malaysian conditions," *Energy,* vol. 35, pp. 3245-3255, 2010.

[67] EIP Water, "European Innovation Partnership Water - Strategic Implementation Plan," Brussels, 2012.

[68] J. Marcos, L. Marroyo, E. Lorenzo, D. Alvira and E. Izco, "Power output fluctuations in large scale PV plants: one year observations with one second resolution and a derived analytic model," *Progress in Photovoltaics: Research and Applications,* vol. 19, pp. 218-27, 2011.

[69] J. Fernández-Ramos, L. Narvarte-Fernández and F. Poza-Saura, "Improvement of photovoltaic pumping systems based on standard frequency converters," *Solar Energy,* vol. 84, no. 1, pp. 101-109, 2010.

[70] J. Zhang, J. Liu, P. E. Campana, R. Zhang, J. Yan and X. Gao, "Model of evapotranspiration and groundwater level based on photovoltaic water pumping system," *Applied Energy,* vol. 136, pp. 1132-1137, 2014.

[71] Z. A. Firatoglu and B. Yesilata, "New approaches on the optimization of directly coupled PV pumping systems," *Solar Energy,* vol. 77, pp. 81-93, 2004.

[72] O. Deveci, M. Onkol, H. O. Unver and Z. Ozturk, "Design and development of a low-cost solar powered drip irrigation system using Systems Modeling Language," *Journal of Cleaner Production,* vol. 102, pp. 529-544, 2015.

[73] I. Kougias, S. S., N. Scarlat, F. Monforti, M. Banja, K. Bódis and M. Moner-Girona, "Water-Energy-Food Nexus Interactions Assessment: Renewable energy sources to support water access and quality in West Africa," European Commission, Luxembourg, 2018.

[74] MASLOWATEN, "MASLOWATEN project," 2018. [Online]. Available: www.maslowaten.eu.

[75] Instituto de Energía Solar - Universidad Politécnica de Madrid, "SISIFO - Simulación de Sistemas Fotovoltaicos," [Online]. Available: http://sisifo.info.

[76] J. S. Ramos and H. M. Ramos, "Sustainable application of renewable sources in water pumping systems: Optimized energy system configuration," *Energy Policy,* vol. 37, pp. 633-643, 2009.

[77] A. del Campo García, Las Comunidades de Regantes de España y su Federación Nacional, Madrid: FENACORE, 2018.

[78] A. Closas and E. Rap, “Solar-based groundwater pumping for irrigation: Sustainability, policies, and limitations,” *Energy Policy,* vol. 104, pp. 33-37, 2017.

[79] J. Fernandez Ramos, L. Narvarte Fernandez, R. Hogan Teves de Almeida, I. Barata Carrêlo, L. M. Carrasco Moreno and E. Lorenzo Pigueiras, “Method and control device for photovoltaic pumping systems”. Spain Patent ES 2 607 253 B2, 1 3 2018.

[80] R. H. Almeida, L. Narvarte and E. Lorenzo, “PV arrays with delta structures for constant irradiance daily profiles,” *Solar Energy,* vol. 171, pp. 23-30, 2018.

[81] M. Das and R. Mandal, “A comparative performance analysis of direct, with battery, supercapacitor, and battery-supercapacitor enabled photovoltaic water pumping systems using centrifugal pump,” *Solar Energy,* vol. 171, pp. 302-309, 2018.

[82] F. Fu, D. Feldman, R. Margolis, M. Woodhouse and K. Ardani, “US Solar Photovoltaic system cost benchmark: Q1 2017,” National Renewable Energy Laboratory, 2017.

[83] Fraunhofer Institute for Solar Energy Systems, “Photovoltaics report,” Fraunhofer ISE, Freiburg, 2017.

[84] C. Kost, S. Shammugam, V. Jülch, T.-H. Nguyen and T. Schlegl, “Levelized cost of electricity renewable energy technologies,” Fraunhofer ISE, Freiburg, 2018.

[85] J. Fernandez Ramos, L. Narvarte Fernandez, R. Hogan Teves de Almeida, I. Barata Carrêlo, L. M. Carrasco Moreno and E. Lorenzo Pigueiras, “Sistema de bombeo fotovoltaico hibridado hidráulicamente con la red eléctrica o con grupos diésel para aplicaciones de riego”. Spain Patent ES 2608527 B2, 2017.

[86] J. Fernández-Ramos, L. Narvarte Fernandez, R. Hogan Teves de Almeida, I. Barata Carrêlo, L. M. Carrasco Moreno and E. Lorenzo Pigueiras, "Sistema de riego por bombeo fotovoltaico hibridado eléctricamente". Spain Patent ES 2 619 555 B2, 2017.

[87] H. Ammar, A. Melit, M. Adouane and M. T. Bouziane, “Techno-economic evaluation of a hybrid PV/diesel water pumping system for different pumping heads,” in *3rd International Renewable and Sustainable Energy Conference*, Marrakech, 2015.

[88] Y. Bakelli, B. Gherbi, B. Taghezouit, O. Hazil and H. Mahammed, “Techno-economic evalualution of different hybrid photovoltaic/diesel pumping systems with water tank storage,” in *8th International Conference on Modelling, Identification and Control*, Algiers, 2016.

[89] E. M. Rogers, Diffusion of Innovations, The Free Press, 1962.

[90] European Commission, Joint Research Centre, “Photovoltaic Geographical Information System (PVGIS),” [Online]. Available: http://re.jrc.ec.europa.eu/pvgis/.

[91] U. Jahn, B. Grimmig and W. Nasse, “Analysis of Photovoltaic Systems (Report IEA-PVPS T2-01: 2000),” International Energy Agency, 2000.

[92] J. Leloux, L. Narvarte and D. Trebosc, “Performance Analysis of 10,000 Residential PV Systems in France and Belgium,” in *26th European Photovoltaic Solar Energy Conference and Exhibition*, Hamburg, 2011.

[93] N. H. Reich, B. Mueller, A. Armbruster, W. van Sark and C. Reise, “Performance ratio revisited: is PR > 90% realistic?,” *Progress in Photovoltaics - Special Issue: 26th EU PVSEC, Hamburg, Germany 2011,* vol. 20, no. 6, pp. 717-726, 2012.

[94] Instituto Português do Mar e da Atmosfera, "Situação de Seca Meteorológica - 31 de outubro de 2017 (in Portuguese)," IPMA, Lisbon, 2017.

[95] J. Rockström, L. Karlberg, S. P. Wani, J. Barron, N. Hatibu, T. Oweis, A. Bruggeman, J. Farahani and Z. Qiang, “Managing water in rainfed agriculture - The need for a paradigm shift,” *Agricultural Water Management,* no. 97, pp. 543-550, 2010.

[96] F. Crundwell, Finance for Engineers, London: Springer-Verlag London Limited, 2008.

[97] B. I. Ouedraogo, S. Kouame, Y. Azoumah and D. Yamegueu, “Incentives for rural off grid electrification in Burkina Faso using LCOE,” *Renewable Energy,* no. 78, pp. 573-582, 2015.

[98] K. Branker, M. Pathak and J. Pearce, “A review of solar photovoltaic levelized cost of energy,” *Renewable and Sustainable Energy Reviews,* no. 15, pp. 4470-4482, 2011.

[99] Trading Economics, “Portugal Inflation Rate,” Trading Economics, [Online]. Available: https://tradingeconomics.com/portugal/inflation-cpi. [Accessed 10 10 2018].

[100] Trading Economics, “Portugal Interest Rate,” Trading Economics, [Online]. Available: https://tradingeconomics.com/portugal/interest-rate. [Accessed 10 10 2018].

[101] Trading Economics, “Morocco Inflation Rate,” Trading Economics, [Online]. Available: https://tradingeconomics.com/morocco/inflation-cpi. [Accessed 10 10 2018].

[102] Trading Economics, “Morocco Interest Rate,” Trading Economics, [Online]. Available: https://tradingeconomics.com/morocco/interest-rate. [Accessed 10 10 2018].

[103] J. Remund, C. Calhau, L. Perret and D. Marcel, “Characterization of the spatio-temporal variations and ramp rates of solar radiation and PV,” Internation Energy Agency - Photovoltaic Power Systems Programme, 2015.

[104] G. Litjens, E. Worrell and W. van Sark, “Influence of demand patterns on the optimal orientation of photovoltaic systems,” *Solar Energy,* vol. 155, pp. 1002-1014, 2017.

[105] E. Luiz, F. Martins, A. Gonçalves and E. Pereira, “Analysis of intra-day solar irradiance

variability in different Brazilian climate zones," *Solar Energy,* vol. 167, pp. 210-219, 2018.

[106] J. Munoz, J. Carrillo, F. Martínez-Moreno, L. Carrasco and L. Narvarte, "Modeling and simulation of large PV pumping systems," in *Proceedings of the 31th European Photovoltaic Solar Energy Conference and Exhibition*, Hamburg, 2015.

[107] O. Vilela, N. Fraidenraich and C. Tiba, "Photovoltaic pumping systems driven by tracking collectors. Experiments and simulation," *Solar Energy,* vol. 74, no. 1, pp. 45-52, 2003.

[108] L. Narvarte and E. Lorenzo, "Tracking and ground cover ratio," *Progress in Photovoltaics. Research and Applications,* vol. 16, no. 8, pp. 703-714, 2008.

[109] Z. Lan and G. Tie Yu, "Performance and reliability of tracker and fixed-tilt mounting systems," *PV- Tech Power,* vol. 1, 2015.

[110] J. Shingleton, "One-Axis Trackers - Improved reliability, durability, performance and cost reduction," Subcontract Report NREL/SR-520-42769 NREL, 2008.

[111] R. Bruno, P. Bevilacqua, L. Longo and N. Arcuri, "Small Size Single-axis PV Trackers: Control Strategies and System Layout for Energy Optimization," *Energy Procedia,* vol. 82, pp. 737-743, 2015.

[112] GmbH, G.C.G., "Manuals and Tools for Promoting SPIS - Workshop "Promotion of Solar-Powered Irrigation Systems (SPIS)" - minutes of the workshop," GFA, GIZ, Eschborn, 2015.

[113] W. Nsengiyumva, S. Chen, L. Hu and X. Chen, "Recent advancements and challenges in Solar Tracking Systems (STS): A review," *Renewable and Sustainable Energy Reviews,* vol. 81, pp. 250-279, 2018.

[114] R. Velik, "East-South-West orientation of PV systems and neighbourhood energy exchange to maximize local photovoltaics energy consumption," *International Journal of Renewable Energy Research ,* vol. 4, no. 3, 2014.

[115] H. Ruf, "Limitations for the feed-in power of residential photovoltaic systems in Germany - An overview of the regulatory framework," *Solar Energy,* vol. 159, pp. 588-600, 2018.

[116] G. Barbose, R. Wiser and M. Bolinger, "Case studies of state support for renewable energy - Designing PV incentive programs to promote performance: a review of current practice.," Final report under Task2 of MPO No. DEK-6-66278-01., 2006.

[117] D. Panico, P. Garvison, H. Wenger and D. Shugar, "Backtracking: a novel strategy for tracking PV systems," in *22nd IEEE Photovoltaic Specialists Conference*, Las Vegas, 1991.

[118] E. Lorenzo, L. Narvarte and J. Munoz, "Tracking and back-tracking," *Progress in Photovoltaics: research and Application,* vol. 19, no. 6, pp. 474-753, 2011.

[119] D. Erbs, S. Klein and J. Duffie, “Estimation of the diffuse radiation fraction for hourly, daily and monthly-average global radiation,” *Solar Energy,* vol. 28, no. 4, pp. 293-302, 1982.

[120] M. Collares-Pereira and A. Rabl, “The average distribution of solar radiation-correlations between diffuse and hemispherical and between daily and hourly insolation values,” *Solar Energy,* vol. 22, no. 2, pp. 155-164, 1979.

[121] R. Perez, R. Stewart, C. Arbogast, R. Seals and J. Scott, “An anisotropic hourly diffuse radiation model for sloping surfaces: Description, performance validation, site dependency evaluation,” *Solar Energy,* vol. 36, no. 6, pp. 481-497, 1986.

[122] F. Martínez-Moreno, J. Muñoz and E. Lorenzo, “Experimental model to estimate shading losses on PV arrays,” *Solar Energy Materials and Solar Cells,* vol. 94, no. 12, pp. 2298-2303, 2010.

[123] I. de la Parra, M. Muñoz, E. Lorenzo, M. García, J. Marcos and F. Martínez-Moreno, “PV performance modelling: A review in the light of quality assurance for large PV plants,” *Renewable and Sustainable Energy Reviews,* vol. 78, pp. 780-797, 2017.

[124] M. Fuentes, G. Nofuentes, J. Aguilera, D. Talavera and M. Castro, “Application and validation of algebraic methods to predict the behaviour of crystalline silicon PV modules in Mediterranean climates,” *Solar Energy,* vol. 81, no. 11, pp. 1396-1408, 2007.

[125] E. Caamaño, E. Lorenzo and C. Lastres, “Crystalline silicon photovoltaic modules: Characterization in the field of rural electrification.,” *Progress in Photovoltaics: Research and Applications,* vol. 10, no. 7, pp. 481-493, 2002.

[126] IEC-60891:2009, “Photovoltaic devices - Procedures for temperature and irradiance corrections to measured I-V characteristics,” IEC, 2009.

[127] M. Jantsch, H. Schmidt and J. Schmid, “Results of the concerted action on power conditioning and control,” in *11th Photovoltaic Solar Energy Conference*, Montreux, 1992.

[128] OMRON, “RX-series Variable Frequency Drives,” [Online]. Available: https://assets.omron.eu/downloads/datasheet/en/v4/i116e_rx-series_variable_frequency_drives_datasheet_en.pdf. [Accessed 24 7 2018].

[129] Grundfos, “Grundfos RSI - AC drives: Installations and operating instructions,” 2016.

[130] E. Lorenzo, Electricidad solar fotovoltaica, volumen III: ingeniería fotovoltaica, Sevilla: Progensa, 2014.

[131] A. E. Fitzgerald, C. Kingsley and S. D. Umans, Electric Machinery, sixt edition, New York: McGraw-Hill, 2003.

[132] I. B. Carrêlo, R. H. Almeida, L. M. Carrasco, F. Martínez-Moreno and L. Narvarte, “A 360 kWp PV irrigation system to a water pool in Spain,” in *33rd European Photovotaic Solar Energy*

Conference and Exhibition, Amsterdam, 2017.

[133] R. H. Almeida, I. B. Carrêlo, L. M. Carrasco, F. Martínez-Moreno and L. Narvarte, “Large-scale hybrid PV-Grid irrigation system,” in *33rd European Photovotaic Solar Energy Conference and Exhibition*, Amsterdam, 2017.

[134] Caprari, “iPump - Caprari,” Caprari, [Online]. Available: https://ipump.caprarinet.net. [Accessed 2018].

[135] I. B. Carrêlo, R. H. Almeida, F. Martínez-Moreno, L. M. Carrasco and L. Narvarte, “A 160 kWp constant pressure PV Irrigation system in Spain,” in *33rd European Photovotaic Solar Energy Conference and Exhibition*, Amsterdam, 2017.

[136] R. H. Almeida, I. B. Carrêlo, L. Narvarte, J. Fernández-Ramos, F. Martinez-Moreno and L. M. Carrasco, “Main final results of MASLOWATEN - the H2020 project for market uptake of large power PV irrigation systems,” in *35th European Photovoltaic Conference and Exhibition*, Brussels, 2018.

[137] J. F. Gülich, Centrifugal Pumps, Springer, 2010.

[138] E. Larralde and R. Ocampo, "Centrifugal pump selection process," *World Pumps,* pp. 21-28, 2010.